III

ELECTRON-PHOTON

ANGULAR   CORRELATIONS   FROM

ELECTRON   IMPACT   EXCITATION

OF   ATOMS

BY

NAZIR   AHMAD   MALIK

Thesis submitted to the University
of Stirling for the degree of
Doctor of Philosophy

Institute of Atomic Physics
University of Stirling
Stirling FK9 4LA
SCOTLAND, U.K.

October 1980

ABSTRACT

Electron-photon angular correlations between the inelastically scattered electrons from the excitation of the 2^1P state of helium and the photons emitted in the de-excitation process have been measured for an incident electron energy of 80 eV and for electron scattering angles in the range of $8 - 108^{\circ}$. For these measurements a new apparatus has been designed and constructed. Because of the existing discrepancy between the experimental results of Hollywood et al. and Sutcliffe et al. great care has been taken during the construction of the apparatus to ensure that the collected data were free from systematic errors. An analysis of the data yields λ, the ratio of the differential cross sections for exciting the $M_j = 0$ sublevel to the total differential cross section and the magnitude $|\chi|$ of the phase difference between the $M_j = 0$ and $M_j = 1$ excitation amplitudes. The Fano-Macek orientation and alignment parameters are also derived from the present data. The values of the derived parameters are compared to values which have been obtained in other experiments and theoretical calculations. It is found that none of the known theoretical calculations fully agree with the present data which are in good agreement with the experimental results of Hollywood et al., and Slevin et al. but show a marked discrepancy at large scattering angles ($\theta_e > 70^{\circ}$) with the data of Sutcliffe et al. and recent measurements of Steph and Golden.

Electron-photon angular correlations for the $4p^5(2P_{3/2})$

$5s\ ^3P_1$ and $4p^5(2P_{1/2})\ 5s\ ^1P_1$ states of krypton and $5p^5(2P_{3/2})$ $6s\ ^3P_1$ state of xenon have also been measured. In this case, unlike helium, LS coupling is not valid and spin-orbit interaction in the target atom effects the phase information χ . This effect has been experimentally observed for the first time for an incident electron energy of 60 eV and 36 eV in the case of krypton and 80 eV for xenon at 20° and 30° electron scattering angles.

D E D I C A T E D

to the loving memory

of my mother

ACKNOWLEDGEMENTS

could give the design a practical shape.

I am grateful to Mrs Lyn North of the Education
Department and Mr R R Harrison of the Shared Technical
Services for their help in making some drawings of the
figures.

I would like to express my sincere thanks to Mrs
Hilda Queen who typed the thesis inspite of her other
pressing commitments.

Finally I am much indebted to my wife and children
for their patience, co-operation and help in making this
exercise a success.

CONTENTS

بسم الله الرحمن الرحيم

I - INTRODUCTION

1.1 General

The study of electron scattering by atoms has received much attention since the beginning of this century. Examples include the study and measurement of quantized energy loss of electrons in electron impact excitation as studied in experiments by Frank and Hertz (1914), Ramsauer (1921) and Townsend (1922), electron scattering intereference from electron angular distributions given by Bullard and Massey (1931), spin effects by Mott (1932), Shull et al. (1943), Exchange scattering by Rubin et al (1969), direct scattering by Hils et al. (1972) and atomic compound states revealed through scattering experiments by Schulz (1963).

The past two decades have witnessed many improvements in experimental techniques by way of using improved electron optics, energy loss analysis of the scattered electrons, single pulse counting and digital data recording. This has facilitated better data collection and detailed analysis of results. In this regard experiments of Rubin et al (1969) where a polarized atomic beam was used in a recoil experiment to determine the ratio of spin flip to total differential cross sections for electron-alkali atoms inelastic scattering, Hils et al (1972) who measured the polarization of electrons scattered from polarized alkali atoms, Hanne and Kessler (1974) who successfully used polarized electrons in a scattering experiment with mercury atoms, Hertel and Stoll (1974) who made measurements of super elastic collisions between low energy electrons and laser excited sodium atoms, can be

mentioned as some of the interesting new methods in the field
of experimental atomic physics.

In recent years a new experimental technique has been
developed for studying inelastic electron-atom collisions.
In this method electrons, or other particles, and photons
are detected in delayed coincidence as described by
Eminyan et al. (1973, 1974) for 2^1P excitation in helium.
This technique as well as the experiments mentioned above,
all explore the elementary collision processes in more
detail than do the usual measurements of differential and
total cross sections. At the same time they reduce the
number of fundamental collision parameters which must be
averaged over before a comparison with theory can be made.

Before discussing the coincidence technique which
forms the basis of this research work, it is worthwhile
to review the traditional methods of investigating electron
impact excitation of atoms. These methods depend largely
on the energy range to be studied. The experimental work
involves observations of the effects arising from the
passage of a beam of electrons through a gas or in crossing
a second beam of neutral atoms or ions.

1.2 Energy Loss Spectra and Optical Excitation Functions

Traditional experimental techniques used in the study
of the excitation process fall into two main categories.
One relating to those experiments where observations are
made on the scattered electrons or recoiling atoms, while
the other involves measurements of the electric dipole
radiation which results from the decay of the excited states.

Using an appropriate energy selector, measurements are made of the angular distribution of electrons scattered with an energy loss corresponding to the excitation energy of the state being studied thus yielding values for the differential cross sections.

Many studies involving the experimental measurements of energy loss spectra have concentrated on electron collisions with helium because helium is a simple gas atom and easy to work with. Some of the earlier works include those of Kupperman et al. (1968) and Imhof and Read (1971).

Energy loss studies on other rare gases have also been carried out, for example, by Delage et al. (1975) on krypton, Williams et al (1973) and Swanson et al. (1976) on xenon. Williams and Crowe (1975) and Williams and Willis (1975) have measured the absolute differential cross sections for a number of rare gases which covered a wide range of incident electron energies and scattering angles. Energy loss spectra of rare gases have recently also been studied by Al-Shamma (1978).

The measurements on the electric dipole radiation resulting from the decay of the excited states are again made in two ways. One measures the intensity of light emitted at the magic angle of 55° which yields the total cross sections as a function of incident electron energy (optical excitation function). The other measures the polarization of the emitted light observed at 90° to the electron beam axis. The latter measurement gives information on the averaged relative population of the magnetic sublevels excited by electron scattering at all angles.

The structure of an excitation function is characterized by the onset at threshold energy of a maximum (or several maxima) characteristic of the transition and the atom and also by the monotonic fall of the excitation function at large electron energies.

The gross structure as initially observed during the first quantitative measurements of the optical excitation function by Bricout (1927), Hanle (1927) and Hanle and Schaffernicht (1930) did not change much until more recent measurements by Pichanic and Simpson (1968), J. Williams (1975) and Brunt et al. (1977a,b) for example, showed the existence of a detailed structure sometimes having several maxima or minima in the excitation function close to threshold. The reason for most of these structures has been attributed to the presence of resonances in the inelastic electron scattering process (Williams, 1978). Such structure is related to the compound states Feshbach (Type I) resonances or Shape (Type II) resonances characterized by a given electron configuration. Ottley and Kleinpoppen (1975), Heddle et al. (1973, 1976), Al-Shamma and Kleinpoppen (1978) during their experiments on excitation functions have also observed similar effects.

1.3 Polarization of Emitted Radiation

The atomic line radiation excited by a unidirectional beam of electrons is in general partially polarized and the emitted photons will have an anisotropic angular distribution.

Earlier polarization measurements by Skinner (1926, 1927), Elett et al. (1926), Eldridge and Oslen (1926), Quarder (1927) and Elanbass (1929), for example, gave polarization

values which were much lower than those predicted by theories given by Oppenheimer (1927, 1928) and Penny (1932). The experimental values tended towards zero as the electron energy approached the threshold value. According to the theoretical predictions, the polarization should have a maximum value at threshold.

Baranger and Gerjouy (1958) associated this anomaly with the formation of atomic compound states. Percival and Seaton (1958) tried to explain this by developing a theory within the framework of quantum mechanics by taking into account the finite level width of the excited fine and hyper-fine structure states.

Failure to find unambiguous values for the polarization in earlier experiments led to further experiments close to threshold. The measurements of polarization with improved resolution, by McFarland (1964, 1967), Fedorov and Mezentov (1965), Heddle and Keesing (1967), Whitker and Dolby (1968) and Heidman et al (1969) for example, showed a rapid change of polarization close to threshold for a number of lines where the theoretical polarization was actually large. Similar results were observed by Enemark and Gallagher (1972), Ehler and Gallagher (1973) and Ottley and Kleinpoppen (1975) which were in good agreement with the theoretical values.

The measurements with improved energy resolution clearly demonstrate that the earlier experiments which seemed to indicate that the polarization tends to zero as the incident electron energy is lowered to the threshold value, lacked sufficient energy resolution to reveal detailed structure in the polarization near threshold.

Comprehensive reviews on polarization are given by
Kleinpoppen (1969, 1975, 1977), Fano and Macek (1973)
and by Heddle (1976).

1.4 Electron-photon Angular Correlations

The measurements of differential cross sections, total
cross sections and polarization of line radiation as such,
do not provide complete information due to a number of
factors which affect the interpretation of data. For
example, the detection of emitted photons are subject to
error due to cascades from higher excited states. Also
while measuring the differential and total cross sections
we need to place them on an absolute scale which involves
either absolute experimental calibration or normalization
to a theoretical model. Again, in comparing experimental
results with theoretical models it is necessary to average
the theoretical results over all the unresolved parameters
of the experiment which results in a loss of information.

The measurement of differential cross sections gives
the probability of scattering in different directions where-
as the total cross section is the sum of the scattering
into all angles and represents an average of the complete
interaction for electrons at a given energy. The differential
cross sections cannot distinguish between excitations to
the different degenerate sublevels of the excited atoms and
have until quite recently suffered from uncertainties in
absolute value (Williams and Willis 1975). The line polari-
zation measurements, however, do separate excitations from
the magnetic sublevels but since the analysis of the radia-
tion takes place without regard to the electron scattering

angles, important details are lost in the averaging process. Moreover, these experimental arrangements have cylindrical symmetry about the incident beam direction, implying that the excited state of the atom is representable as an incoherent superposition of pure states. Such problems have been discussed extensively by Moisewitsch and Smith (1968) and Williams (1975). These problems can be avoided by carrying out an experiment in which scattered electrons and photons from the same scattering event are observed in coincidence. Here we obtain the differential cross section ratio λ which does not need calibration to an absolute scale, whereas σ is not measured directly and one has to determine its value by other methods. The electron-photon coincidence technique requires both a high degree of experimental sophistication and substantial theoretical analysis with regard to relations between observables extracted from the angular correlations on the one hand and coherence parameters on the other hand.

Rubin et al. (1969), Macek and Jaecks (1971) and Wykes (1972) gave the theory of the electron-photon coincidence technique by relating the coincidence rates to "collisional parameters" such as inelastic scattering amplitudes. The electron-photon angular correlations have been related to "target parameters" such as orientation and alignment parameters and also to state multipoles of the atoms during the collisional excitation process by Fano and Macek (1973), Macek and Hertel (1974) and Blum and Kleinpoppen (1975).

The experiments on electron-photon angular correlations were first motivated while dealing with the question of how threshold polarization (Kleinpoppen 1967) and differential

magnetic sublevel cross sections could be extracted from such correlations. In these experiments the observation is restricted to radiations emitted by only those atoms which scattered the electrons with a given energy in a given direction defined by the detector. It is also assumed that excitation and de-excitation are independent processes, which requires that the atomic lifetimes are sufficiently long to allow the projectile electrons to leave the atom before a noticeable number of these will have decayed. At intermediate electron energies, the collision time is shorter than any characteristic time and this makes the process coherent (Macek and Jaecks 1971).

In order to determine the excitation amplitudes, an electron-photon coincidence experiment can be performed in two equivalent ways. Firstly electron-photon angular correlations can be made between the inelastic scattered electrons and the photons emitted during the de-excitation from which λ and $|\chi|$ parameters can be obtained. Alternatively the same information can be obtained by measuring the polarization of the emitted radiation. However the sign of χ, the phase difference between the excitation amplitudes cannot be found from the angular correlation measurements. For this one has to measure the circular polarization of the emitted radiation.

Delayed coincidence techniques have been used extensively in nuclear physics (RE Bell, 1966). It is only relatively recently that it has become widely used in atomic physics. The electron-photon coincidence technique was first adopted by Imhof and Read (1969) to eliminate cascades from the

higher states in the measurement of the excited state lifetime of 4^1S state of helium. This technique has since been used again by Imhof and Read (1971a,b,c) and many others (for example, Smith et al. 1973, 1975, Shaw et al. 1975, King and Adam 1974, King et al. 1975a) to measure lifetimes in atoms and molecules. Imhof and Read (1977) have reviewed the measurement of lifetimes in atoms, molecules and ions using the coincidence technique.

King et al. (1972) used the electron-photon coincidence technique to study the polarization of radiation from atoms excited by electron impact.

This technique has also been applied to measure absolute differential excitation cross sections for atomic levels which could not be separated in the scattered electron detector as described by Pochat et al. (1973), Kleinpoppen and McGregor (1979).

Besides using the electron-photon delayed coincidence technique, atomic and molecular lifetimes have also been measured by measuring delayed coincidences (photon-photon coincidence) between cascade photons as by R D Kaul (1966); Camhey Valari et al. (1970), Holt and Pipkin (1974), Brannen et al. (1975) and King and Read (1975). In another type of experiment (electron-electron coincidence) scattered electrons have been detected in coincidence with secondary electrons ejected in ionizing collisions as described by Ehrhardt et al. (1969).

The first electron-photon angular correlation measurements were reported by Eminyan et al. (1973, 1974) who measured the angular correlation function in helium at 80 eV

higher states in the measurement of the excited state lifetime of 4^1S state of helium. This technique has since been used again by Imhof and Read (1971a,b,c) and many others (for example, Smith et al. 1973, 1975, Shaw et al. 1975, King and Adam 1974, King et al. 1975a) to measure lifetimes in atoms and molecules. Imhof and Read (1977) have reviewed the measurement of lifetimes in atoms, molecules and ions using the coincidence technique.

King et al. (1972) used the electron-photon coincidence technique to study the polarization of radiation from atoms excited by electron impact.

This technique has also been applied to measure absolute differential excitation cross sections for atomic levels which could not be separated in the scattered electron detector as described by Pochat et al. (1973), Kleinpoppen and McGregor (1979).

Besides using the electron-photon delayed coincidence technique, atomic and molecular lifetimes have also been measured by measuring delayed coincidences (photon-photon coincidence) between cascade photons as by R D Kaul (1966); Camhey Valari et al. (1970), Holt and Pipkin (1974), Brannen et al. (1975) and King and Read (1975). In another type of experiment (electron-electron coincidence) scattered electrons have been detected in coincidence with secondary electrons ejected in ionizing collisions as described by Ehrhardt et al. (1969).

The first electron-photon angular correlation measurements were reported by Eminyan et al. (1973, 1974) who measured the angular correlation function in helium at 80 eV

incident energy for inelastically scattered electrons and photons from the 2^1P state, at an electron scattering angle of 16° and photon angles from 30° to 130°, and later extended the range of electron scattering angles from 10° to 40° for a range of incident energies from 40 to 200 eV. The angular correlation data were used to calculate the differential cross section ratio λ and relative phase $|\chi|$ of the corresponding excitation amplitudes a_o and a_1 for exciting the magnetic substates M = o and M = ±1 of the n^1P state. The working range for the 3^1P state in helium was also extendend to include a range of electron scattering angles from 10° to 30° for incident electron energies from 50 to 150 eV by Eminyan et al. (1975). Tan et al. (1977) and Ugbabe et al. (1977) in their angular correlation measurements used a linear polarization filter to analyse the 2^1P - 1^1S de-excitation radiation and thus determined the λ and $|\chi|$ parameters. These measurements were made at an electron energy of 50 eV over a range of electron scattering angles from 5° to 42° and at a fixed electron scattering angle of 42° over a range of electron energies from 30-80 eV.

The electron-photon coincidence technique has also been applied to the 2^1P state of atomic hydrogen by Williams (1975), Dixon et al. (1978), Hood et al. (1979) and Slevin et al. (1980). Ugbabe et al. (1977) and Arriola et al. (1975) reported the measurements of electron-photon angular correlations on neon and argon respectively. Malcolm and McConkey (1979) used this technique to study the λ and $|\chi|$ parameters and also threshold polarization for the resolved

104.8 and 106.7 nm lines of argon. Kleinpoppen and McGregor (1979) studied the angular correlations for the 116.5 and 123.6 nm lines of krypton and determined the collision parameters λ and $|\chi|$.

Using the coincidence technique, linear and circular polarization measurements for the $3^1P \to 2^1S$ (501.6 nm) line of helium has been done by Standage and Kleinpoppen (1976). Zehnle et al. (1978) applied this method for the vector polarization analysis of the potassium ($4^2P - 4^2S$) photons for the K - He collisions. Anderson et al. (1979) performed similar measurements of the Stokes parameters for magnesium ($3^2P - 3^2S$) photons. Recently the electron-photon coincidence technique has been applied to measure linear and circular polarization of the $6^3P_1 - 6^1S_0$ line of mercury in order to determine the partially coherent nature of the excitation/de-excitation process by Zaidi et al. (1980).

The electron-photon angular correlation measurements for the 2^1P excited state of helium by Sutcliffe et al. (1978) Hollywood et al. (1979), Slevin et al. (1980) and Steph and Golden (1980) have been extended to much larger scattering angles. It has been observed from the experimental data obtained by these authors that there exists marked disagreement between the values for the parameter λ at large scattering angles obtained by Sutcliffe et al. (1978) and Hollywood et al (1979). The recent measurements of Slevin et al (1980) tend to agree with the results of Hollywood et al. (1979) while those of Steph and Golden (1980) show agreement with the results of Sutcliffe et al.

(1978). There does not seem much variation in the value of the $|\chi|$ parameter obtained by these groups indicating that the value of $|\chi|$ perhaps is not sensitive to different experimental conditions.

The disagreement in the value of λ at large scattering angles have stimulated much interest in electron-photon angular correlation experiments in which differential cross sections for electron impact excitation of the 2^1P state of helium are measured. The importance of this experimental study increases in view of the fact that many elaborate theoretical calculations for λ and $|\chi|$ parameters have been proposed using differing approaches like distorted wave, many body, close coupling, second order potential, pseudostate expansions, multichannel eikonal etc. (Branden and McDowell 1977, 1978) all giving differing results. It has become difficult to judge the merits of each method since the authors have not only all used different approximations but have also all used different atomic potentials.

The disagreement in the experimental data as obtained by Sutcliffe et al. (1978) and Hollywood et al. (1979) is thus of considerable importance. More authentic and reliable experimental measurements especially at larger scattering angles are required to clarify the experimental disagreement in the existing data and lay out new guidelines for sound theoretical interpretation of the results.

In the present experiment an effort has been made to resolve the discrepancy existing between the data of Hollywood et al. (1979) and Sutcliffe et al (1978) as

later extended by Steph and Golden (1980). Because of
this disagreement special attention has been given to the
analysis of the systematic errors which could effect the
coincidence data.

1.5. <u>Present Work</u>

The work presented in this thesis has been carried
out in three phases. In the first phase a new electron-
photon angular correlation measurement apparatus has been
designed and built. The existing apparatus (Eminyan et al.
1974, Standage and Kleinpoppen, 1976 and Kleinpoppen and
McGregor 1979) because of its design limitation could only
be used for small scattering angle studies with low current
electron beam ($\sim$nA) and was not suitable for the present
work requiring large angle electron scattering measurements.

The new apparatus once built was given a number of
tests to check its operation and validity of the measure-
ments.

In the second phase, the apparatus was used to study
the electron-photon angular correlations for the excitation
of the 2^1P state of helium. For this angular correlation
measurements have been made at the electron scattering
angles of 8°, 18°, 30°, 35°, 50°, 60°, 80°, 90°, 100° and
108°.

The angular correlation data are analysed to yield the
ratio of the differential cross section λ for the excitation
of the degenerate magnetic sublevel of the 2^1P state of
helium and the phase difference between the corresponding
excitation amplitude $|\chi|$. Fano-Macek orientation and

alignment parameters 0^{col}, $A_o{}^{col}$, $A_{1+}{}^{col}$, $A_{2+}{}^{col}$ have also been derived from the λ and $|\chi|$ parameters.

The results are compared with the existing data by Sutcliffe et al. (1978), Hollywood et al. (1979), Slevin et al. (1980), Steph and Golden (1980) and some of the others who have worked in the small scattering angle range.

In the third phase of the experiment electron-photon angular correlation measurements have been made for the triplet $4s^55s^3P_1$ ($\lambda = 123.6$ nm) and singlet $4p^55s^1P_1$ ($\lambda = 116.5$ nm) states of krypton and the triplet $5p^56s^3P_1$ ($\lambda = 146.9$ nm) state of xenon. In the light of recent comments on the interpretation of electron-photon coincidence experiments by Blum et al. (1980), these measurements have been made in two planes. One set of measurements was taken by rotating the photon multiplier in the plane of scattering while the other set of measurements was made in a plane at an azimuthal angle of 135°. These measurements have been made at electron scattering angles of 20 and 30 degrees.

The data have been interpreted in terms of the new parameters σ, λ, $\cos \overline{\chi}$ and $\cos \varepsilon$ as suggested by Blum et al. (1980), Blum and Kleinpoppen (1980). These new parameters take into consideration the spin-orbit interaction experienced in heavy atoms and do not apply to helium where the spin orbit coupling is negligible for the scattered electrons at low energies.

Some theoretical aspects regarding the electron-photon angular correlation measurements with crossed beam apparatus are discussed in Chapter II. Chapter III describes the

design and development of the apparatus. The validity of
the measurements carried out with the apparatus is checked
by tests described in Chapter IV. The results of the
measurements on helium, krypton and xenon are presented
and discussed in Chapter V while Chapter VI includes the
conclusions of the present work and the suggestions for
future work.

2. THEORY OF ELECTRON-PHOTON
ANGULAR CORRELATION

2.1 General

In electron-photon coincidence experiments, we consider collisions between atoms and electrons in which some of the atoms are excited, and subsequently decay by photon emission. The basic assumptions for the interpretation of results with light atoms are that excitation-de-excitation are independent processes, the Hamiltonian characterizing the collision contains no explicit spin dependent terms and the excitation process is considered to be adequately described in the LS coupling scheme. Experimentally a certain subensemble of atoms is selected and the observation is restricted to radiation emitted by only those atoms which scattered the electrons with a given energy in a given direction defined by the detector.

The atom initially in the ground state is excited to a set of degenerate or nearly degenerate upper states by electron impact. The atomic system in turn decays from the upper levels to a set of closely spaced lower levels. As pointed out by Macek and Jaecks (1971), in a collision at intermediate energies, the excited states are populated in a time of the order of 10^{-15} sec. which is much shorter than any characteristic time of these states such as lifetime or reciprocals of transition frequencies of spin-orbit and hyperfine structure interactions. The important feature of this excitation is that the upper states are

excited coherently even if they are completely resolved and therefore can interfere during the decay.

The theory of the measurements in which photons are detected in delayed coincidence with scattered electrons has been developed by Macek and Jaecks (1971) who relate the coincidence rates for electron-photon angular correlations to scattering amplitudes thus investigating the "collision parameters" of the electron atom excitation process which include the differential inelastic cross sections, excitation amplitudes and their phase differences. The "target parameters", such as orientation and alignment parameters and the multipole states of the excited atoms have been described by Fano and Macek (1973), Blum and Kleinpoppen (1975,76). Electron-photon angular correlations in atomic physics have been comprehensively reviewed by Blum and Kleinpoppen (1979). Recently Blum et al. (1980) have introduced new parameters to interpret the electron-photon angular correlations where spin-orbit effects are significant during the scattering process as is the case when heavy atoms (e.g. xenon, krypton and mercury) are excited by electron impact.

2.2 Excitation of 2^1P State of Helium

If one neglects spin-orbit and spin-spin interactions, which is a good approximation for the excitation process $1S_0 \rightarrow n^1P_1 \rightarrow 1^1S_0$ in helium, the excitation into the excited states can be described as a coherent superposition of excitation into degenerate magnetic sublevels. The 2^1P state of helium excited from the 1^1S ground state by electron impact can be described by the state vector

$$| \psi > = a_{+1} |11> + a_0 |10 > + a_{-1} |1\text{-}1> \qquad (2.1)$$

where the amplitudes a_M with $M=0, \pm1$ describe the excitation to particular magnetic substates $| JM >$ of the excited state.

The state vector $| \psi >$ (Eq. 2.1) can be normalized so that:

$$< \psi | \psi > = a^*a = |a|^2 = \sigma \qquad (2.2)$$

where σ is the inelastic differential cross section for exciting the ^1P state

Moreover $< \psi | \psi > = (\Sigma_{M'} a^*_{M'} <JM' |) (\Sigma_M a_M |JM >)$

$$= \Sigma_{M'M} a^*_{M'} a_M <JM'|JM> \qquad (2.3)$$

From the orthogonality of the base states

$$<JM'|JM> = \delta_{M'M} \qquad (2.4)$$

follows

$$< \psi | \psi > = \Sigma a^*_{M'} a_M \ \delta_{M'M}$$

$$= \Sigma_M |a_M|^2$$

$$= \sigma \text{ from eq.(2.2)}$$

and

$$|a_{+1}|^2 + |a_0|^2 + |a_{-1}|^2 = \sigma_{+1} + \sigma_0 + \sigma_{-1}$$

where σ_M , $M = 0, \pm1$, is the partial differential cross section for exciting the M substate.

The mirror symmetry of the scattering process in the plane of scattering implies that $a_1 = -a_{-1}$.

We therefore have $\sigma_{+1} = \sigma_{-1}$ and hence

$$\sigma = \sigma_0 + 2\sigma_1 = |a_0|^2 + 2|a_1|^2 \qquad (2.5)$$

In the coherent excitation of the magnetic substates in a given excitation process determined by the excitation energy and the scattering angle, the excitation amplitudes a_1 and a_0 are expected to have a fixed phase relationship to each other. The amplitudes a_M are in general complex numbers. However since $|\psi\rangle$ is defined only up to an overall phase factor, a_0 may be assumed real and positive. The relative phase χ between a_1 and a_0 is then defined by

$$\bar{a}_1 = |a_1|e^{+ i\chi} \qquad (2.6)$$

Therefore for a given incident electron energy E_i, electron scattering angle θ_e and the photon angle θ_γ, $|\psi\rangle$ is completely described by the parameters

$$\lambda = \frac{|a_0|^2}{(2|a_1|^2 + |a_0|^2)} = \frac{\sigma_0}{\sigma} \quad (0 \leqslant \lambda \leqslant 1) \qquad \text{and}$$

$$\chi \qquad (-\pi \leqslant \chi \leqslant \pi)$$

Thus a measurement of σ, λ and χ constitutes a complete determination of the scattering process. σ is the probability of electron scattering in a particular direction, the dimensionless quantities λ and χ describe the state of the atom after the collision.

The excitation amplitudes can be determined by performing coincidence experiments in two almost equivalent ways. Electron-photon angular correlation measurements yield the excitation amplitudes which can alternatively be determined

from coincidence polarization measurements of the emitted radiation. The scheme of these two types of coincidence measurements is shown in Fig. 2.1 (a) and (b).

2.2.1 Angular Correlations

Atoms excited to the 2^1P states in helium by electron impact, decay to the ground state with a lifetime of 0.58 ± 0.04 ns (Williams and Fry 1968) giving off 58.4 nm UV photons in the directions described by $(\theta_\gamma \; \phi_\gamma)$. Macek and Jaecks (1971) in their theory of the measurements for the photon-particle delayed coincidence technique describe the angular correlations between the photons and the scattered electrons in terms of the scattering amplitudes. Their results (summed over photon polarization) in the case of the 2^1P state of helium (Eminyan et al. 1976) can be written as:

$$\frac{d^2P_C}{d\Omega_e d\Omega_\gamma} = \frac{\sigma dP_C}{\Sigma d\Omega_\gamma} \qquad (2.7)$$

where

$$\frac{dP_C}{d\Omega_\gamma} = \frac{3}{8\pi} \left[\lambda \sin^2 \theta_\gamma + \left(\frac{1-\lambda}{2}\right) (\cos^2\theta_\gamma + 1) \right.$$

$$- \left(\frac{1-\lambda}{2}\right) \sin^2\theta_\gamma \cos 2 (\phi_\gamma - \phi_e)$$

$$\left. + \{\lambda(1-\lambda)\}^{\frac{1}{2}} \cos\chi \sin 2\theta_\gamma \cos(\phi_\gamma - \phi_e) \right]$$

Here in eq. (2.7)

$\dfrac{d^2P_C}{d\Omega_e d\Omega_\gamma}$ is the probability density for scattering of electrons in directions (θ_e, ϕ_e) in any 2^1P excitation, with subsequent emission of the photon in direction $(\theta_\gamma, \phi_\gamma)$,
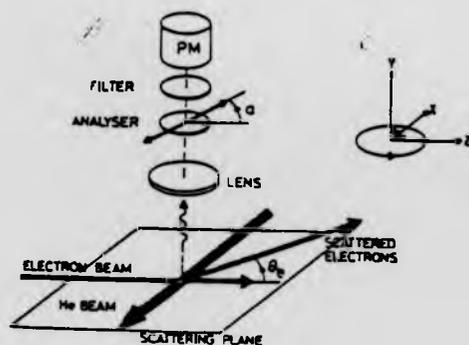
(a)
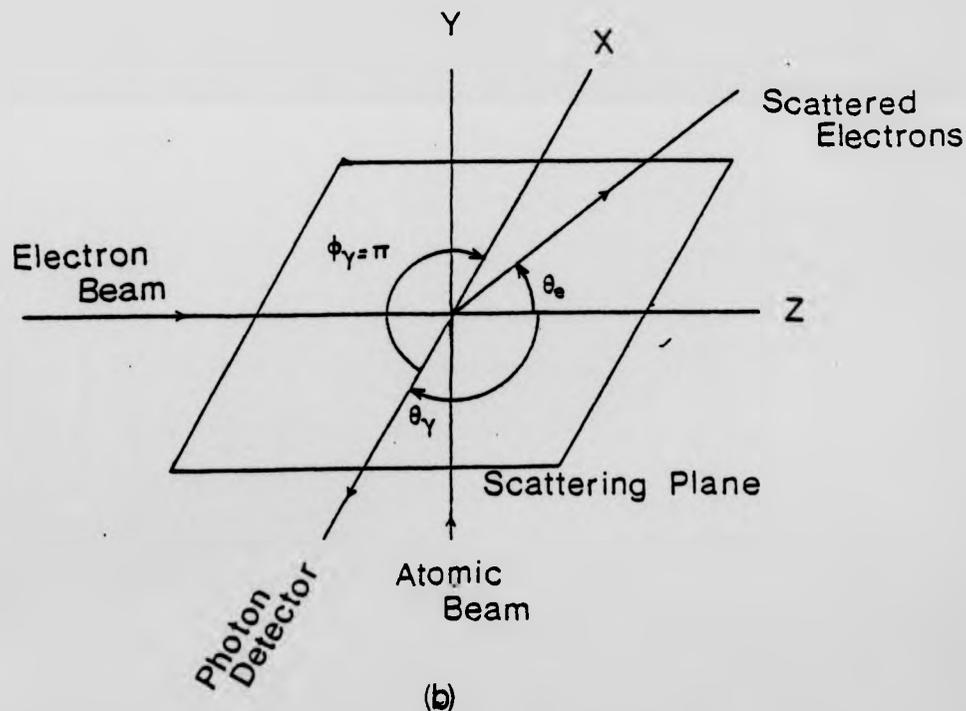
(b)

Fig. 2.1 (a)

A typical schematic layout for the polarization measure-
ment. The X-Z plane is the scattering plane; the photons
are detected by the photomultiplier (PM) along the Y axis.
Scattering angle θ_e and linear polarization angle α are
measured in the X-Z plane.

Fig. 2.1 (b)

The geometry of the electron-photon coincidence experi-
ment using crossed beam technique.

Σ is the total (integrated) cross section for excitation of the 2^1P state at energy E_i

and $\dfrac{dP_c}{d\Omega_\gamma}$ is the probability density for photon emission after electron scattering in a particular direction upon which λ and χ depend.

In the present experiment, the primary electron beam is incident in the Z direction on the target located at the origin of the co-ordinates. Inelastically scattered electrons are analysed by a 127° electron analyser whose position defines the scattering plane XZ. Therefore, the azimuthal angle $\phi_e = 0$ for all detected inelastically scattered electrons. The photon detector is also placed in the XZ plane but on the opposite side of the electron beam from the analyser at the azimuthal angle $\phi_\gamma = \pi$. Under these conditions following Macek and Jaecks (1971) we have from eq. (2.7):

$$\frac{dP_c}{d\Omega_\gamma} = \frac{3}{8\pi} N$$

where N is the angular correlation defined by

$$N = \lambda \sin^2 \theta_\gamma + (1-\lambda) \cos^2 \theta_\gamma -$$

$$2 \{ \lambda(1-\lambda) \}^{\frac{1}{2}} \cos \chi \sin \theta_\gamma \cos \theta_\gamma \qquad (2.8)$$

By fitting the experimental data obtained from the measurements of the angular distribution of the time correlated photons to the angular correlation function in eq.(2.8),

the collision parameters λ and $|\chi|$ at a particular scattering angle can be extracted.

2.2.2 Polarization Measurements

By setting a linear polarizer at an angle α (Fig. 2.1a) in front of the photon detector, the probability density for scattering an electron in a given direction with subsequent emission and observation of the photon is

$$\frac{d^2P_C}{d\Omega_e d\Omega_\gamma}(\alpha) = \frac{\sigma}{\Sigma}\left[\left(\frac{dP_C}{d\Omega_\gamma}\right)_{\hat{\epsilon}^{(1)}}\cos^2\alpha + \left(\frac{dP_C}{d\Omega_\gamma}\right)_{\hat{\epsilon}^{(2)}}\sin^2\alpha\right] \quad (2.9)$$

where

$\left(\dfrac{dP_C}{d\Omega_\gamma}\right)_{\hat{\epsilon}^{(i)}}$ is the probability density for photon

emission polarized along the direction of the polarization unit tensor $\hat{\epsilon}^{(i)}$

Thus

$$\left(\frac{dP_C}{d\Omega_\gamma}\right)_{\hat{\epsilon}^{(1)}} = \frac{3}{8\pi}\{\lambda\sin^2\theta_\gamma + (\frac{1-\lambda}{2})\cos^2\theta_\gamma\left[1 + \right.$$

$$\cos 2(\phi_\gamma - \phi_e)\left] + \left[\lambda(1-\lambda)\right]^{\frac{1}{2}}\right.$$

$$\cos\chi\sin 2\theta_\gamma\cos(\phi_\gamma - \phi_e)\}$$

and $\left(\dfrac{dP_C}{d\Omega_\gamma}\right)_{\hat{\epsilon}^{(2)}} = \dfrac{3}{8\pi}\{(\dfrac{1-\lambda}{2})\left[1 - \cos 2(\phi_\gamma - \phi_e)\right]\}$ (2.10)

Therefore for the photon detector set at a fixed angle out of the plane of the scattering $\left[\text{i.e.}(\phi_\gamma - \phi_e) \neq 0, \pi\right]$ the measurement of

$$\frac{d^2P_C}{d\Omega_e d\Omega_\gamma}(\alpha)$$

obtained by rotating the polarizer axis yields values for λ and $|\chi|$.

From the above it is clear that the information obtained from a measurement of the linear polarization is identical to that obtained from a photon angular distribution.

2.3 Excitation of Heavy Rare Gas Atoms

The theories developed for coincidence experiments by Macek and Jaecks (1971), Fano and Macek (1973), Blum and Kleinpoppen (1975) and the general formula derived by Macek and Jaecks (1971) for helium, have been applied by Eminyan et al. (1974, 1975) to analyse electron-photon coincidence experimental data for the electron impact excitation of the 2^1P state of helium with the approximations that (a) the spin-orbit coupling effect in the collision is negligible for the scattered electrons at low energies (b) the initial and the final states of the target are singlet and (c) the states have no fine or hyperfine structure.

In a more recent study, the general theory of Macek and Jaecks (1971) has also been applied by Ugbabe et al. (1977) Malcolm and McConkey (1979) to interpret their experimental results for neon and argon respectively. McGregor et al (1980) have studied the excitation of krypton.

In deriving eq. (2.7) from the general theory of Macek and Jaecks (1971) it was necessary to assume the validity of the mirror symmetry of the scattering process in the plane of scattering, i.e.

$$a_{-M} = (-1)^M a_M$$

This transformation property of the amplitudes holds good only if LS coupling is a good description of the target atom. Such is the case for He (i.e. $^1P \rightarrow {}^1S$ transition). For the heavier atoms LS coupling is not valid and as is discussed by Macek and Jaecks (1971) and more recently by Blum (1979) eq.(2.7) cannot be applied in this case. In effect, since a_{-1} is no longer related to a_{+1} (due to the loss of mirror symmetry in the scattering plane) the theory has one more parameter. Herman & Hertel (1978), Blum (1979) and Blum et al. (1980) introduced a new parametrisation of the atomic states having spin orbit effects for the interpretation of their angular correlation measurements defined as under:

$$\sigma = \sigma_0 + 2\sigma_1$$

$$\lambda = \frac{\sigma_0}{\sigma}$$

$$= \frac{\sigma_0}{\sigma_0 + 2\sigma_1}$$

$$\cos \overline{\chi} = \frac{Re\langle a_0 a_1 \rangle}{\sqrt{\sigma_0 \sigma_1}} \quad , \quad \sin \phi = \frac{Im\langle a_0 a_1 \rangle}{\sqrt{\sigma_0 \sigma_1}}$$

$$\cos \epsilon = -\frac{\langle a_1 a_{-1} \rangle}{\sigma_1} \tag{2.11}$$

The parameters σ and λ are the same as defined previously (Eminyan et al. 1973, 1974) and determine the population of the state with M = ±1, O , $\overline{\chi}$ and ϕ characterize the interference between the states M = ±1 and M = -1. When spin-orbit coupling holds we have in particular $\cos \epsilon < 1$ and the deviation from 1 is a measure of the strength of spin-orbit coupling.

It can be shown that if LS coupling holds during the

scattering process, then $\cos \epsilon = 1$ and $\cos \bar{\chi} = \cos \chi$

Using these definitions, and with our present notation eq. (2.7) takes on the new form,

$$\frac{dNc}{d\Omega d\Omega^-} = B\sigma \left(\lambda \cos^2 \beta + \frac{1-\lambda}{2} \sin^2 \beta + \frac{1-3\lambda}{2} \cos^2 \beta \cos^2 \theta^- \right.$$

$$+ \sqrt{\lambda(1-\lambda)} \cos \bar{\chi} (\sin 2 \theta^- \cos \phi^- \cos^2 \beta - \sin 2\beta \sin \theta^- \sin \phi^-$$

$$+ \frac{1-\lambda}{2} \cos \epsilon \left[(\cos^2 \beta \cos^2 \theta^- - \sin^2 \beta) \cos 2\phi^- \right.$$

$$\left. \left. - \sin 2\beta \cos \theta^- \sin 2\phi^- \right] \right) \qquad (2.12)$$

With $B = vn_o n_A \frac{3}{8\pi} \frac{\gamma^1}{\gamma}$ where vn_o is flux,

n_A atomic beam density and γ/γ^1 is the branching ratio.

(This notation has been retained for ease of reference otherwise in the formula $\theta^- = \theta_\gamma$ the photon angle and $\phi^- = \phi_\gamma$ photon detector azimuthal angle).

In the present experiment on the triplet $4p^5 5s\,^3P_1$ ($\lambda = 123.6$ nm), the singlet $4p^5 5s\,^1P_1$ ($\lambda = 116.5$ nm) states of krypton and the triplet $5p^5 6s\,^3P_1$ ($\lambda = 146.9$ nm) state of xenon, the angular correlation measurements have been made in two planes, one parallel to the scattering plane XZ (azimuthal angle $\phi_\gamma = 180^o$) and the other in a different plane at an azimuthal angle of 135°. An azimuthal angle of 135° has been selected in order to simplify the calculations using eq. (2.12). By fitting the experimental data to the angular correlation functions, the value of λ, $\cos \bar{\chi}$ and $\cos \epsilon$ parameters are extracted. In fact for the 50% abundant isotope of xenon, the elimination of hyperfine structure (nuclear spin $I \neq o$) poses special experimental difficulties and requires even more general

parametrization. In the present study, however, we have
made the observations for xenon also in two planes as for
the 90% abundant isotope of krypton having I = 0. For
these two planes at the azimuthal angles $\phi_\gamma = \pi$ and $3\pi/4$,
eq. (2.12) then becomes:

$$\frac{dN_C}{d\Omega d\Omega'} = B\sigma \left\{ \frac{1+\lambda}{2} + \frac{1-3\lambda}{2} \cos^2 \theta' - \cos \epsilon \frac{1-\lambda}{2} \sin^2 \theta' \right.$$

$$\left. -\sqrt{\lambda(1-\lambda)} \cos \overline{\chi} \quad \sin 2 \theta' \right\} \qquad (2.13)$$

and

$$\frac{dN_C}{d\Omega d\Omega'} = B\sigma \left\{ \frac{1+\lambda}{2} + \frac{1-3\lambda}{2} \cos^2 \theta' \right.$$

$$\left. - \sqrt{\frac{\lambda(1-\lambda)}{2}} \quad \cos \overline{\chi} \quad \sin 2 \theta' \right\} \qquad (2.14)$$

respectively.

3. APPARATUS

3.1. General

A new electron-photon angular correlation measurement apparatus has been designed and built for this work. Two different types of experiment are possible with this apparatus. The first has a broad resolution ($\sim$0.5 eV) and high current electron beam ($\sim 10^{-5}$A) which does not require a monochromator whereas the second with high resolution ($\sim$0.02eV) and low electron beam current ($\sim 7.10^{-8}$A) requires a monochromator. In the present experiment the work has been carried out with high currents and therefore a monochromator was not used. Fig. 3.1 shows an interior view of the apparatus while a general schematic diagram of the apparatus is shown in Fig.3.2. The main components are a 127° electron analyzer with associated input and output optics, an electron gun assembly, a Faraday cup, photon multiplier and gas nozzle, all housed inside the excitation chamber and mounted on a triple turntable assembly. The electrodes of the various elements were connected to the outside, via electrical feedthroughs to the associated electronics and power supplies.

The vacuum system used for the experiment was initially set up by Koschmieder (1974), Raible (1974) and later used by Al Shamma (1978). A description of the main parts of the apparatus is given in the following sections.

3.2. The Vacuum System

The vacuum system consisted of a T shaped stainless steel chamber of 600 mm length and with an internal diameter of 350 mm. The chamber had two 350 mm diameter openings, one at each end, with a few smaller parts which could be
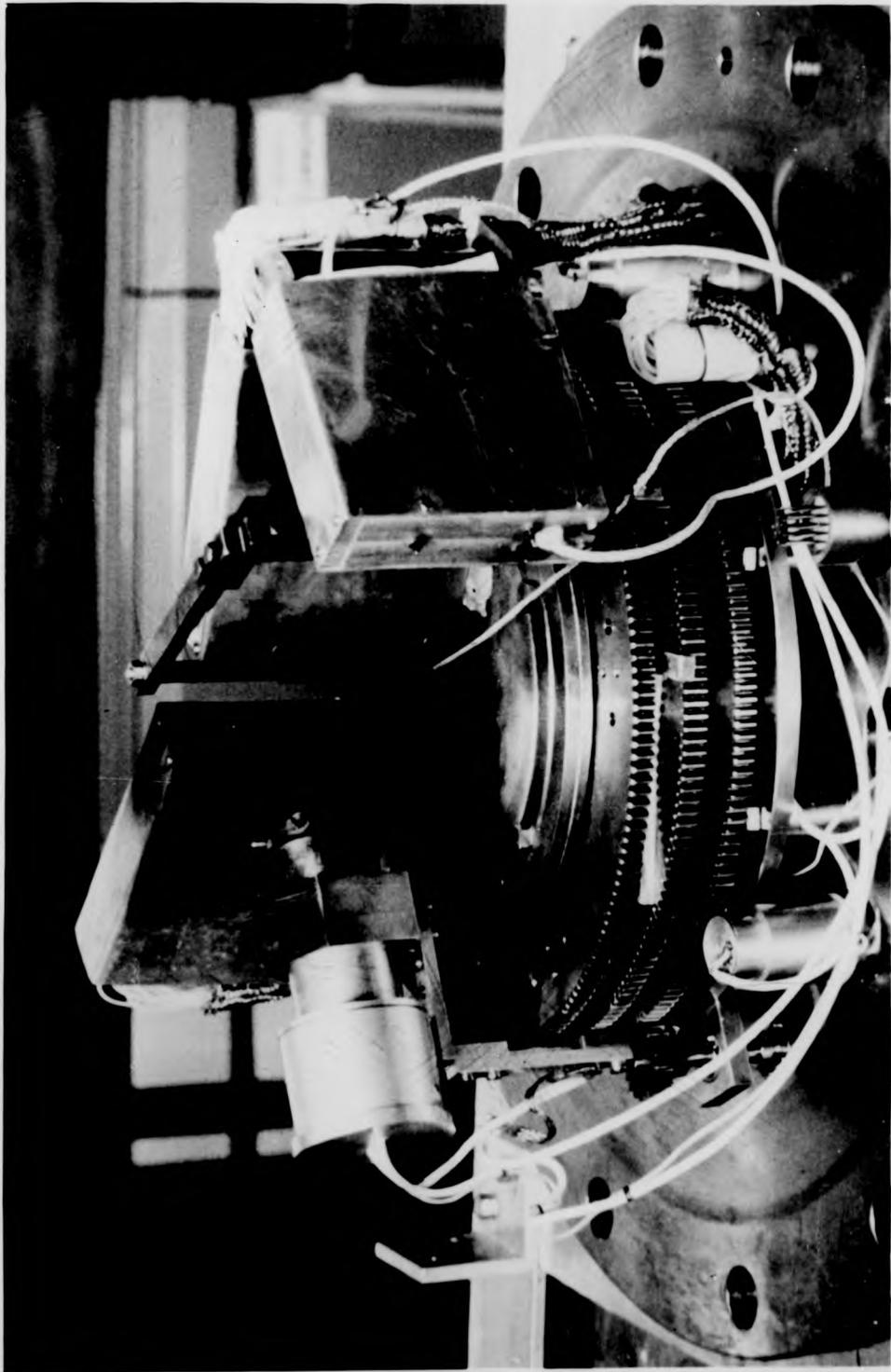
Fig 3.1 An interior view of the apparatus
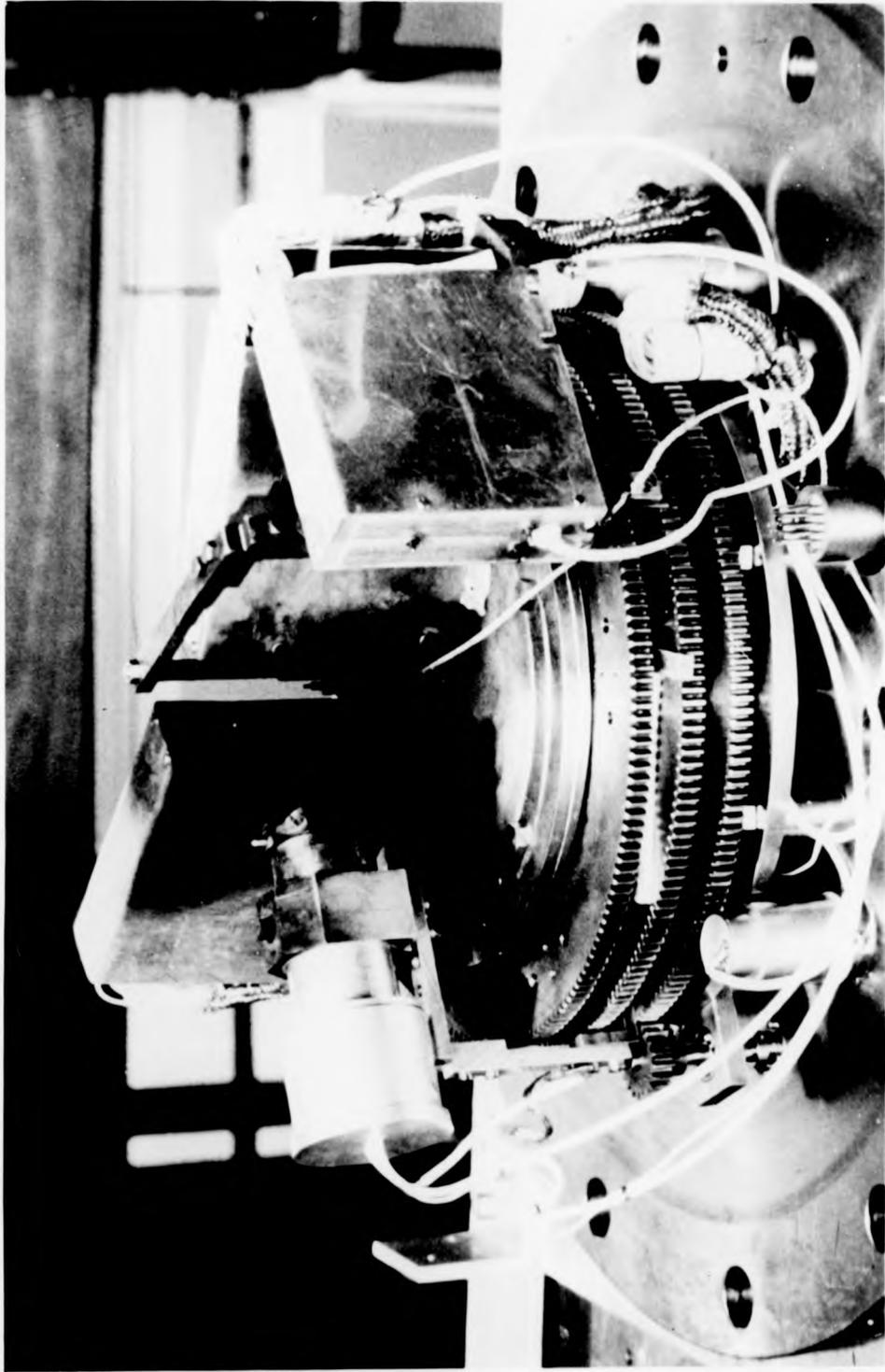
Fig 3.1 An interior view of the apparatus
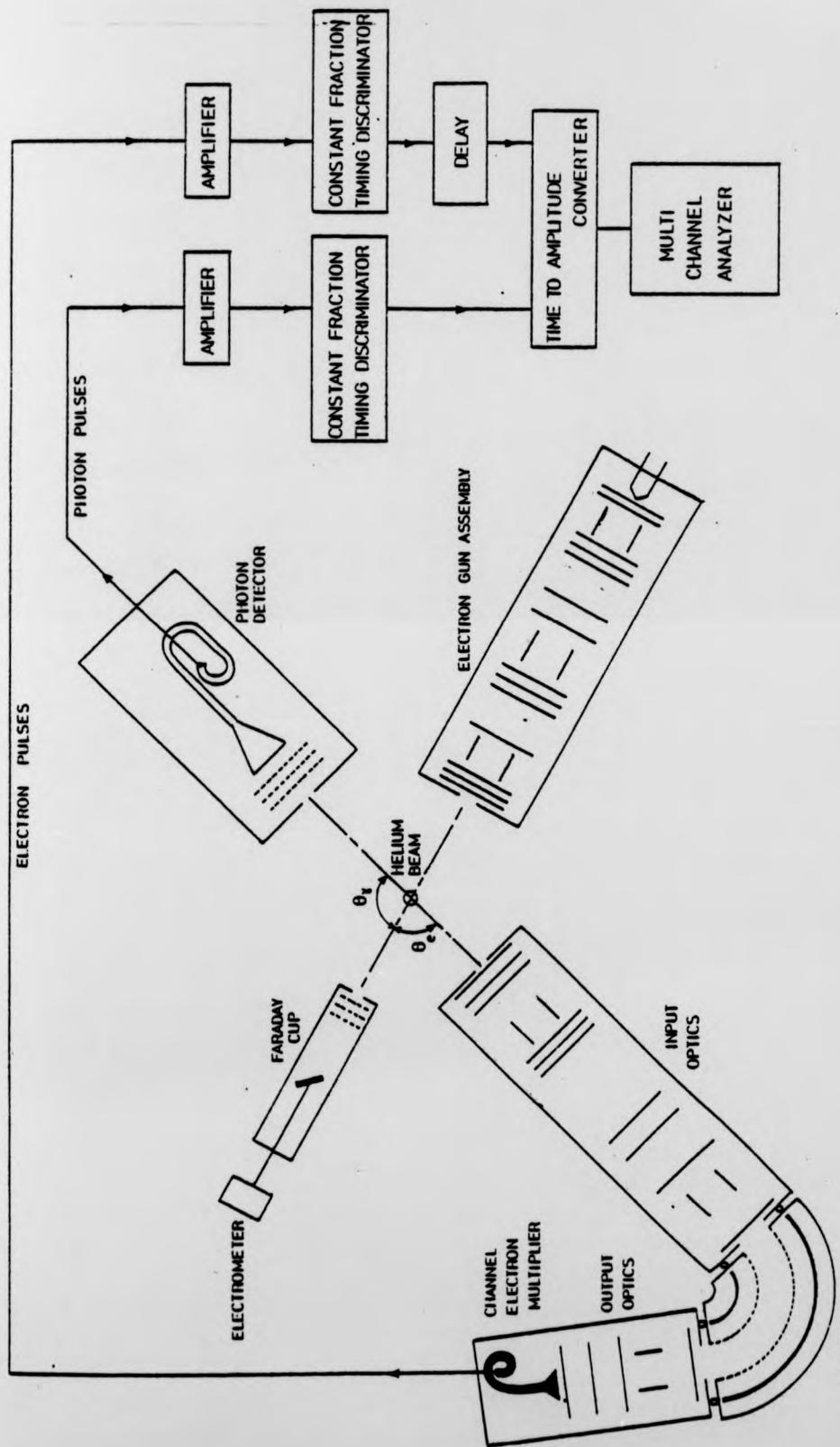
FIG. 3.2 Schematic diagram of the apparatus for electron - photon angular correlation measurements

used for fixing other components as required. Four such ports have been used in the present experiment, i.e. for the foreline bypass, the air admittance valve, the Pirani gauge head and the ionization gauge head. One side end flange had nine 38 mm ports to take all the rotary feed-throughs, electrical feedthroughs and the gas leak valve used for the experiment. A schematic diagram of the vacuum system is shown in Fig.3.3. The side view of the vacuum chamber gives the placement of the electrical feedthroughs (Vacuum Generator EFT19, EFT20 and EFT1), Rotary feed-throughs (Vacuum Generator RD-1 Rotary Motion Drive) and gas leak valve (Vacuum Generator MD-6),were all fixed on the same side flange. Viton 'O' rings and copper gaskets were used to vacuum seal the flanges with the chamber.

The chamber was pumped by a four stage jet system oil diffusion pump (Heraeus DI3000) through a 250 mm part joined with a T joint at the top of freon and water cooled baffles placed on the diffusion pump.

In the beginning, the diffusion pump was not giving pressures lower than 10^{-6} Torr. To improve upon this the diffusion pump was stripped apart, thoroughly cleaned and on the recommendation of the manufacturers (Leybold Heraeus) the existing oil Santovac 5 was replaced with Silicone 705 oil. This improved the performance of the diffusion pump and a base pressure better than 1.5×10^{-7} Torr was finally reached. The existing backing pump (Heraeus DK100) also showed substandard performance. This was, therefore, replaced by a new rotary piston vacuum pump (Edwards model ES 2000) which had a pumping speed of 126 m^3/hour.

Gate Valve

Freon

Water
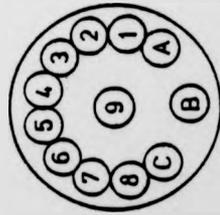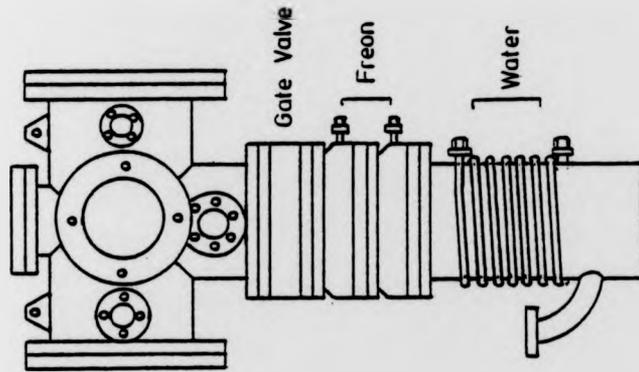
Feed throughs and gas leak valve

ROTARY FEED THROUGHS

A   Analyzer
B   Faraday Cup
C   Photon Multiplier

ELECTRICAL FEED THROUGHS

1   EFT 19 Filament & FC
2   EFT 19 Electron Gun Assembly
3   EFT 20 Electron Signal
4   EFT 1 HT for CEM
5   EFT 19 Analyser Assembly
6   EFT 19 Photon Multiplier
7   EFT 20 Photon Signal
8   EFT 1 HT for Photon Multiplier

9   MD6   VG. Gas Leak Valve

FIG.3.3 SCHEMATIC LAYOUT OF VACUUM SYSTEM

The diffusion pump could be separated from the vacuum chamber by means of an electro-pneumatically operated gate valve. This gate valve could be used to isolate the vacuum chamber from the diffusion pump, in case the chamber was required to be exposed to atmospheric pressure for working inside. This allowed the diffusion pump to be kept working all the time thus saving the time required for cooling and heating the pump during such operations. (This feature proved extremely useful in this experiment where in the initial setting up and operation, the system had to be opened up quite frequently).

The vacuum chamber could be baked by heater coils wrapped around the vessel. The ba-king temperature did not exceed 120°C to avoid damage to the vacuum seals (Viton 'O' rings).

The vacuum chamber was suspended from a metal beam using castor wheels. The triple turntable holding the apparatus was mounted on one end flange. This could be moved out of the chamber "en block" by unbolting the nuts and separating the flange from the chamber by moving it on the ball races placed on a metal frame specially built for this purpose. The flange once taken out of the chamber could be laid on the frame structure to allow easy access to the apparatus. This procedure facilitated the tracing of any faults in the apparatus. After inspection or rectification of faults, the flange could be easily lifted upright and moved on the ball races to replace the apparatus inside the vacuum chamber.

3.3. The Triple Turntable Assembly

The triple turntable used for fixing the different parts

of the electron-photon angular correlation measurement
apparatus is shown in Fig. 3-4. The triple turntable
assembly made of 310 non-magnetic stainless steel, was
fixed permanently to one end flange with the centre of
the flange coinciding with the centre of the turntable
assembly. The table had four concentric circular plates
each having a diameter of 246 mm. and 8 mm thickness. The
bottom plate was fixed while the upper three could be
rotated individually from outside the vacuum system by means
of rotary feedthroughs (Vacuum Generator RD1 Rotary Motion
Drive). The three rotating turntables had 200 teeth on
their periphery each driven by a phosphor-bronze gear wheel
having 20 teeth and fixed to a rotary feedthrough. The
rotating tables moved individually on 3 mm ϕ ruby balls
situated in circular tracks machined into the lower plates.
The rotary feedthroughs had 360 divisions marked on their
knobs. The gear ratio of 200 : 20 implies a rotation of
36° for each full turn of the feedthroughs.

It was found convenient to keep the electron gun
assembly fixed on the bottom table and mount the photon
multiplier on the first turntable, the Faraday cup on the
second turntable and the 127° electron analyser assembly
on the topmost (third) turntable.

The design of earlier experiments (i.e., Eminyan et
al. 1974) allowed measurements of angular correlations at
scattering angles up to only 40°. In the present design,
the sizes of the turntables, and electron optical elements
were chosen so that measurements at both smaller and larger
scattering angles were possible. The present fitting of the
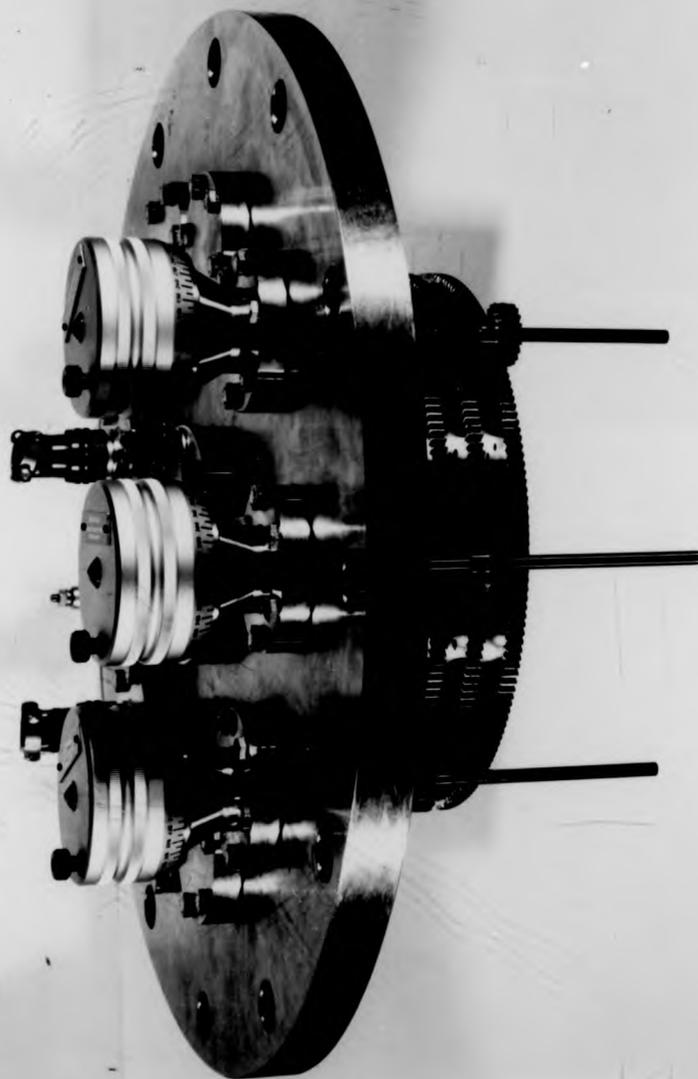
Fig 3.4 The Triple Turntable Assembly
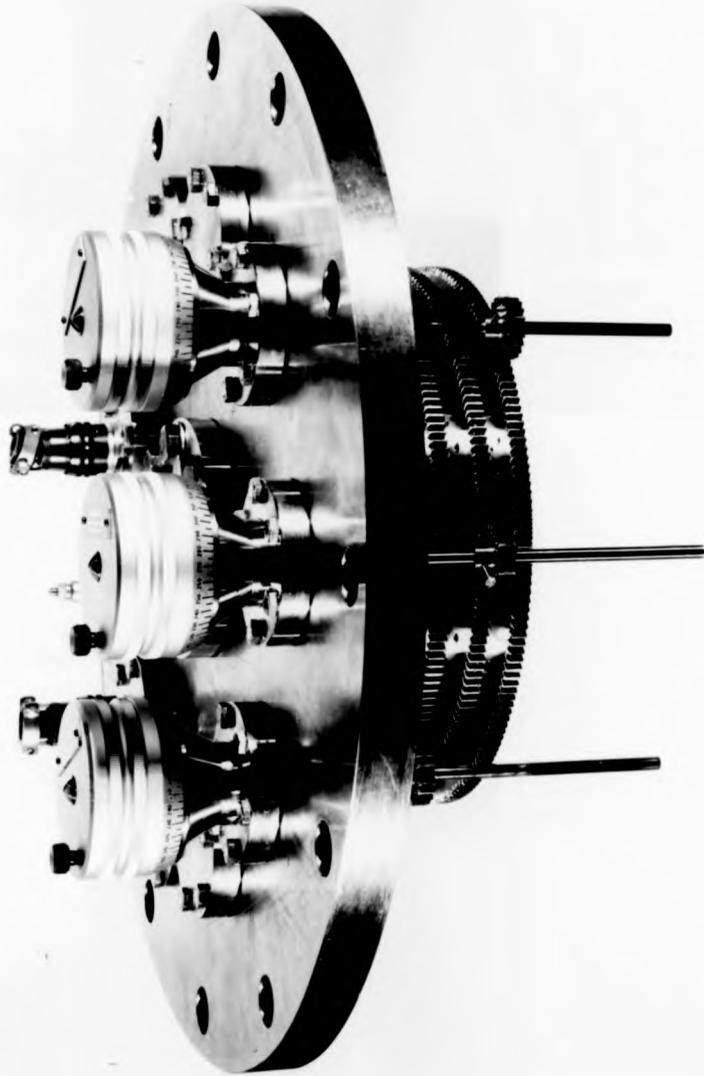
Fig 3.4 The Triple Turntable Assembly

electron gun assembly, 127° electron analyser, photon
multiplier and Faraday cup on the triple turntable assembly
allows the following angular range of measurements:

Electron Gun Assembly	-	Fixed at 0° axis
127° Electron Analyser Assembly	-	-40° to +108°
Photon Multiplier	-	-40° to +122°
Faraday cup	-	±40° from 0° axis.

After calibration of the angular ranges, metal stoppers
were fixed on the table-tops to facilitate finding the
angular locations from outside the vacuum system, and pre-
venting the analyser and photon multiplier from hitting the
electron gun or Faraday cup and disturbing the alignment
of the system.

3.4. Atomic Beam Source

For efficient functioning the beam emerging from the
source should be strongly peaked in the forward direction,
that is, it should be directional, the directionality being
measured by the ratio of the intensity in the forward
direction to the total effusion or by the angular width of
the beam at half intensity points. A simple aperture source
has the disadvantage of a broad cosine distribution of
intensity and therefore it was decided to use a long canal
source for this equipment.

Giordmaine and Wang (1960) carried out a study of beam
formation by long tubes and derived expressions for both the
intensity and the angular distribution for cylindrical tubes
and verified them experimentally. They showed that the peak
intensity and the collimation of the beam are essentially
determined by inter-molecular collision in the tube and the

beam intensities depend on the ratio of the mean free path λ to the radius r and length ℓ of the tube. For the highest directionality the condition $\lambda \gg \ell$ must be satisfied. But under this condition the source pressure is so low that the forward intensity is inadequate for many applications. Use of a multiple capillary tube permits an increase in the allowable pressure without loss of directionality in the source but the beam intensity is correspondingly increased. If the pressure is further increased however, the beam width will also increase along with the total gas flow. At very low pressures, where $\lambda \gg \ell$ and $\lambda \gg r$, we have simple molecular effusion. As the pressure is increased to the point where λ is no longer large compared to the length of the tube, i.e. $\lambda \gg r, \lambda < \ell$, inter-molecular collisions still do not play a significant role and the total flow rate is given by

$$N = \frac{8}{3} \ \frac{r}{\ell} \ \frac{n_0 \bar{\nu}}{4} \ (\pi r^2) \ \text{atoms sec}^{-1}$$

where n_0 is the particle density in the course behind the tube and $\bar{\nu}$ is the average molecular velocity of the particles. However the forward peak intensity $I(\theta = o)$ is now given by (Giordmaine and Wang 1960)

$$I(o) = \frac{1}{2^{\frac{1}{4}} \ 8 \ \delta} \ (\frac{3\bar{\nu}rN}{\pi})^{\frac{1}{2}} \ \text{atoms Sterad sec}^{-1} \qquad (3.1)$$

where δ is the atomic diameter, $\bar{\nu}$ is the average velocity of the atoms in the source.

In the present experiment the tube length was 20 mm with a diameter of 0.5 mm. With a base pressure of 1.5×10^{-7} Torr and the load pressure with gas injected up to 1.4×10^{-6} Torr we can assume that $\lambda \gg r$ and $\lambda < \ell$

and the condition for the applicability of eq. (3.1) was fulfilled.

The average velocity of atoms in the beam is given by (Ramsey 1956)

$$\bar{v} = (\frac{9\pi KT}{8m})^{\frac{1}{2}} = (\frac{9\pi KT \; N_a}{8A})^{\frac{1}{2}} \qquad (3.2)$$

where K is the Boltzmann constant, T is the absolute temperature, m is the mass of the atom, N_a is the Avogadro's number and A is the atomic weight.

The forward peak intensity I at a distance d cm from the aperture is given by eq. (3.1) to be

$$I = I(o)/d^2 = \frac{1}{2^{\frac{1}{2}} \; 8 \; \delta d^2} (\frac{3\bar{v}rN}{\pi})^{\frac{1}{2}} \text{ atoms cm}^{-2} \text{ sec}^{-1} \quad (3.3)$$

When the system is running in an equilibrium state then the effusion rate N in atoms sec^{-1} is related to the pressure P in Torr through the overall pumping speed S_o in litres sec^{-1} by,

$$N = 3.54 \times 10^{19} \; S_o \times P \qquad (3.4)$$

where the numerical factor converts the flow rate in Torr ℓ sec^{-1} into atoms sec^{-1}

In the present experiment helium, krypton and xenon have been studied. As the calculations for finding the beam intensity give only the estimated values, the beam density in the interaction region has been calculated only for xenon and the result should give a rough idea about helium and krypton beam densities too.

For a xenon background pressure of $\sim 1 \times 10^{-6}$ Torr and an overall pumping speed of ~ 3000 ℓ sec^{-1} the flow rate according to eq. (3.4) is given by

$$N = 10.62 \times 10^{16} \text{ atoms sec}^{-1} \tag{3.5}$$

The values of different parameters in eq. (3.3) for xenon are as follows:-

$\delta = 4.93 \times 10^{-8}$ cm (Lew, 1967)

$d = 0.5$ cm

$\bar{v} = 2.54 \times 10^{4}$ cm sec^{-1} (calculated from eq. (3.2)

$r = 0.025$ cm

$N = 10.62 \times 10^{16}$ atoms sec^{-1} (given by eq. (3.5)

Substituting these values in eq. (3.3), the density in the interaction region comes out to be

$$I = 6.82 \times 10^{16} \text{ atoms cm}^{-2} \text{ sec}^{-1}$$

Hence the beam density is given by

$$\rho = \frac{I}{\bar{v}} = 2.69 \times 10^{12} \text{ atoms cm}^{-3}$$

3.5 The Electron Gun Assembly

A multistage high current gun producing a well collimated beam has been designed on the principles described in the literature by Simpson and Kuyatt (1963), Harting and Read (1976). Unipotential guns such as diodes are not capable of saturating a given space below a certain minimum voltage which depends on the beam convergence angle. The maximum current which can be put through a space characterised by its length ℓ and diameter $2r$ or equivalently in terms of convergence angle γ and length ℓ (Fig. 3.5) is set by the repulsive action of the electrons and is given by

$$I = 38.5 \, E^{3/2} \, (\tan \gamma)^2$$

where I is in μ amps if E the electron energy is in volts.
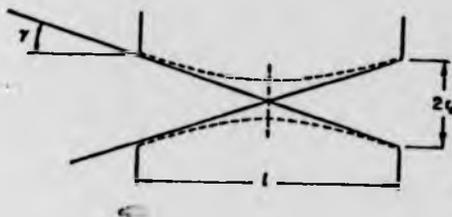
Fig. 3.5 Dashed lines show ideal space charge
          limited beam profile required to
          saturate a given space.

To achieve this upper limit, one has to launch the
electron beam through a hole of diameter $2r_o$ and under an
angle such that in the absence of space charge forces a
crossover would occur in the centre of the volume.

The limitations on the use of unipotential guns are
imposed by,

    (1) Space charge effects, and

    (2) The Helmholtz Lagrange law of (electron) optics.

The multistage principle essentially overcomes these
difficulties by extracting the electrons from the cathode region
at some higher energy to avoid the space charge problem and
then decelerating the electron beam to its final energy.

A schematic layout of the electron gun assembly used is
shown in Fig. 3.6. The gun has two main parts, a triode

FIG. 3.6 Schematic diagram of Electron Gun Assembly.

F – Filament

G – Grid

A – Anode

D-1,D-2,D-3–Deflection plates

W-1,W-2 – Windows

P-1   – Pupil

L-1,L-2,L-3–Einzel lenses

electron gun (extraction stage) formed by a cathode, grid and anode, and a three stage focussing system (deceleration stage) comprising three electrostatic einzel lenses L - 1, L - 2 and L - 3 and three pairs of deflection plates D - 1, D - 2 and D - 3. The diameter and angular extent of the electron beam is best described in terms of windows and pupils. Windows W - 1 and W - 2 define the apertures of lenses L - 1 and L - 3 and the pupil P - 1 defines the angular extent of the rays accepted by the lens L - 2. The deflection plates D - 1, D - 2 and D - 3 are used to correct any misalignment of the electron beam.

The cathode was a directly heated hairpin filament made from tungsten wire 0.1 mm ϕ. Grid and anode, deflection plates and all the elements of the electrostatic lenses were made from 0.1 mm thick molybdenum sheet. Duraluminium was used to make spacers (separator elements) and insulation between electrodes was achieved by 0.1 mm thick PTFE spacers.

The shape of all the elements in the electron gun was rectangular with sides 25 x 50 mm. Keeping in view the height of the 127° electron analyser (62.5 mm) to be used, it was preferable to use the lens system with rectangular slits. The slit widths varied from 0.4 mm to 5 mm and had heights from 0.4 mm to 10 mm.

The elements of the electron gun, einzel lenses, deflection plates and spacers were joined together by a system of three 3 mmϕ ceramic rods which passed through all the elements. The whole assembly was mounted on a PTFE block fixed on a specially made aluminium base on the

triple turntable assembly. The filament could easily be replaced by removing the filament holder from the rear by releasing another PTFE block used as stopper and leaving the rest of the electron gun assembly intact on the turntable.

Electrical connections to all the elements were made through 0.1 mm ϕ stainless steel wires covered with PTFE sleeving except for the filament which was connected through 1 mm ϕ insulated copper wire. All connecting wires were bunched together and after carefully shielding them with copper braiding, were connected to the electrical feedthroughs, 19 pins located inside the vacuum chamber with crimp connectors. The electron gun assembly was then covered with aluminium casing and the portions visible to the interaction region were sooted to avoid reflections of electrons from the metal surfaces.

3.6. The Electron Spectrometer

3.6.1. General

The energy of an electron beam can be described by its most probable value E and the energy spread ΔE. The energy spread ΔE can be defined as the energy between the half maxima points of the electron beam current distribution. This current distribution due to a thermionic cathode emitter can be described by the Maxwell distribution

$$I(E) = I_0 \left(\frac{E}{KT} \right) e^{-E/KT}$$ where I_0 is the total

current, E is the electron energy measured in eV, T is the emitter temperature measured in degrees Kelvin and K is the

Boltzmann constant.   This leads to an energy spread

$$\Delta E = 2.45 \; KT$$

One therefore can expect an energy spread of between 0.2 eV
and 0.6 eV depending on the temperature of the thermionic
emitter used.   In the present experiment, T was estimated
to be $\sim 2000^\circ$K, therefore,

$$\Delta E_{\frac{1}{2}} \simeq 0.45 \; eV$$

The energy spread at high current densities in the electron
beam broadens owing to the space charge effects and the
distribution then does not remain Maxwellian (Simpson and
Kuyatt, 1966).

When better energy resolution is required devices such
as electron monochromators are used, which filter the inci-
dent beam and reduce the half width below that of its
thermionic source.   In the present experiment high resolu-
tion was not required, instead high beam currents were to
be utilized for coincidence measurements.   For this no mono-
chromator was used.   However, in the present study an energy
selector has been used to analyse the scattered electrons.

3.6.2. 127° Electron Analyser

Two types of electrostatic analysers are commonly used
in atomic physics.   They are the 180° spherical and the 127°
cylindrical analysers.   Both are based on the deflection
properties of the electrostatic field established between
two concentric electrodes which deflect the electrons
according to their energies.   By adjusting this electrostatic
field, the desired energy electrons are focussed if the
deflection angle is equal to π radians (180°) for the

spherical analyser and $\frac{\pi}{\sqrt{2}}$ (127°) for the cylindrical one.

Both types of analysers have their advantages and disadvantages. Where the 180° spherical analyser being a double focussing device has better transmission efficiency and better resolving power than that of a 127° cylindrical analyser of the same radius of curvature (Purcell, 1938), it is seriously affected by space charge effects which are more serious than in the 127° analyser (Froitzheim et al. 1975). A 127° analyser has been used in the present experiment for its simpler mechanical design.

The theory of the 127° cylindrical analyser was first developed by Hughes and Rojonsky (1929) who showed that a beam of electrons entering the cylindrical field through a slit and having a small beam divergence α with respect to the slit normal, is focussed at an angle of $\frac{\pi}{\sqrt{2}}$ radians or 127°.17′. Hughes and McMillan (1929) built the first device based on this theory and experimentally found that it could be used as an energy selector. However their design had a rather poor resolution owing to the use of sheet metal for the cylindrical electodes which caused space charge problems. These space charge effects were avoided by Marmet and Kerwin (1960) who replaced the solid cylindrical electrodes by high transparency grids with collector plates behind them. This resulted in the unwanted electrons causing space charge problems, leaving the selector field and being collected by the outer collector plates, at the same time improving the energy resolution by reducing the possibility of undesired electrons passing through the exit slit after metal reflections.

The general transmission function of an analyser is given by

$$\frac{\Delta r}{r_o} = A \frac{\Delta E}{E_o} - B\alpha^2 - C\beta^2$$

where r_o is the radius of the central path of the electrons through the analyser $(r_o = \frac{r_1 + r_2}{2})$, Δr is the slit width of the identical entrance and exit slits, E_o is the mean energy, ΔE, the energy spread measured in terms of full width at half maxima intensity, α is the half angle of angular divergence of the beam in the horizontal plane (Fig. 3.7) and β is the same quantity perpendicular. A, B and C are constants and have different values for various analysers.

For a 127° cylindrical analyser, A = 1, B = 4/3 and C = 1.

The energy resolution for such an analyser is therefore given by (Rudd, 1972) as

$$\frac{\Delta E}{E_o} = \frac{\Delta r}{r_o} + \frac{4}{3} \alpha^2 + \beta^2 \tag{3.6}$$

The effects of α and β can be reduced by a pre-selector injector system. Eq.(3.6) shows that for better resolution the slit widths should be kept small and the analyser should be operated at low energies.

Fig. 3.7 shows the electron trajectories in a 127° cylindrical analyser. The electrons are injected into the space between the two cylinders through the entrance slit S, with an energy $E_o = eV_o$.

The radial field due to potentials V_1 and V_2 at a distance r_o is given by
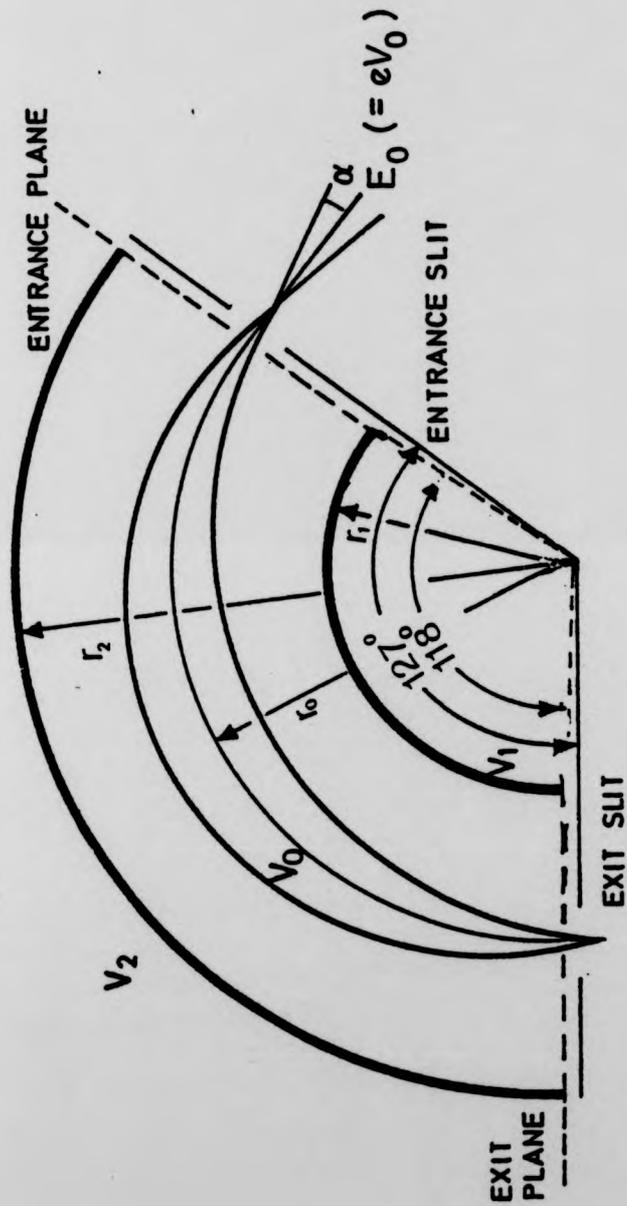
Fig. 3.7 Electron trajectories in a 127° cylindrical analyser

$$E(r) = \frac{1}{r} \frac{V_1 - V_2}{\ln \frac{r_2}{r_1}}$$

where r_1 and r_2 are the radii of the inner and outer cylinders respectively and $r_0 = \frac{r_1 + r_2}{2}$ is the mean radius. An electron emerging perpendicularly from the entrance slit with energy $E_0 = eV_0$ describes a circular path with radius r_0 and is transmitted through the exit when the focussing condition,

$$V = \frac{V_1 - V_2}{2\ln \frac{r_2}{r_1}}$$

is fulfilled. V_0 is the potential at the central orbit and V_1 and V_2 are roughly symmetric with respect to V_0.

It can be shown that the potential at the inner grid is

$$V_1 = V_0 \left\{ 1 + 2\ln \left(\frac{r_0}{r_1} \right) \right\}$$

and that at the outer grid is

$$V_2 = V_0 \left\{ 1 + 2\ln \left(\frac{r_0}{r_2} \right) \right\}$$

The effect of fringing fields at the ends of the electrodes in the region of the slits poses a special problem. The electric fields for which these analysers are designed are considerably distorted at the ends. This field distortion has the effect of slightly changing the position of the focus from 127° to a slighly smaller value, implying that for correct focussing of the electron beam at the exit slit a little bit smaller sector angle than 127° is required. Pavlovic et al. (1972) used a sector angle of 112° and Roy et al. (1975) employed an angle of $121^\circ.6$. A sector angle of 118° was used in designing the present analyser.

3.6.3. Mechanical Design

The 127° Electron Analyser shown in Fig. 3.8 was built along the lines outlined by Mermet and Kerwin (1960). In order to reduce the fringe effects, the total height of the cylinders was increased to 62.5 mm. The other dimensions of the analyser were as follows:-

Radius of the inner grid	=	9.725 mm
Radius of the outer grid	=	14.750 mm
Mean Radius	=	12.238 mm
Radius of the inner collector Plate	=	6.125 mm
Radius of the outer collector Plate	=	20.80 mm
Slit width (Entrance)	=	1 mm
Slit length (Entrance)	=	10.0 mm
Slit width (Exit)	=	0.4 mm
Slit length (Exit)	=	10.0 mm

Immaculate V stainless steel was used for the machined parts of the analyser. The deflection grids were made by spot welding 0.1 mm ϕ tungsten wire 58 mm long, to the stainless steel frame forming inner and outer grids. A uniform gap of 0.05 mm between the wires ensured ∿30% transparency for the grids (Fig. 3.9). Behind these transparent electrodes were placed the solid collector plates which were biased positively with respect to grids so as to collect the electrons which escaped through the grids. The insulation between grids was achieved by four 1.6 mm ϕ ruby balls placed on each grid structure and holding the plates by stainless steel screws passing through ceramic tubes. The analyser assembly was isolated from the input and output slits which formed part of the analyser
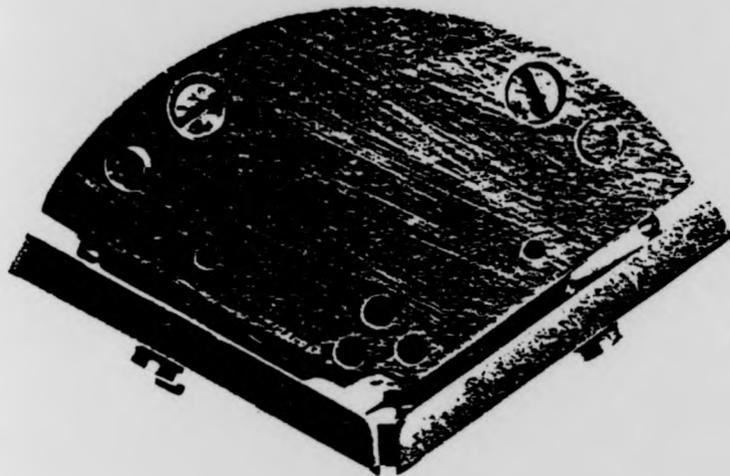
(a)
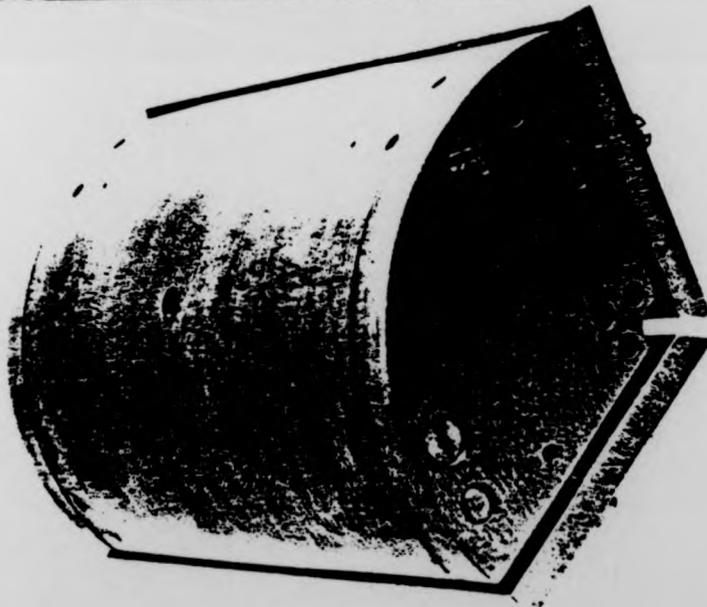
(b)

Fig. 3.8 (a) and (b)
127° Electron energy analyser (a) Top view
(b) Side view.
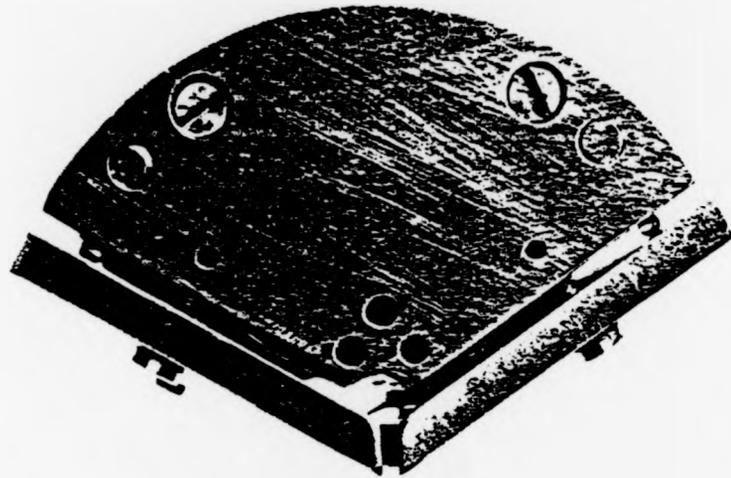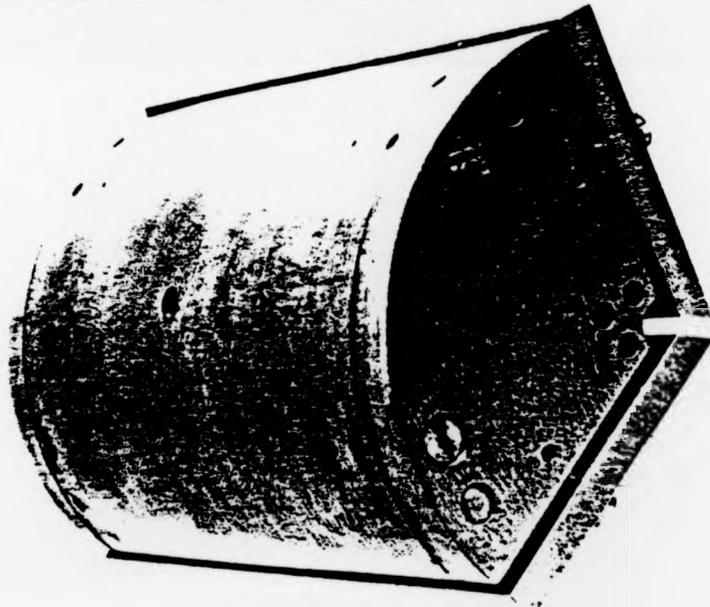
(a)

(b)

Fig. 3.8 (a) and (b)

127° Electron energy analyser (a) Top view (b) Side view.

(a)

(b)
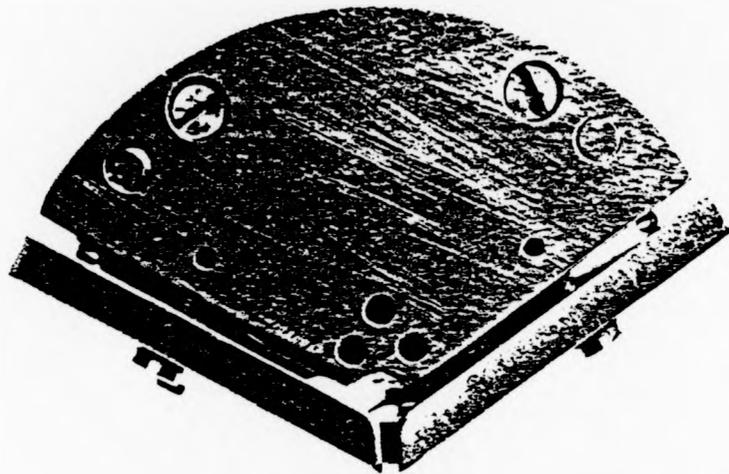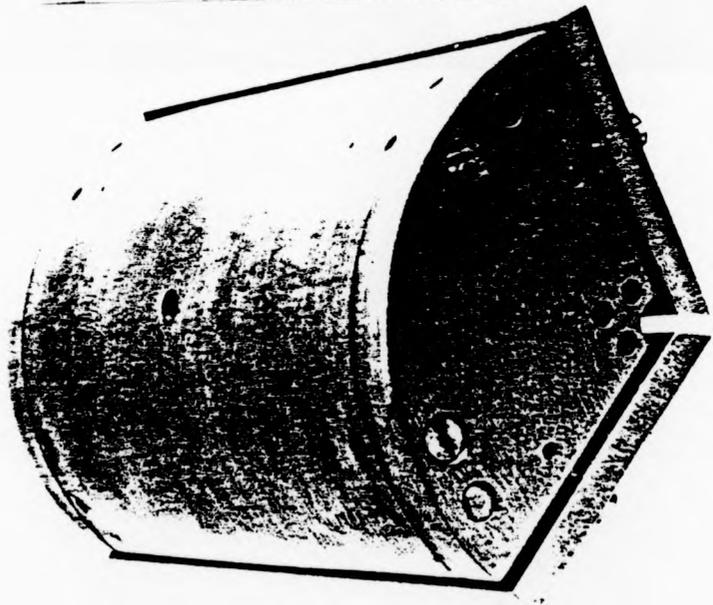
Fig. 3.8 (a) and (b)
127° Electron energy analyser (a) Top view
(b) Side view.

(a)

(b)
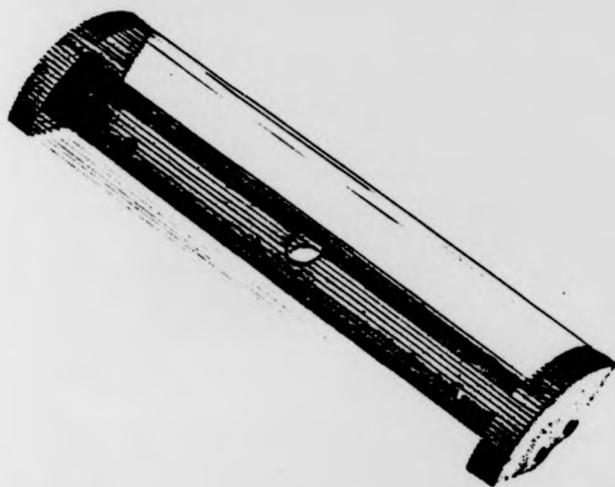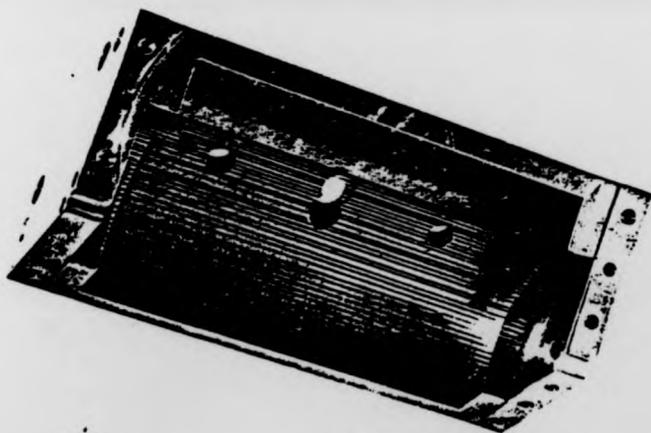
Fig. 3.9 (a) and (b)

127° Electron energy analyser (a) Inner grid
(b) Outer grid.

(a)

(b)
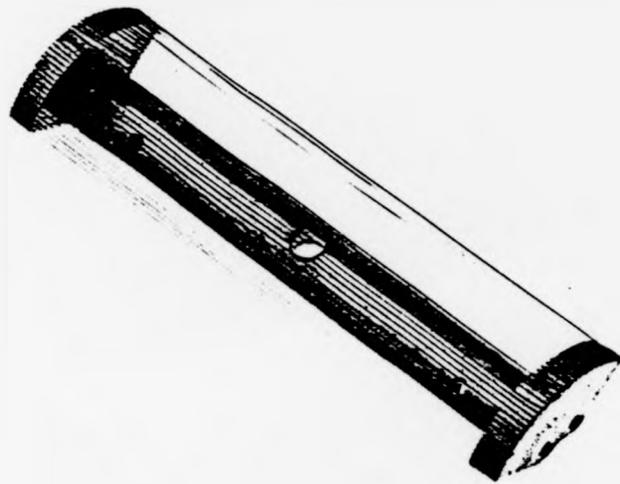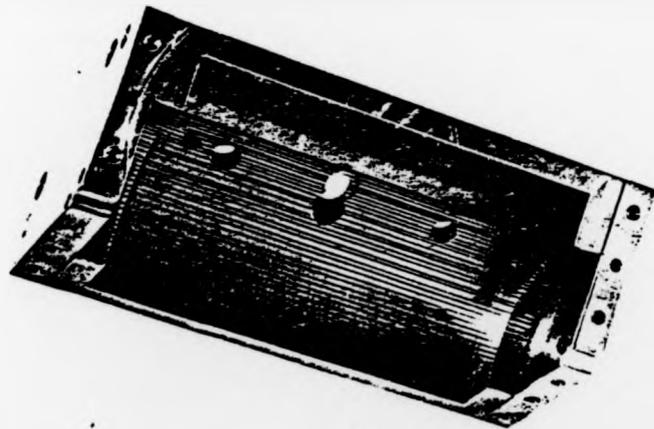
Fig. 3.9 (a) and (b)

127° Electron energy analyser (a) Inner grid
(b) Outer grid.

input optics and the output optics by means of 2.4 mm ϕ ruby balls placed between the optics assemblies and the top and bottom sides of the analyser (Fig. 3.8). The field section (sector angle of the focussing electrodes) was 118° and not 127°, to minimize the effect of fringing field at the input and output planes of the analyser (section 3.6.2).

3.6.4. The Electrostatic Lens System

To reduce the effects of the angular divergence of the electron beam (α and β) on the energy resolution of the analyser, a preselector injector system was designed. The system consisted of one einzel lens, two 2 element electrostatic lenses and two pairs of deflection plates. The material, shapes and sizes of the electrodes, spacers and the deflection plates were similar to those used in the electron gun assembly (Fig. 3.6).

A similar lens system was designed for the analyser exit. The system was formed by one pair of deflection plates and a two element electrostatic lens.

A schematic diagram of the whole analyser assembly is shown in Fig. 3.10. The analyser assembly was mounted to the turntable by placing the input and output optics arms of the analyser on separate PTFE bases fixed on a dura-aluminium base which was attached to the turntable. All electrical connections were made with 0.1 mm ϕ stainless steel wires covered with PTFE sleeving, and spot welded to the electrodes. The wires were bunched together and after carefully shielding with copper braiding, they were terminated at the EFT 19 pins inside the vacuum system. The elements of the input optics and the output optics were

FIG. 3.10 SCHEMATIC DIAGRAM OF ANALYSER ASSEMBLY

covered with aluminium cases and then wrapped with Aluminium foil to close any opening for the stray electron to enter the analyser assembly. To avoid reflection of electrons from metal surfaces, the parts visible to the interaction region were blackened with soot.

The scattered electrons entering the analyser input optics through a 5X1 mm^2 slit aperture, 29 mm away from the centres of interaction region were first accelerated to a high energy by lens L-4. They then passed through an energy changing lens V_4 and a condenser lens (Einzel lens L-5) to the window W_3. The electrons were then decelerated to about 5 eV and focussed on to the analyser entrance slit V_6 by lens L-6. The electrons transmitted through the analyser were then re-accelerated and focussed by means of a 2-element electrostatic lens L-7 on to the input of the channeltron electron multiplier. Any misalignment of the electron beam was corrected by means of pairs of deflection plates D-4, D-5 and D-6.

3.7. Detection of Scattered Electrons

Some of the scattered electrons in the interaction region after passing through the analyser input optics, 127° electron analyser and the analyser output optics were detected by the channel electron multiplier housed in a PTFE block and placed 1 mm from the last slit of the output optics of the analyser. Keeping the channeltron close to the slit ensured that most of the electrons were collected by the channeltron and at the same time prevented stray electrons from entering the CEM.

The high voltage to the channeltron was provided through a filter network $C_2C_3R_2R_3$ connected to the high voltage electrical feedthrough (Vacuum Generator EFT-1). An integrating circuit C_1R_1 was used to shape the electron pulse at the output of the channeltron. A schematic diagram of the integrating circuit and the HT voltage supply to the channeltron is shown in Fig.3.11.

3.8 Detection of Photons

Two types of photon detectors have been used in this experiment. A channel electron multiplier with retarding grids mounted at the channeltron entrance was used for the helium experiment and a UV photon detector Bendix 762 was used for the krypton and xenon measurements.

3.8.1. Channel Electron Multiplier (CEM)

A schematic diagram of the channel electron multiplier (CEM) for the photon detection is shown in Fig. 3.12(a). The channeltron used was a Mullard type B 419 BL/01. Three grids, each made up of four 0.1 mm ϕ tungsten wires (transparency $\simeq$ 90%) were placed in front of the detector and biased to prevent charged particles from entering the CEM. The whole detector assembly was housed inside an aluminium box (Fig. 3.13b) and fixed to a specially made aluminium mount which was attached to the triple turntable assembly. The detector was normally operated at 3200 volts. Because of its low efficiency at wavelengths above 1000 A$^{\circ}$, it was used for the detection of UV photons emitted from decay of 2^1P state of helium radiating photons at 58.45 nm
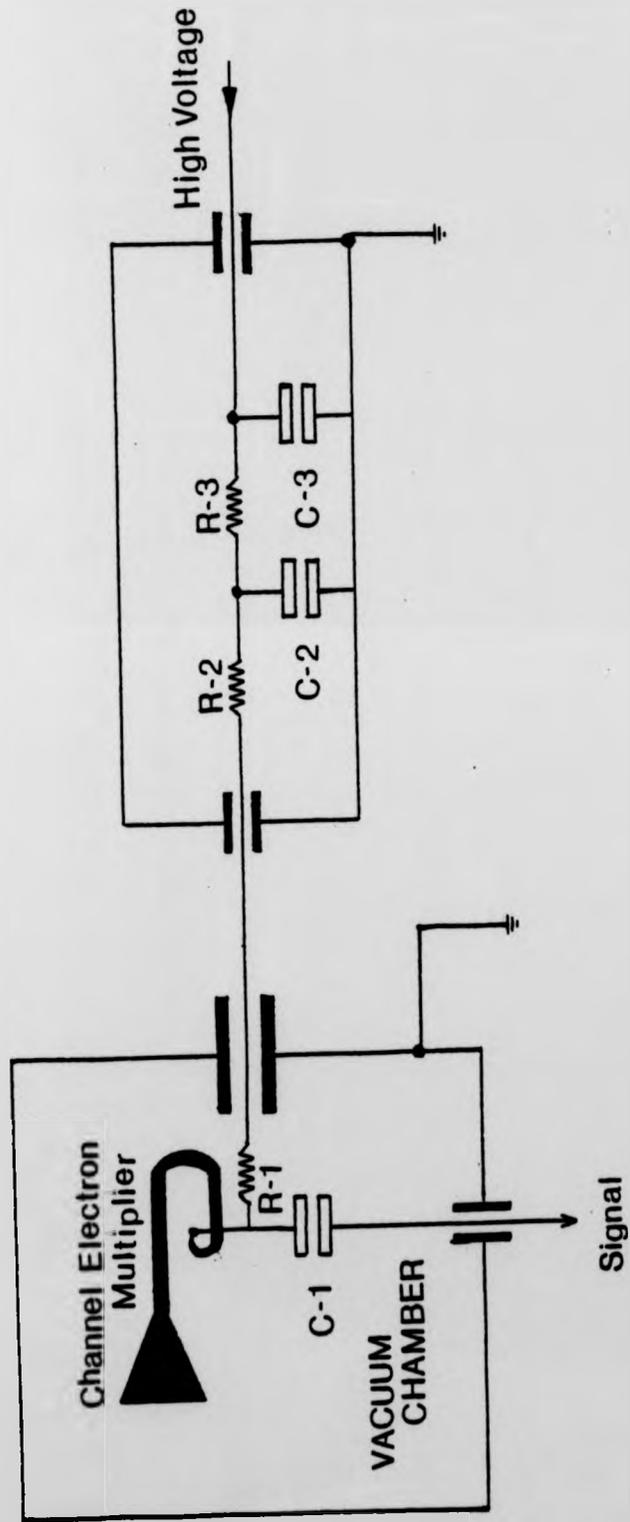
Fig. 3.11: High voltage supply to the channel electron multiplier showing the filter circuit and the pulse shaping integrating network.

(a)
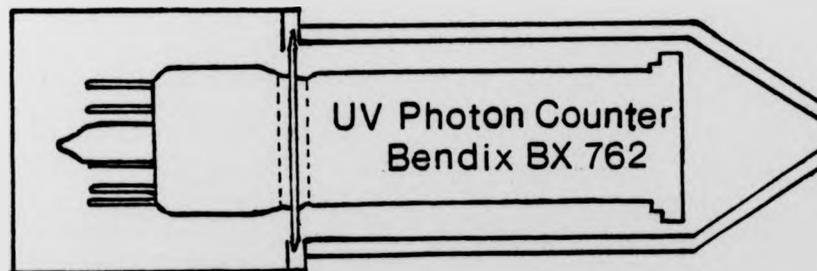
(b)

Fig. 3.12

    (a)   Channel Electron Multiplier with biasing grids used as a photon detector.

    (b)   UV photon counter (Bendix BX 762) used for krypton and xenon.

(a)

(b)
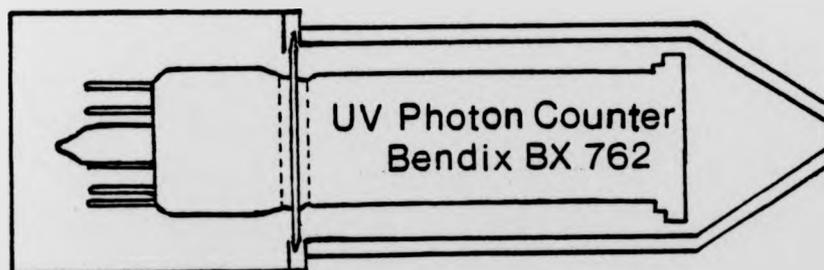
Fig. 3.12

    (a)   Channel Electron Multiplier with biasing
           grids used as a photon detector.

    (b)   UV photon counter (Bendix BX 762) used for
           krypton and xenon.

3.8.2. UV Photon Detector (Bendix BX 762)

A schematic diagram of this photon detector is shown in Fig. 3.12(b). The phototube is equipped with a magnesium fluoride window (Bendix BX 762). The cathode which is funnel shaped, is coated with cesium iodide, and electron multiplication is accomplished by a channeltron. The short wavelenth cut off of the magnesium fluoride window is at 114 nm and on the long wavelength side the quantum efficiency of the cesium iodide photo cathode drops to 0.008% at 200 nm compared with a value of 5% at 150 nm

This photon detector was used for the detection of the UV photons emitted from krypton and xenon. The wavelengths of the radiations emitted from the transitions studied lie between 110 nm and 150 nm.

3.9. The Faraday Cup

The electron beam emerging from the electron gun was collected by a Faraday cup placed opposite to the electron gun assembly. The Faraday cup used in this experiment is shown in Fig. 3.13 (a). The collector is a rectangular piece of molybdenum of size 2 x 13 mm^2 connected to an electrometer (Keithley Model 610 CR) by a screened wire. The electrometer measured the electron beam traversing the interaction region. Three grids were placed in front of the collector which were biased differently. The grid nearest to the interaction region was at ground potential, the middle grid was made slightly negative to absorb any ions present and the third grid was made slightly positive to absorb any secondary emission of electrons.
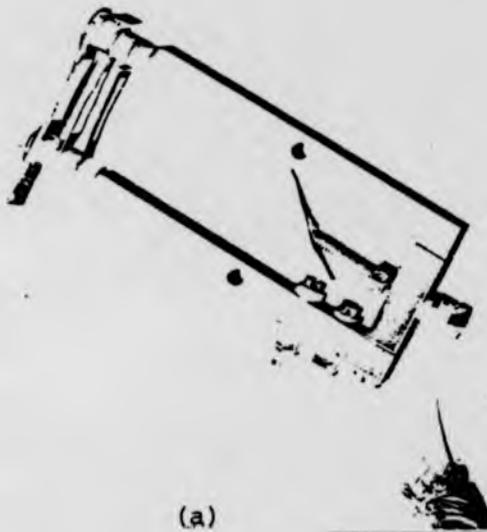
(a)
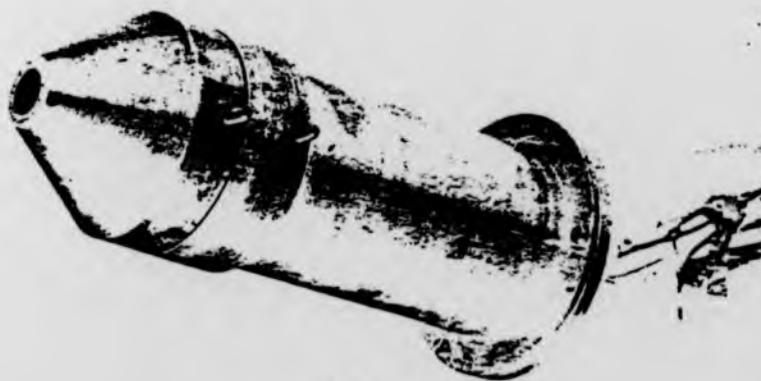
(b)

Fig. 3.13 (a) and (b)

(a) Faraday cup with three biasing appertures
(cover removed)

(b) Aluminium cover for the photon multiplier

(a)

(b)
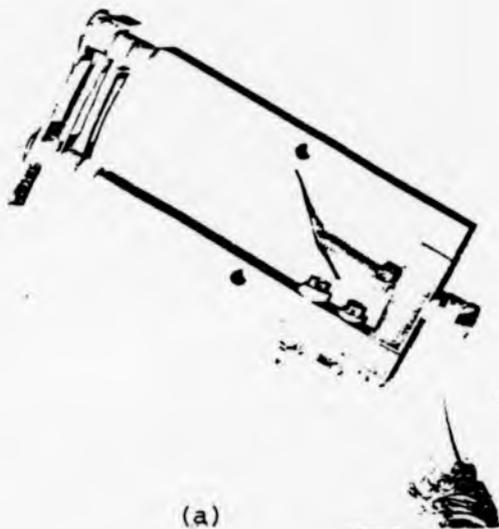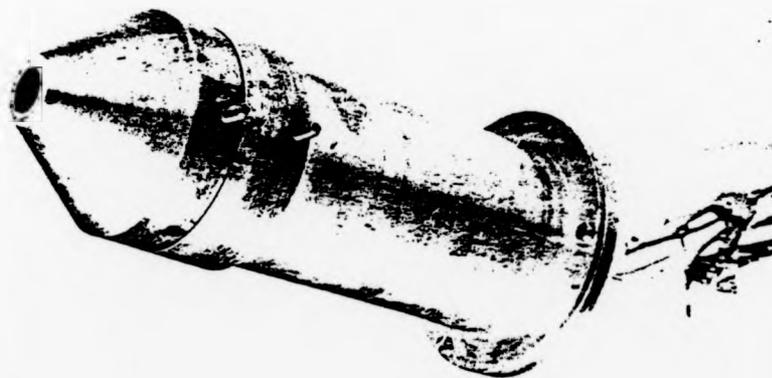
Fig. 3.13 (a) and (b)

(a) Faraday cup with three biasing appertures
   (cover removed)

(b) Aluminium cover for the photon multiplier

The collector and the three biasing grids were all
housed inside an immaculate V stainless steel case at
ground protential. Surfaces visible to the electrons in
the interaction region were sooted to reduce reflection
of electrons from there

3.10   Alignment of Electron Optics and Detection System

In all angular distribution measurements an accurate
alignment of the primary beam source, analyser input optics,
photon detector entrance aperture and Faraday cup is very
important. In view of the large number of electrostatic
lenses used, the alignment had to be checked very carefully.
The procedure followed for the alignment of the system was
as follows:

A stainless steel piece of wire 0.1 mm ϕ was inserted
into the gas nozzle. The target wire was then illuminated
with a torch light and then viewed through the slits against
a bright background of white paper. Alignment was first
checked from the filament side of the electron gun (filament
removed to allow observation through the lens assembly slits)
and the position of the electron gun assembly was adjusted
to a position from where the shining wire was seen exactly
in the centre of the retangular slits of the first and the
last electrodes. Then the Faraday cup aperture was aligned
by viewing straight through the electron gun assembly to the
Faraday cup entrance slit. The electron gun assembly was
correctly aligned to the Faraday cup when the first and the
last slit of the electron gun assembly and the entrance slit
of the Faraday cup were in a straight line intercepting the

wire target in the gas nozzle. The turntable position of
the Faraday cup was noted and the analyser was then placed
in front of the electron gun after moving the Faraday cup
away from the centre. The first slit of the analyser input
optics was viewed through the electron gun slits. The
analyser alignment was completed when the three apertures
coincided. The analyser was then rotated over the full
angular range and when viewed through a hole at the rear of
the analyser, the target wire in the gas nozzle always re-
mained in the centre of the analyser input optics slits.
The photon multiplier housing aperture was then aligned by
viewing through the analyser input optics across the target
wire in the gas nozzle. The position of the photon multiplier
housing was set by viewing the target wire exactly through
the centre of the circular aperture when viewed through the
analyser input optics slits.

3.11 Power Supplies to the System

The arrangements to supply power (at low voltages) to
the various electrodes in the system are shown in Fig. 3-14.
All power supplies used for the system were highly stabilised,
constant dc voltage sources. The variations in the output
voltage of these supplies due to temperature effects over a
period of 24 hours were less than 0.2 mV. Two potential
distribution panels were built each having twelve 10 turn
helipots (100 k Ω, 5W) connected in parallel. The input
to these was taken from separate 0-425 volts power supplies
(Kepco, ABC 425 M). One distribution panel supplied power
voltages to the electron gun assembly and the other to the
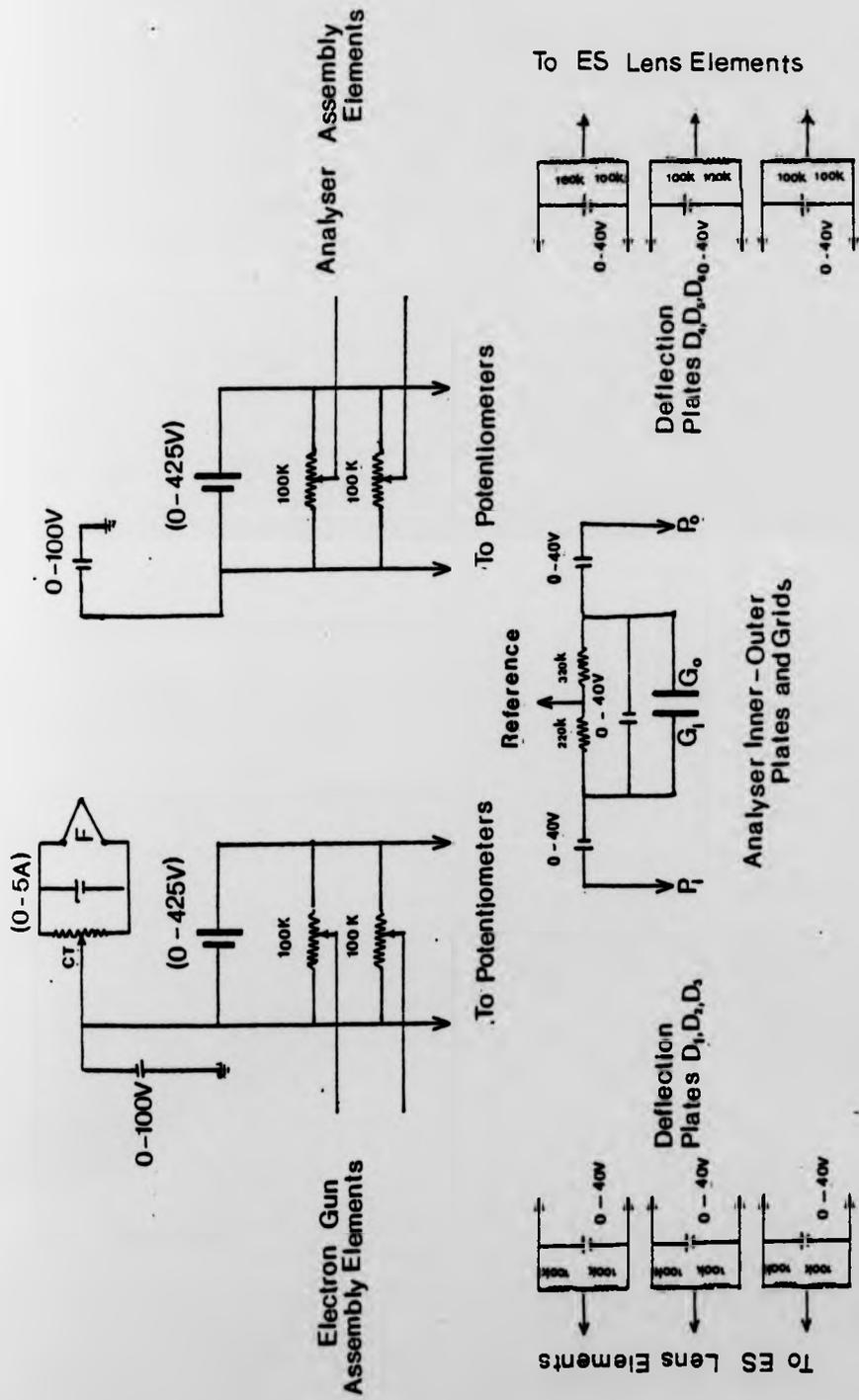
Fig. 3.14:

Schematic layout of the low voltage power supplies for the elements of
Electron Gun Assembly and 1270 electron analyser.

127° electron analyser assembly. All the voltages derived were relative to a separate reference potential for the electron gun and analyser and were biased with separate 0-100 v supplies to off-set these voltages.

The advantage of using such a system of power supplies, which are derived from a single input source, is that any proportionate drift in the voltages would be equally experienced by all the elements involved and hence the ratio of the voltages would remain the same.

The electron gun filament was heated by a separate constant current power supply (5A,20v) built by the Electronics Workshop.

The voltages required for the deflection plates were derived from six separate power supplies. These dc power supplies (0-40 V) were built by the Electronics Workshop to our specifications and have a high stability and low noise performance.

A separate stabalized power supply (0-40 V, Farnell) was used to supply biasing voltages to the grids of the analyser. The inner and outer plates were made $\stackrel{\sim}{\sim}$ 10 V positive with respect to the corresponding grids by another two power supplies (0-40 V).

High voltage power supplies 0-6 kV (Fluke Model 408B) were used to supply HT voltages to the channel electron multiplier and the photon detector.

All the outputs were floating and were applied to the electrodes in the system through screened wires.

Three separate constant current power supplies were used to supply current to the three pairs of Helmholtz coils used for the neutralization of the earths magnetic field

inside the vacuum chamber

3.12 <u>Cancellation of Electric and Magnetic Fields</u>

Stray magnetic or electric fields can disturb the electrons beam considerably in electron scattering experiments. It was therefore necessary to neutralize these fields.

The effect of stray electric fields were reduced by keeping all surfaces exposed to the electron beam in the interaction region at earth potential. To achieve this the last element in the electron gun assembly and the first element of the analyser input optics were placed at earth potential. Similarly the outer grids of the Faraday cup and photon multipliers were also kept at earth potential. This produced a field free interaction region. Insulations between electrodes were achieved by using slightly under-sized 0.1 mm thick PTFE sheet spacers. This prevented them from being seen by the electron beam, thus any chance of an electric field being produced by charging up of the insulators and interfering with the electron beam was eliminated.

Magnetic fields in the interaction region result from the earths field and from the residual magnetization of the steel components used in the system. The static magnetic field in the interaction region was reduced by three mutually perpendicular pairs of Helmholtz coils placed around the scattering chamber. The interaction region was made the centre of all the three sets of coils, which consisted of 50 turns of insulated copper wire wound on duraluminium frames. These coils were finally attached to the scattering chamber and their position so adjusted that the centre of the

coils coincided with the interaction region.

The current for these coils was supplied by three independent constant current supplies. A Hewlett Packard magnetic probe was used to check the field cancellation in the centre of the interaction region and over a radius of 10 cms in the scattering plane, the region in which the electron beam was expected to traverse through the analyser and electrostatic lenses before being detected by the channel electron multiplier. By adjusting the current in the coils, the field was reduced to less than 1 μT in the region.

3.13 Protective System

An interlock system has been designed to ensure safety of operation of the apparatus. Possible breakdown of the electrical supply, compressed air supply and the water supply used for cooling purposes, all lead to the shut down of the diffusion pump. Any such failure causes a steep pressure rise which is detected by the ionization gauge control unit. The ionization gauge control unit is wired to the interlock system through a relay which energises in the event of steep pressure rise and switches off the power supplies used in the apparatus.

The interlock system works in two possible modes. In the first when the system switch is in the 'DAY' position, that is when someone is present in the laboratory, there is a twenty minutes delay in the shut off procedure to enable the person present to carry out any required adjustments without completely switching off the power supplies. In

the second mode, when the system is in the 'NIGHT' position, that is when the apparatus is left unattended any failure causes an immediate shut down of the system. This interlock system has proved very successful on several occasions.

3.14 Suppression of Stray Electrons

Stray electrons pose a serious problem in all electron scattering experiments. Such electrons either leave the electron gun before passing through the final aperture or find their way to the electron detector outside the normal path through the analyser. Great care has been taken in designing the metal spacers for the optics used in this experiment (Fig. 3.6) so that the beam of the electrons moving either in the electron gun assembly or through the analyser and its associated optics, travels in an enclosed path. This special design of the electron optics assemblies reduced the stray electron counts to almost zero. In addition the electron gun and the analyser optics have been covered with cases made of aluminium. The analyser assembly was further wrapped with thin copper foil to ensure covering any possible openings for the stray electrons to enter the detector.

Another source of stray electrons is the small fraction of the primary electron beam which is not collected by the Faraday cup. These electrons reach the analyser after metal reflection and are transmitted, thus causing significant contribution to the background signal. For this reason all metal objects seen by the electron beam while passing through the interaction region to the Faraday cup were covered with soot. The special design of the three aperture Faraday cup

(Fig. 3.13(a)) also helped in reducing the reflected electron component. The electron count rate with the target gas beam switched off was only a few counts per second.

3.15 Suppression of Electrical Pickup

Electrical pickup in the detection system causes spurious counts which must be eliminated. Mains ground loops were such a problem and therefore special attention was given to proper shielding and grounding of all the pieces of the apparatus. Power supply racks, electronic apparatus racks and the stainless steel vacuum chamber were earthed by using thick copper braids. The individual earth leads were terminated at one common point on the vacuum chamber from where a single earth connection was taken to the physical earth point outside the laboratory. This prevented earth loops which often cause spurious signals.

Special attention was given to the siting of the apparatus and all electrical connecting wires were made to cross perpendicularly the existing electrical wiring in the laboratory to prevent pickups due to magnetic field induction.

3.16 The Timing Electronics

A schematic diagram of the timing electronics used for the coincidence measurements is shown in Fig. 3.15.

Pulses from photon and electron detectors are fed into the fast amplifiers (dual bipolar linear amplifier LeCroy Model 333). These amplifiers with an overall gain of 40 db
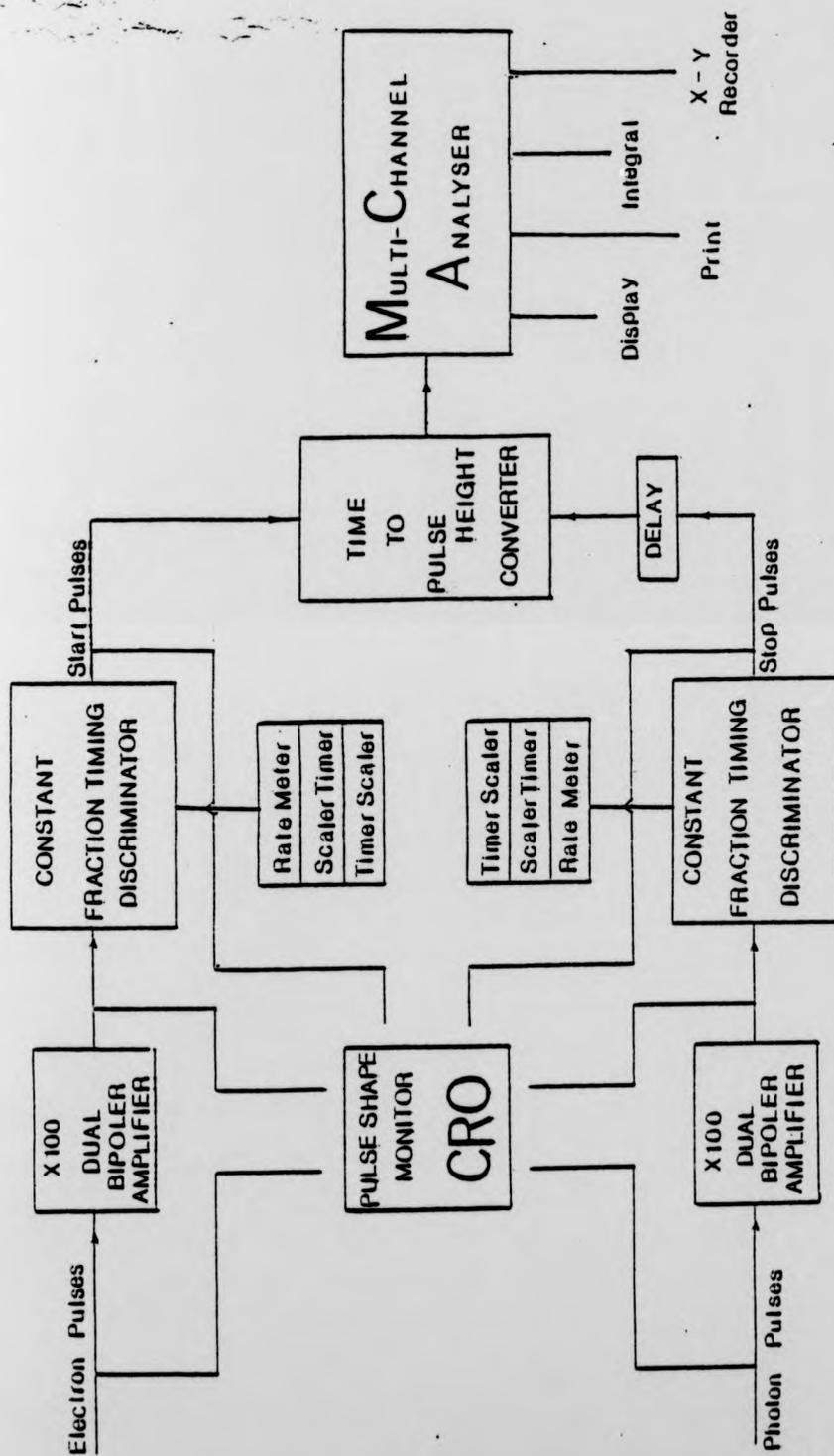
Fig. 3.15

Schematic layout of the timing electronics used for electron-photon angular
correlation measurements.

or 100 times amplification were placed at the shortest possible distance from the vacuum chamber to avoid pick up noise. The amplified pulses from these amplifiers were then fed into constant fraction timing discriminators (ORTEC, Model 473). The electron timing pulses from the constant fraction discriminator provided the start pulses for the Time to Amplitude Convertor (ORTEC, Model 467). For stop pulses, photon timing pulses were used with appropriate delay. The output signal from the Time to Amplitude Convertor (TAC) whose amplitude is proportional to the time difference between the start and stop pulses was connected to a multichannel analyser (NORLAND INO TECH 5300). The Multichannel Analyser allows all the events in a spectrum to be viewed simultaneously.

A cathode Ray oscilloscope (Tetronics, Model 454) was used as a pulse shape monitor. Electron and photon pulse shapes were first viewed direct from detector. A clean pulse showed the correct functioning and efficiency of the detectors. Similarly pulses could be monitored after the amplifiers or Constant fraction discriminators to confirm the correct processing of the pulses and proper functioning of electronics before feeding them into the Time to Pulse Height Convertor and Multichannel Analyser.

3.18 Apparatus for the out of Scattering Plane measurements on krypton and xenon

The apparatus described in the preceding sections was designed and used to study electron-photon angular correlation in the scattering plane only that is, the photon multiplier was rotated in a plane at an azimuthal

angle (ϕ_γ) of 180°. In the light of recent publications
of Blum et al. (1980), Blum and Kleinpoppen (1980), an
attempt has been made to study the spin orbit effects in
the electron impact excitation of krypton and xenon from
the electron-photon angular correlation measurements. In
order to extract the parameters λ, $\cos\bar{\chi}$ and $\cos \epsilon$ of the
excited atomic states as outlined by these authors for
the heavy atoms, out of the scattering plane measurements
have also been carried out for krypton and xenon. These
measurements have been taken with the apparatus initially
built by Eminyan et al. (1974) which has now been modified
to allow electron-photon angular correlation measurements
to be made at an azimuthal angle of 135° in addition to
the usual scattering plane measurements.

A schematic layout of the apparatus is given in
Fig. 3.16. The main parts of the apparatus are, a 127°
cylindrical electrostatic monochromator, a 127° electron
analyser with associated electron optics, atomic beam
source and a photon detector all housed within a vacuum
chamber.
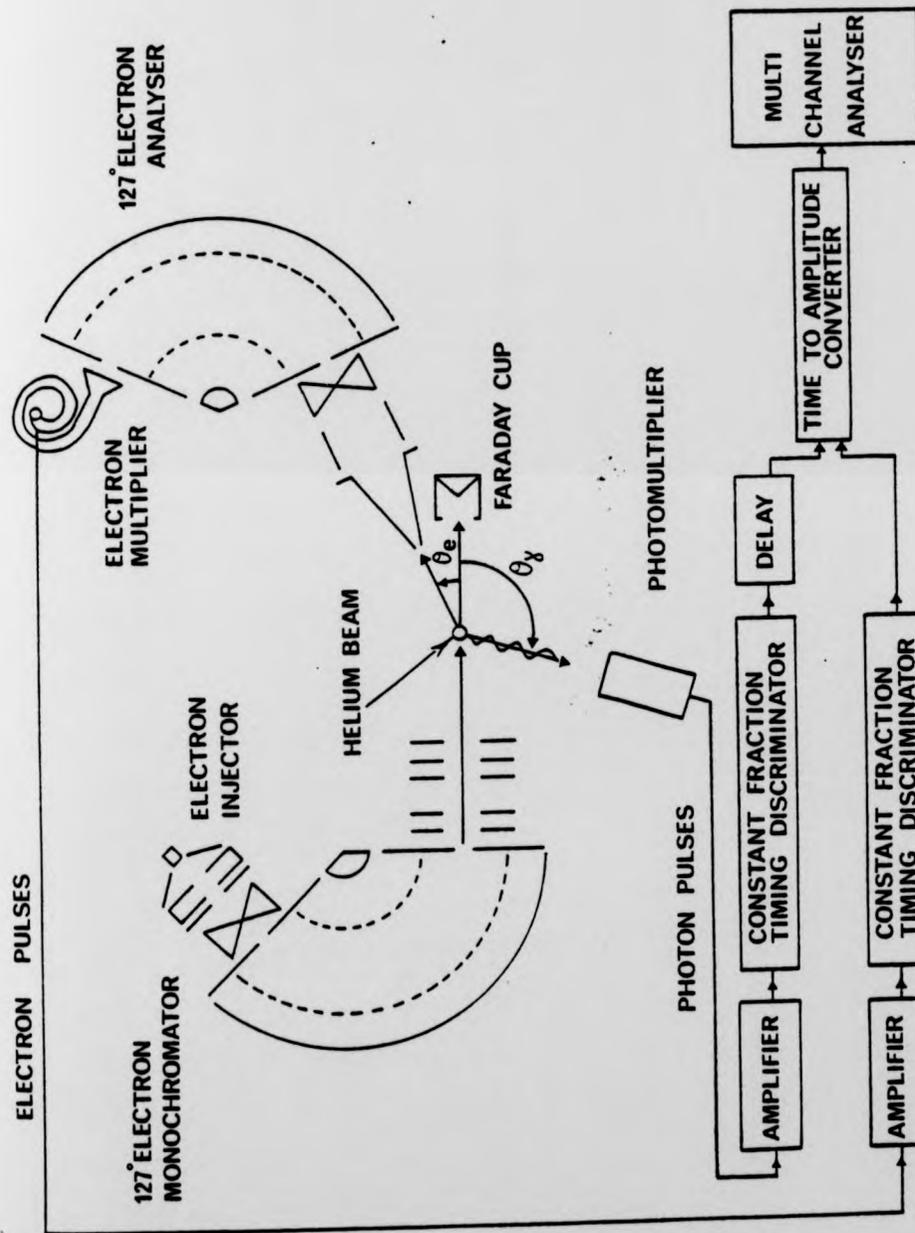
Fig. 3.17 Apparatus used for out of the scattering plane measurements on krypton and xenon

4 - VALIDATION OF MEASUREMENTS

4.1 General

After the design and completion of the apparatus, it was then necessary to ensure that the individual parts of the apparatus were functioning satisfactorily. The operation of the electron gun, the performance of the electron optical elements in the electron gun assembly, the focussing of the primary electron beam in the Faraday cup, the functioning of the analyser and analyser input and output optics and the operation of the photon multipliers were all first tested individually and then as a unit. For the measurements of the 2^1P state of helium, a channel electron multiplier with three biasing grids and for krypton and xenon an UV photon multiplier (Bendix 762) were used to collect photons.

Initially many difficulties were faced in making the apparatus work. Due to the use of very thin PTFE insulators (0.1 mm thick) for the isolation of the electrodes (Fig. 3.6), there were electrical shorts, charging up of PTFE spacers and current leakage problems. These problems were overcome by making the size of the PTFE insulators slightly smaller than the aluminium spacers and removing all the extra bits of carbon soot which was used to reduce the reflection of electrons from shining metal surfaces. Rounding one side top corner of the aluminium spacers to make room for spot welding electrical connections to the electrodes eliminated the risk of shorts due to the tight holding of the elements

by the three ceramic rods passing through all elements of
the electron gun and analyser optics.

In the design of the electron optics, the distances
between the lens elements were calculated approximately
following the guidelines given in various texts and publi-
cations (e.g. Kuyatt and Simpson 1963, 1968, Klemperer and
Barnett (1971), Harting and Read (1976), P Grivet (1972).
The exact working voltages were found by experience, and
optimization of the applied voltages was achieved by monitor-
ing the transmitted current for the best performance. The
electron beam current was monitored by a Keithley electrometer
at various isolated electrodes. The electrostatic lens
performance was monitored at the windows and pupil planes
by isolated electrodes.

In the following sections, certain tests and procedures
are described which were carried out on the apparatus for
checking the validity of measurements.

4.2 Focussing and Angular Distribution of Electron Beam

4.2.1. Electron Gun Assembly

During the initial operation of the electron gun, the
electron beam current detected in the Faraday cup was small.
The Faraday cup was placed 20 mm away from the interaction
region. The alignment of the electron gun assembly was then
checked and the position of the Faraday cup was adjusted to
place it exactly at the geometrical centre of the line of
electron gun assembly slits passing through the centre of
the gas nozzle in the interaction region. The voltages
applied to the lens elements were then optimized by

monitoring the 80 eV electron beam simultaneously at electrodes W-1, P-1 and W-2 (Fig. 3.6) and focussing the beam on to the Faraday cup. The electron beam current measured at the collector of the Faraday cup, which was biased + 100 V with respect to ground, was approximately 8.5 μA. The focussing of the primary electron beam current was then checked. For this the focussed beam was also measured at the slit C, 1.5 mm wide (one nearest to the collector as shown in Fig. 4.1). The measured current was 0.45 μA. This gave a current ratio of $\frac{8.5 \ \mu A}{0.45 \ \mu A} \simeq \frac{20}{1}$ for the currents received at the Faraday cup collector and the smallest visible slit of the grid C. This result indicated that the focussing of the primary electron beam was satisfactory.
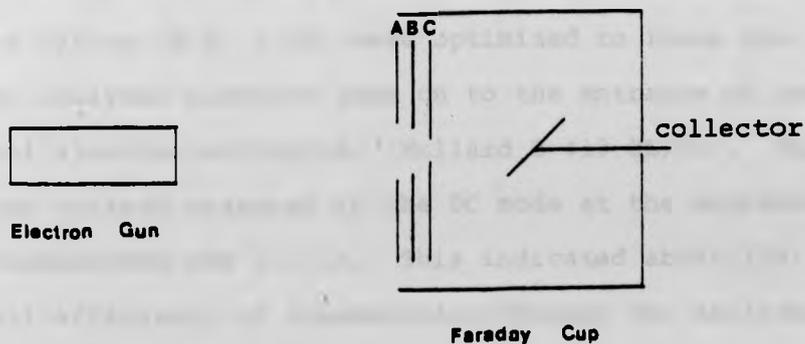
Fig. 4.1   Slit apertures and the collector of
the Faraday cup

4.2.2. 127° Electron Analyser Assembly

After noting the 0° position of the Faraday cup on the turntable, the Faraday cup was moved aside and the analyser was brought in front of the electron gun. Keeping the retarding potential at zero volts, the electron beam was monitored at electrode W-3 (Fig. 3.10) of the analyser input optics. With the help of lenses L-4, L-5 and the deflection plates D-3, the electron beam was focussed at W-3. The electron beam was then monitored at the outre plate/outre grid of the analyser which were joined together and biased + 50 V with respect to ground. 3μ Amps of current was measured in the electrometer verifying that the analyser input optics were functioning correctly.

The analyser was then tuned to pass electrons having 20 eV energy to operate in a broad resolution mode so as to allow a large number of electrons to be transmitted. The voltages applied to the elements of the analyser input and output optics (Fig. 3.10) were optimized to focus the energy analysed electron beam on to the entrance of the channel electron multiplier (Mullard B 419 BL/01). The maximum current measured in the DC mode at the entrance to the channeltron was 1.1 µA. This indicated about 12% overall efficiency of transmission through the analyser.

An angular scan of the primary beam current transmitted through the analyser was then made and the resulting current versus angle graph is shown in Fig. 4.2. The full width at half maximum (FWHM) of $\sim$ 1 degree indicated a satisfactory performance of the electron gun assembly optics.

The analyser was then placed at a 30° scattering angle.
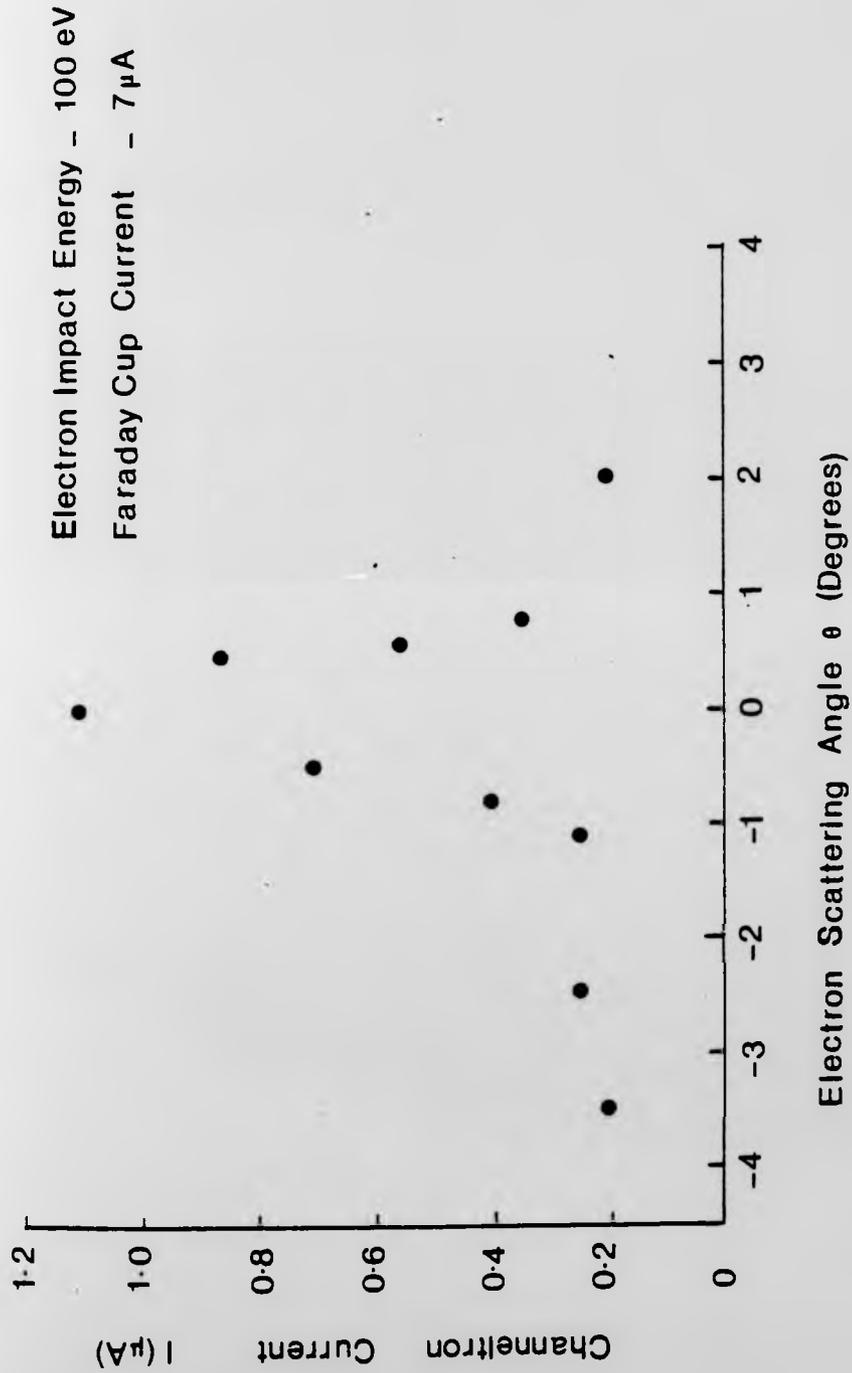
Fig. 4.2:

Angular distribution of the electron beam through 127° electron analyser assembly.

The channeltron was connected to the pulse counting electronics and the electron pulses, after X100 amplication through a bipolar amplifier (LeCroy 333), were monitored with a ratemeter at a rate of $\approx$ 1500 cps. The analyser was scanned through an angular range from 30° to 90° over which the measured count rate from elastic scattering by background gas remained about the same ($\approx$ 1500 c.p.s.) independent of whether the primary beam was collected in the Faraday cup or dumped in the chamber. This implied that there were no reflected electrons picked up by the analyser in the vacuum chamber.

4.3 Photon Angular Distribution

The performance of the photon multipliers was checked by studying the anisotropic behaviour of the emitted radiation. Counts were measured as a function of the photon scattering angle θ_γ. Fig. 4.3 shows the results obtained for the photon multiplier (CEM with three biasing grids) used for helium and Fig. 4.4 shows the corresponding results for the UV photon multiplier (Bendix 762) used in the case of krypton and xenon. The observed values in the case of helium are compared with the expected values for the polarized and the non-polarized radiation measurements. The measured photon distributions show the anisotropic behaviour of emitted radiations during the de-excitation process.

4.4 Differential Linearity Test on Time to Pulse Height Convertor

Differential linearity of the Time to Pulse Height Convertor and SCA (ORTEC Model 467) was tested with the
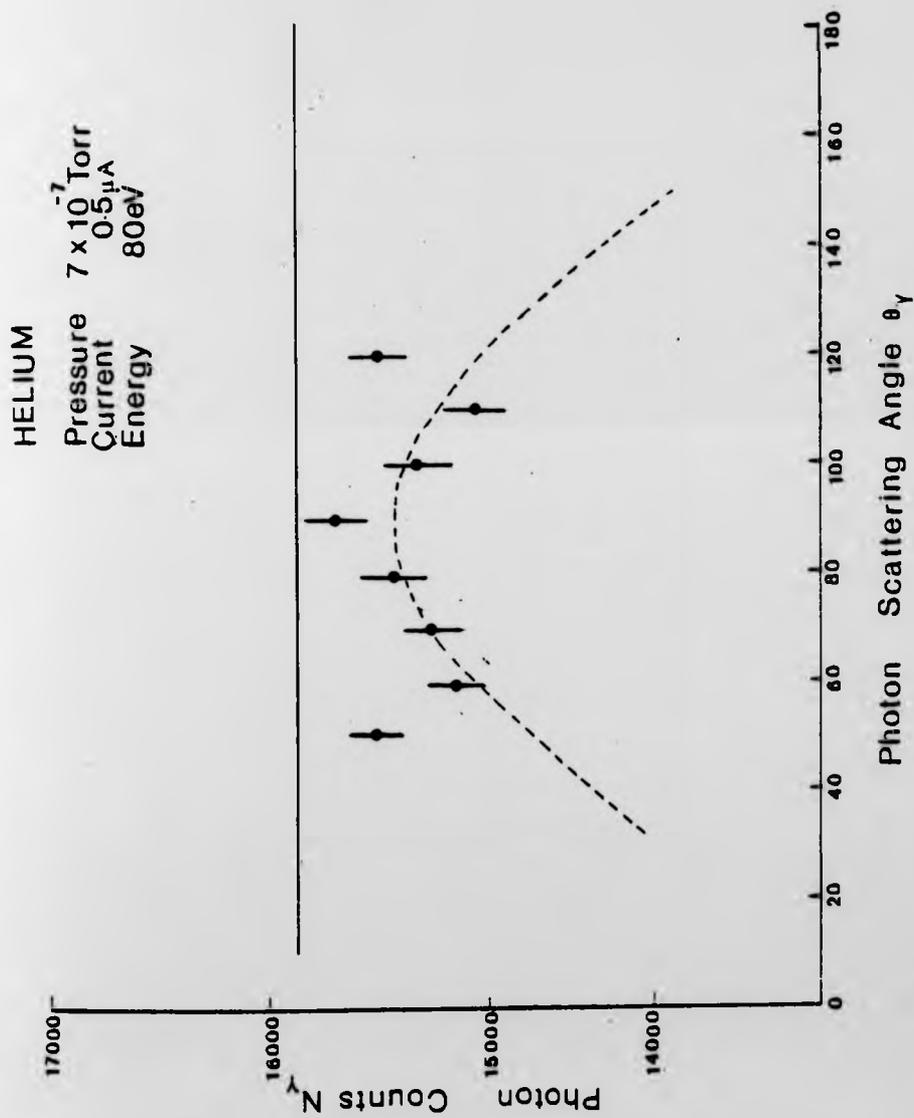
Fig. 4.3 Angular distribution and photons emitted from 2^1P state of helium compared with different polarization conditions.

ϕ, Experimental; ----, Ideal polarized beam (Anisotropic); ———, Ideal non polarized beam (Isotropic).

Fig. 4.3 Angular distribution and photons emitted from 2^1P state of helium compared with different polarization conditions.

$\bullet$, Experimental; -----, Ideal polarized beam (Anisotropic); ———, Ideal non polarized beam (Isotropic).
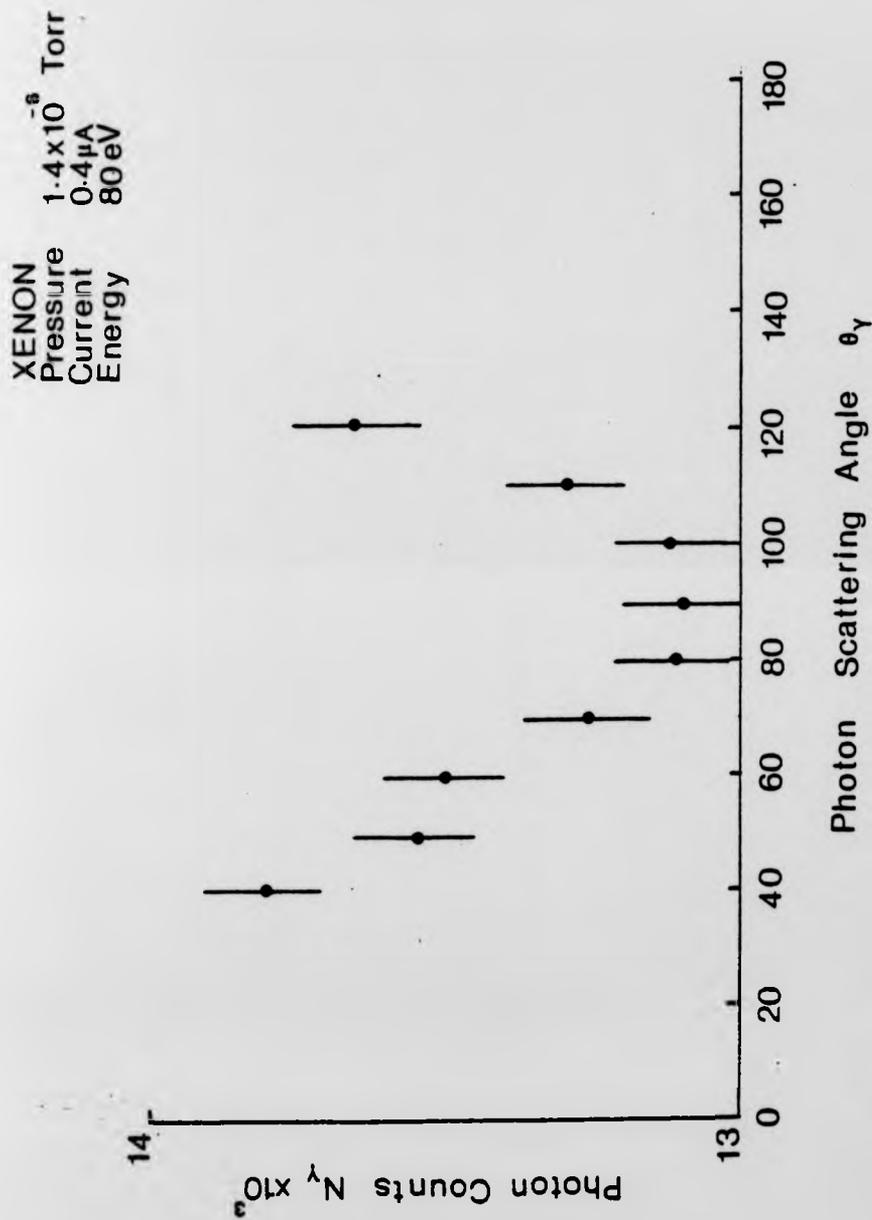
Fig. 4.4:
Angular distribution of photons emitted from $5p^5 6s$ $^3P_1$ state of xenon. Error bars indicate ±1 standard deviation. (For more details on angular distribution of photons see Al Shamma 1978).

help of the system shown schematically in block form in
Fig. 4.5. In this test the start signals were taken from
the electron pulses which provide a random spectrum of
pulses. A pulse generator at a fixed count rate was used
to provide the stop signals. The measurable time interval
between a start and a stop due to the random nature of the
electron pulses, takes on all values and should result in
a flat baseline on the sreen of the Multichannel Analyser,
i.e. for an infinite number of Time to Pulse Height Convertor
outputs the count level for each channel of the MCA should
be equal. In the present test the output pulses were
accumulated over a period of twelve hours. The spectrum as
seen on the Multichannel Analyser had 5000 ± 70 counts per
channel showing that the count level for each channel of
the multichannel analyser was equal within the limits of
the statistical fluctuations. It was concluded that the
Time to Pulse Height Convertor was functioning correctly.

4.5 Pulse Shaping

To optimize the electron and photon pulse shapes in the
present experiment, a pulse generator (Phillips PM 5775) was
used to generate a pulse of $\sim$ 10 ns duration and 40 mV
amplitude closely simulating a channeltron pulse. This
pulse was coupled into the R.C network at the end of the
channeltron (shown in Fig. 3.11). Optimization was achieved
by varying the integrator circuit at the end of a 5 meter
long cable from the signals feedthrough (Vacuum Generator
EFT 20) at the vacuum flange. The value of R C was chosen
so as to produce a clean electron pulse with little or no
ringing.
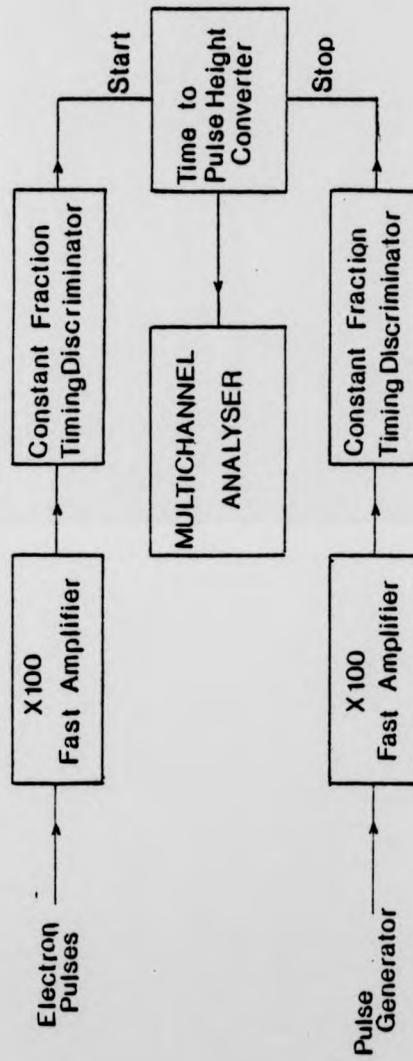
Fig. 4.5:

Schematic layout of the apparatus for the differential linearity test on Time to Pulse Height Convertor.

Fig. 4.6 (a)

Electron pulse from the channel electron
multiplier viewed in the oscilloscope before
amplification.
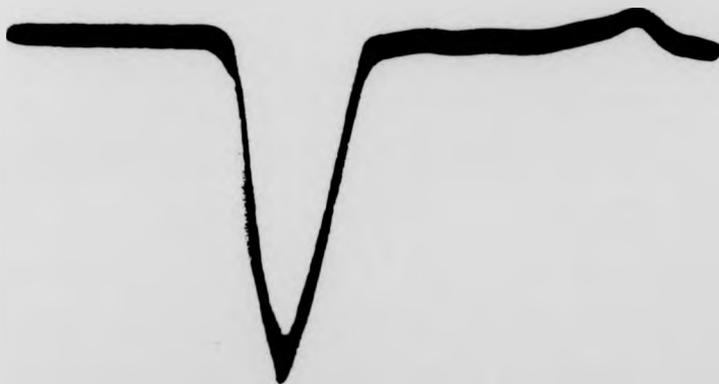
Fig. 4.6 (b)

Photon pulse from the UV photon counter
(Bendix 762) viewed in the oscilloscope
before amplification.

With a new channeltron the maximum amplitude of the pulse without amplification was measured to be 50 mV for the photon multiplier and 40 mV for the channel electron multiplier. Typical photon and electron pulses are shown in Fig. 4.6(a) and (b) respectively.

4.6 Checking the Effect of Variation of the Magnetic Field in the Scattering Plane

Due to the fact that in the present experiment the analyser is rotated over a diameter of about 20 cms in the scattering plane, there is always a possibility that non-uniformities in the earth's residual magnetic field affect the motion of the electron beam in such a way that the mirror symmetry ($\pm \theta$ symmetry) of the scattering processes can be disturbed.

To test for this possibility the inelastic electron scattered counts were measured on both sides of the zero degree axis. Within experimental errors, equal numbers of electron counts were measured at $\pm 20^{\circ}$ and $\pm 30^{\circ}$ scattering angles. This showed that the magnetic field was compensated sufficiently well so as to not affect the experimental results.

4.7 Resolution of the Electron Gun-Analyser System

After checking the performance of the electron gun assembly and the 127° electron analyser individually, the performance of the system as a whole was tested by measuring its energy resolution. For this the analyser was tuned to 80 eV electrons. The electrons transmitted through the analyser, operating at an energy of 5 eV, were

detected by the channel electron multiplier, and the elastic spectrum was obtained on the multichannel analyser, in its multichannel scaling mode, by scanning the reference voltage of the analyser with the ramp voltage supplied by MCA.

An elastic spectrum taken at an electron scattering angle of 30° is shown in Fig. 4.7(a). The resolution of the analyser is obtained by measuring the FWHM of the elastic peak thus obtained. This gives a resolution of 0.45 eV which was considered to be sufficient to resolve the states of interest for the present experiment in helium, krypton and xenon.

4.8   Energy Loss Spectra He, Kr, Xe

Keeping the incident electron energy fixed at 80 eV, the analyser was tuned to accept 58.8 eV electrons so as to transmit the scattered electrons which had excited the helium atoms and suffered an energy loss of 21.2 eV. The helium gas was then injected and an energy loss spectrum was obtained. By varying the retarding potential at the analyser entrance slit or the potential difference between the inner and outer grids of the analyser, a check was made with the ratemeter that the count rate varied with the energy of the electrons. An energy loss spectrum taken at an electron scattering angle of 30° is shown in Fig. 4.7 (b). The spectrum shows two peaks, one corresponding to the unresolved 2^1P 2^3P signals and the other to the 2^3S signals. In the first phase of the experiment the 2^1P state (which decays by the emission of 58.4 nm photons) was studied.

TIME 000000 CUR 0000=000000

(a)

2^1P2^3P

2^3S

TIME 000000 CUR 0000=000000
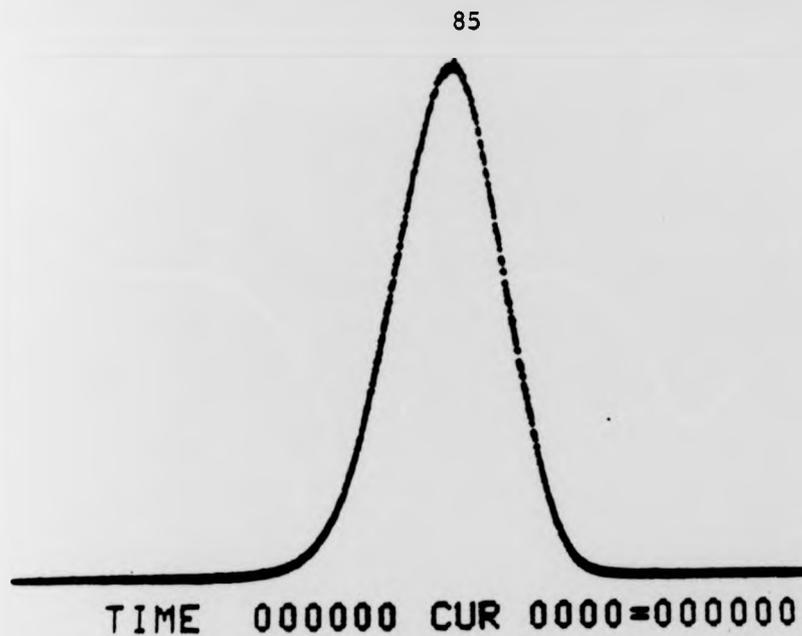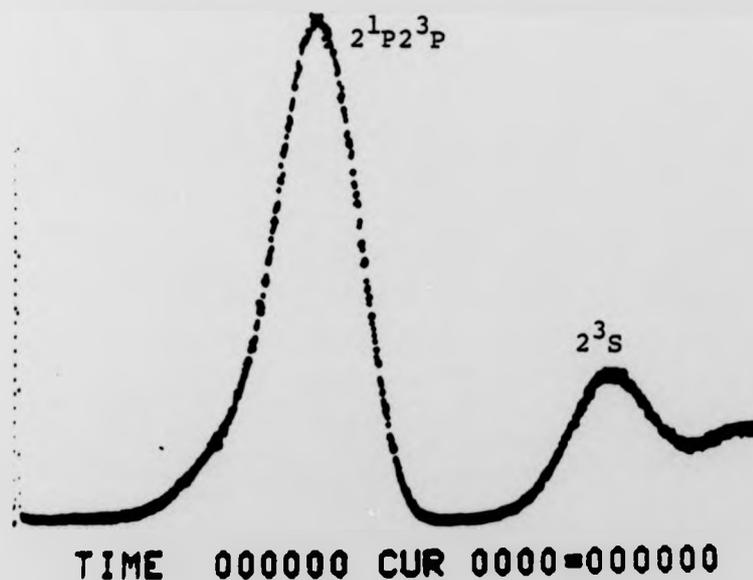
(b)

Fig. 4.7 (a) and (b):

(a) A typical elastic spectrum taken at an
    electron scattering angle of 30° with
    helium pressure = 5 x 10⁻⁷ Torrs, incident
    electron energy 80 eV and Faraday cup
    current 1.0 μA.

(b) Energy loss spectra of helium obtained
    with the experimental conditions as in
    Fig. 4.7(a).

Similarly energy loss spectra for krypton and xenon were obtained by tuning the analyser to accept those scattered electrons which had excited the krypton and xenon atoms and suffered an energy loss of 10.1 eV and 8.44 eV respectively.

The energy loss spectra of krypton is shown in Fig. 4.8 (a) and (b). The two spectra, the second extending the energy scan of the first, show a series of peaks corresponding to different energy levels of the excited states. The energy scale was calibrated with reference to the elastic peak occurring at zero energy loss. Sharp features are observed at energies 10.1, 10.7, 12.4 and 13.1 eV. The energy positions of these features are in good agreement with the energy levels of Moore (1952) at 10.03, 10.64, 12.35 and 13.0 eV respectively,

The energy loss spectra of xenon is shown in Fig. 4.9 (a) and (b). Both the spectra, the second extending the energy scan of the first as before, show a series of peaks corresponding to different energy levels of the excited states. The energy scale was again calibrated with reference to the elastic peak occurring at zero energy loss. Sharp features are observed at 8.4, 9.6, 11.0 and 12.4 eV which are in good agreement with the energy levels of Moore (1958) at 8.43, 9.56, 10.95 and 12.45 eV respectively.

The schematic energy level diagrams for helium, krypton and xenon as given in Candler (1964) are shown in Figs. 4.10 and 4.11 (a) and (b) respectively.

From the energy loss spectra of He, Kr and Xe, it is apparent that many states can be resolved with the present system without using a monochromator. The 2^1P state of

TIME 000040 CUR 0000=000040

(a)

TIME 000032 CUR 0000=000032
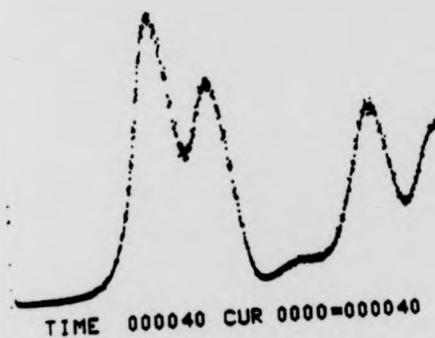
(b)

Fig. 4.8 (a) and (b):

Typical energy loss spectra of krypton
taken at an electron scattering angle
of 20°. Incident electron energy 80 eV
and the Faraday cup current 0.5 μA.

TIME   000000 CUR 0000=000000

(a)

TIME   000000 CUR 0000=000000
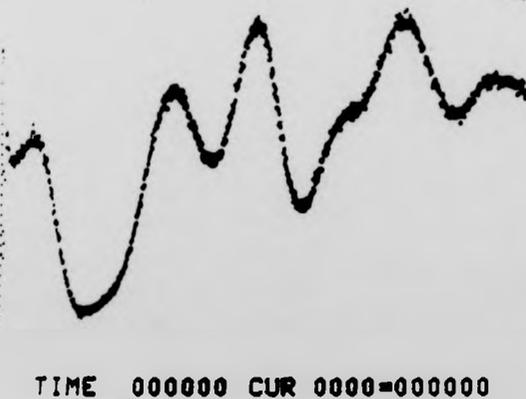
(b)

Fig. 4.9 (a) and (b):

Typical energy loss spectra of xenon
taken at an electron scattering angle
of 30°. Incident electron energy 30 eV
and the Faraday cup current 0.5 µA.
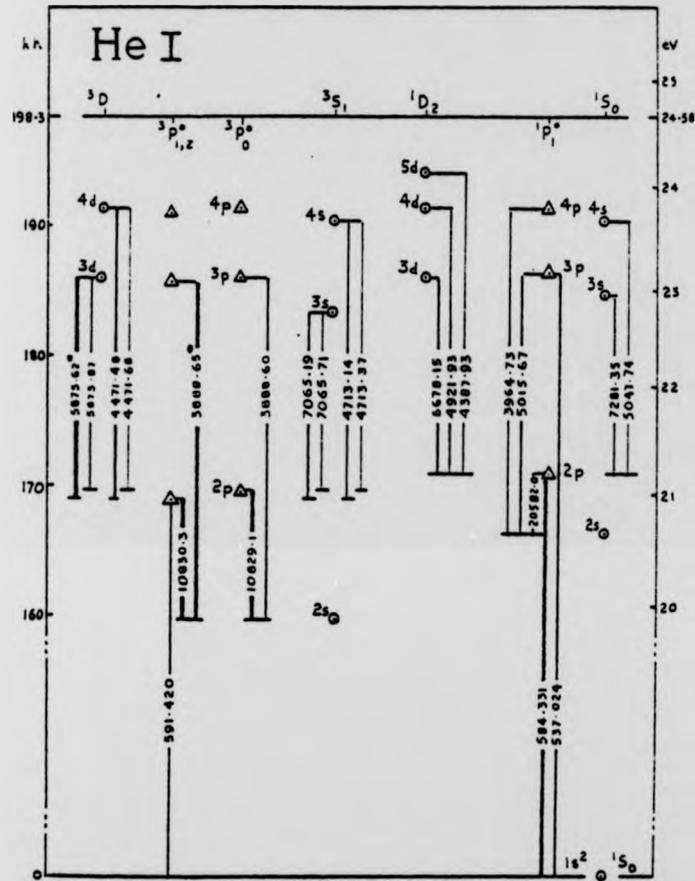
Fig. 4.10:   Energy level diagram for He.
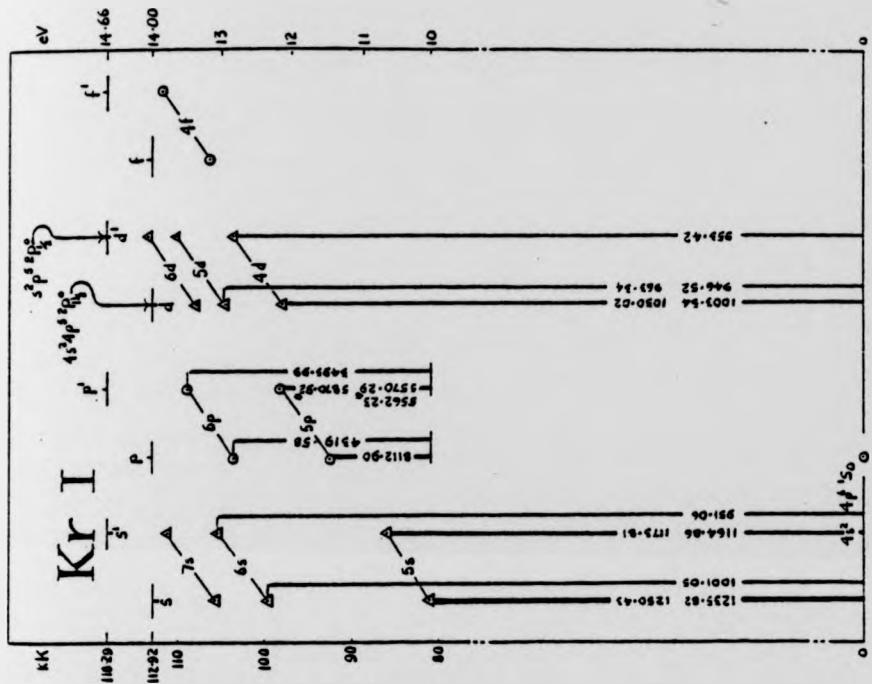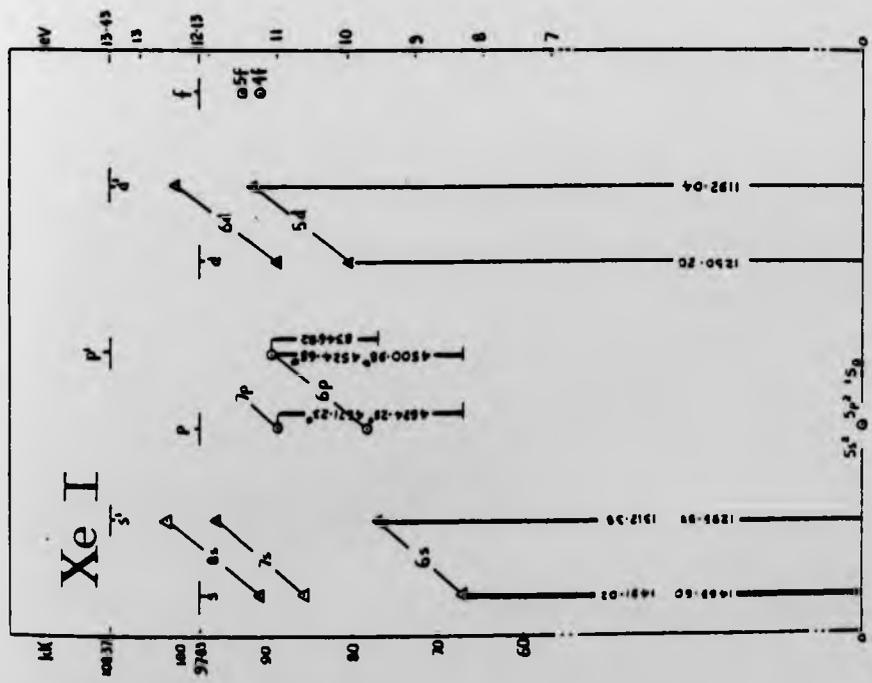
Fig. 4.11 (a) and (b): Energy level diagrams for Xe and Kr.

helium, the $4p^5(^2P_{3/2})5s$ $J = 1$, $4p^5(^2P_{\frac{1}{2}})5s$ $J = 1$ states
of krypton and $5p^5(^2P_{3/2})6s$ $J = 1$ state of xenon are
studied in the present experiment.

4.9 Coincidence Time Spectrum

The geometry of the collision system has been described
in chapter 2 and shown in Fig. 2.1 (b) where in a Cartesian
co-ordinate system, the electron beam is considered to be
incident in the Z direction on the atomic target which is
located at the origin with the atomic beam moving along the
Y direction. The position of the electron detector, which
lies in the XZ plane, defines the scattering plane. The
photons are observed in the same plane. At an incident
electron energy of 100 eV, the 127° electron analyser was
placed at a scattering angle of 15° and tuned to accept
electrons which had lost 21.2 eV energy corresponding to
the excitation of the unresolved 2^1P2^3P states of helium. The
inelastically scattered electrons were detected by the CEM
in the scattering plane after being transmitted through
the analyser assembly. The 2^3P state decays by emitting
infra-red photons ($\lambda = 10830$ A^O) and therefore cannot be
detected with the photon detector using the channel electron
multiplier (Mullard B 419 BL/01).

In this way electrons and photon pulses produced during
the excitation/de-excitation process were fed into the fast
amplifiers with X100 amplification and then into constant
fraction timing distriminators. Thereafter the electron
pulses were fed to the start terminal and photon pulses
through an appropriate delay, were fed to the stop terminal

of a time to pulse height convertor (TPHC) which generates
an output signal whose amplitude is proportional to the
time interval between consecutive start and stop pulses.
The TPHC output signal was finally fed into the multichannel
analyser (MCA) operating in the pulse height operating mode.
In this way electrons and photons from the same $^1S_o - ^1P - ^1S_o$
scattering event produced a definite time correlation result-
ing in a coincidence spectrum on the MCA. This spectrum
consists of true coincidences of the electrons and photons
originated from the excitation/de-excitation of an atom
and random coincidences of the electrons and photons having
no common origin. The true coincidences form a peak on top
of a background of random coincidences, when the time origin
of the 'true coincidences' is brought into the range of
observed times by means of an additional cable delay insert-
ed into the stop channel of the time to pulse height convertor
(Fig. 3.2).

A typical coincidence spectrum obtained for the helium
$^1S_o - 2^1P$ transition is shown in Fig. 4.12 taken at an
electron scattering angle of 15° with the photon multiplier
placed at an angle of 122°.

In Fig. 4.13 another time spectrum taken with 58.4 nm
photon is shown. This time the electron analyser was tuned
to the elastic peak. The resultant uniform spectrum with-
out any peak is expected as photon and electron events in
this case are uncorrelated. It also demonstrates the
correct functioning of the coincidence electronics.
Fig. 4.14 shows different stages of the accumulation of
the coincidence spectrum obtained under the same conditions

TIME 095246 CUR 0000=095246

(a)

TIME 095315 CUR 0000=095315
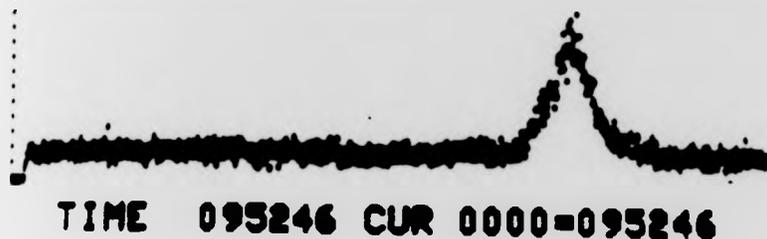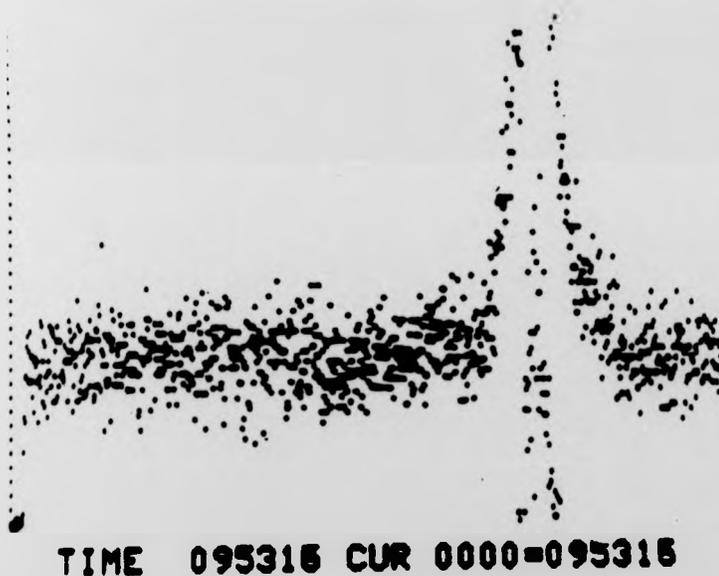
(b)

Fig. 4.12 (a) and (b)

(a) Coincidence time spectrum of He $^1S_0$ - 2^1P transition taken at an electron scattering angle of 15° and photon multiplier placed at an angle of 122°, with an incident electron energy of 100 eV and Faraday cup current of 1μA.

(b) Same spectrum on reduced sensitivity scale.

TIME   059184 CUR 0000=059184

Fig. 4.13:

Coincidence time spectrum taken with 584Å
photon with the electron analyser tuned to
the elastic peak.
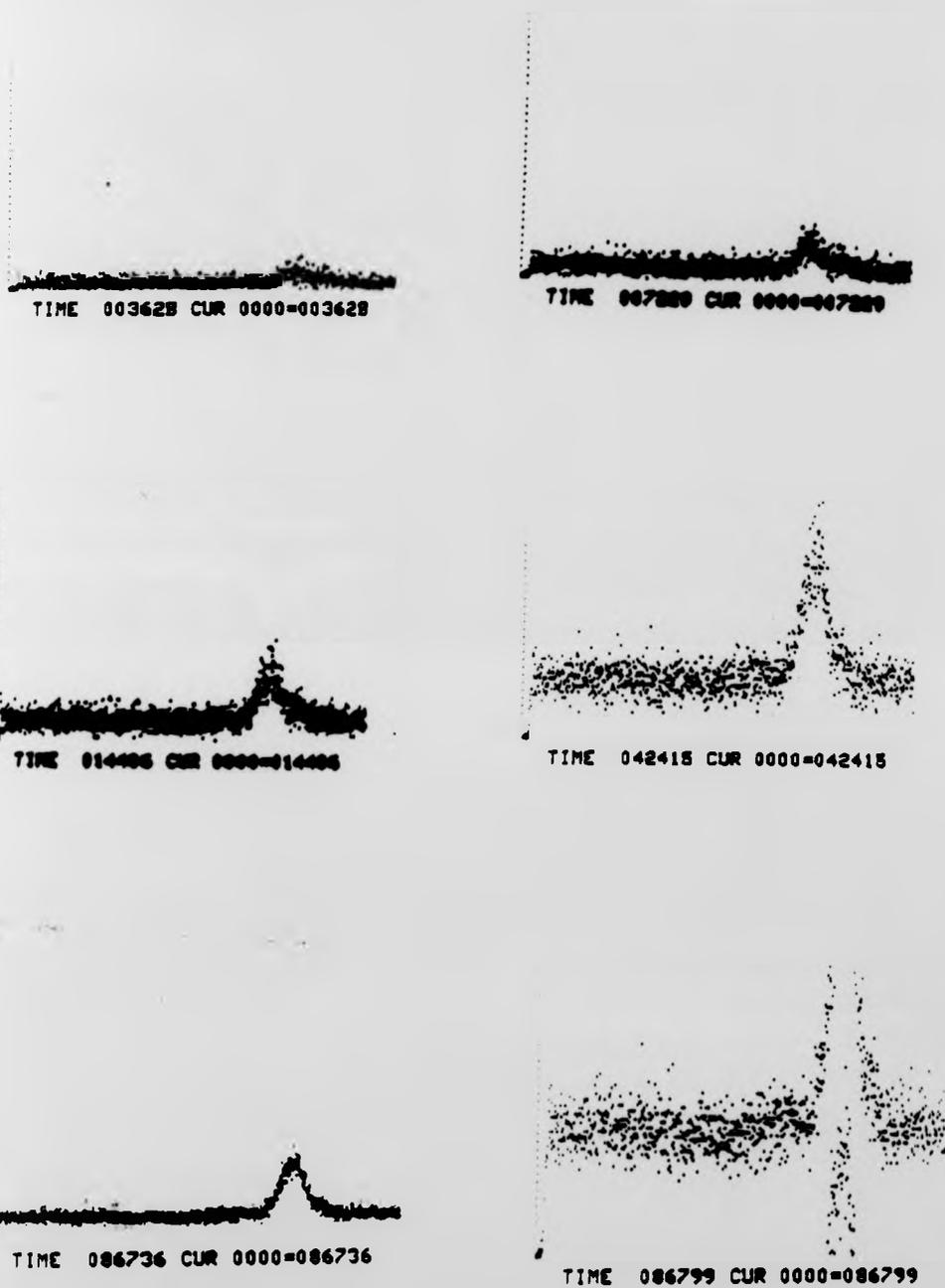
Fig. 4.14:

Different stages of the formation of coincidence time spectrum under the same experimental conditions as for the one shown in Fig. 4.12.

TIME   003628 CUR 0000=003628

TIME   867880 CUR 0000=867880

TIME   014486 CUR 0000=014486

TIME   042415 CUR 0000=042415

TIME   086736 CUR 0000=086736

TIME   086799 CUR 0000=086799
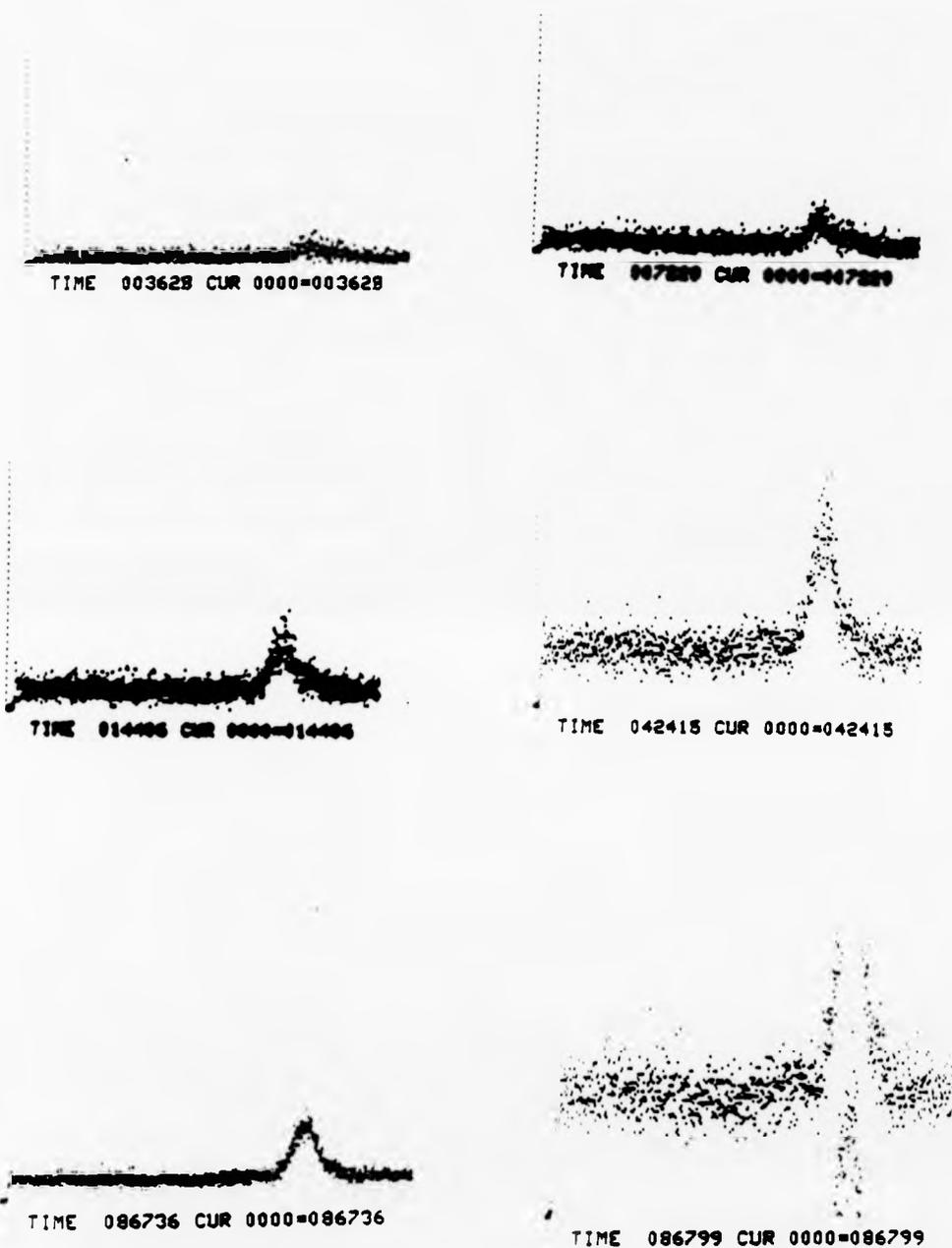
Fig. 4.14:

Different stages of the formation of coincidence time spectrum under the same experimental conditions as for the one shown in Fig. 4.12.

as for the one shown in Fig. 4.12.

4.10 Discriminator Level Setting

The electron and photon pulses from the fast ampli-
fiers still contain noise and electrical pickup which if
not curbed would result in a poor signal to noise ratio.
In order to suppress background noise pulses with an ampli-
tude below the signal level, the discriminator level of the
constant fraction timing discriminators (CFTD) was adjust-
ed so as to eliminate most of the noise pulses. The
constant fraction discriminator (ORTEC Model 473A) has a
discriminator range of -50 mV to -5 V. The electron and
photon pulses after X100 amplification have an amplitude
from 4 to 5 volts which falls within the range of the
CFTD used.

The output pulses from the constant fraction timing
discriminator were monitored on an oscilloscope. At zero
settings of the discriminator level the main probe was
accompanied by a number of spikes which were caused due
to noise and electrical pickup. These spikes were usually
of low amplitude. The discriminator level was increased
from -50 mV to a level where the spikes due to noise and
electrical pickup disappeared. The discriminator levels
for both electron and photon signals from the detectors
were determined which for the present experiment were
1.0 volts for the photon signal and 0.50 volts for the
electron signal.

4.11   Data Acquisition

The 'true coincidences' due to time correlated electrons
and photons appear in certain number of channels of the
multichannel analyser corresponding to a range of times.
These times are determined by the resolution time of the
apparatus and by the lifetime of the excited state.   The
resolution time of the present apparatus was estimated to
be ∿5 ns.

Out of the 512 channels of the multichannel analyser
used in this experiment, the true coincidences fell into
a group of about 100 channels.   The number of true coinci-
dences collected in time T was found by subtracting the
base line counts measured in about 400 channels outside
the range of times of the true coincidences from the total
number of coincidences.   The method of calculating the
base line counts, true coincidence counts and the error in
the number of true coincidences, is explained as follows:
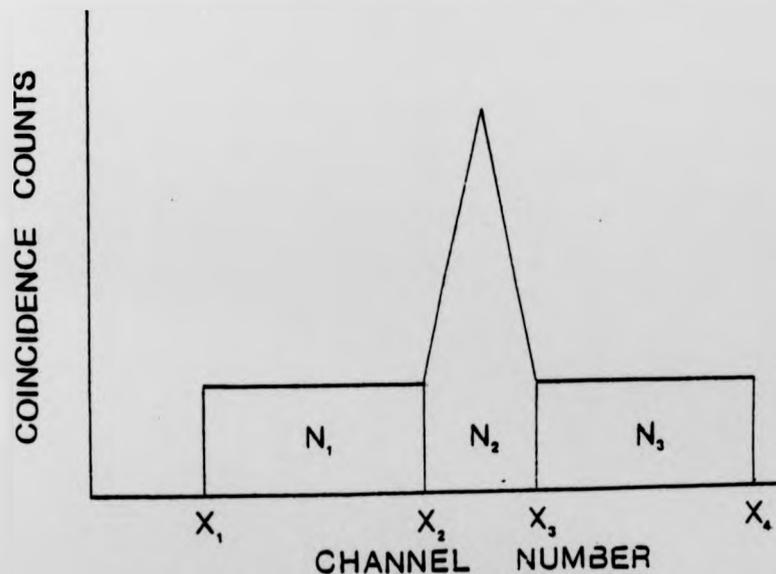
Fig. 4.15   Data acquisition for coincidence analysis

The area under the coincidence time spectrum was divided into three regions N_1, N_2 and N_3 bounded by $(X_2 - X_1)$, $(X_3 - X_2)$ and $(X_4 - X_3)$ where X_1, X_2, X_3 and X_4 represent the channel number on the multichannel analyser screen and N_1, N_2 and N_3 represent the integrals of the coincidence counts in the three regions. (Fig. 4.15)

The random coincidences β under the coincidence peak are given by

$$\beta = \frac{(N_1 + N_3)(X_3 - X_2)}{(X_2 - X_1) + (X_4 - X_3)} \qquad (4.1)$$

The number of true coincidences N_c is

$$N_c = N_2 - \beta \qquad (4.2)$$

The statistical uncertainty of N_c was calculated by assuming that Poisson's statistic was applicable when the standard deviation is given by $\sqrt{N}$. Thus the error δN_c in the number of true coincidences is given by

$$\delta N_c = \sqrt{N_2 + \left\{ \frac{X_3 - X_2}{(X_3 - X_1) + (X_4 - X_3)} \right\}^2 \{N_1 + N_3\}} \qquad (4.3)$$

The total number of 'true coincidences' N_c and the standard deviation δN_c were normalised to the total number of scattered electrons N_e counted during the accumulation time T. The resulting values of $\frac{N_c}{N_e}$ and $\frac{\delta N_c}{N_e}$ were thus insensitive to small variations in electron beam current, target density and efficiency of the electron detector. In order to keep a constant check on the stability of the system, count rates of electrons and photons, Faraday cup current and pressure were observed before and after each run.

For helium, electron-photon coincidence counts were
measured for fixed incident electron energies (80 eV) and
electron scattering angles for various positions of the
photon multiplier in the scattering plane (azimuthal angle
$\phi_\gamma = 180^O$). In the case of krypton and xenon these measure-
ments were taken in the scattering plane ($\phi_\gamma = 180^O$) as
well as out of the scattering plane (i.e. at $\phi_\gamma = 135^O$).

The parameters $\dfrac{N_c}{N_e}$ and $\dfrac{\delta N_c}{N_e}$ have been used in the
computer programmes to derive the values of λ and $|\chi|$ for
helium and $\lambda, \bar{\chi}$ and ε for krypton and xenon.

4.12 Check for Resonance Trapping

The radiation emitted from an excited atomic
state may be absorbed by atoms in the ground state
before being received by the photon detector.
A photon re-emitted after absorption by one of these
atoms will not be anisotropic and will no longer remain
time correlated with the scattered electron that caused
the initial excitation of the atom. This imprisonment of
resonance radiation would affect the experimental results.
It was, therefore, considered necessary to check the effect
of pressure on the coincidence signal in this experiment.
Keeping the excitation parameters the same (i.e. excitation
energy $E_i = 80$ eV and electron scattering angle $\theta_e = 20^O$)
normalised coincidence counts were measured at different
gas pressures. These normalised count rates were then
plotted against the pressure of the gas being studied for
the angular correlation measurements.

Figs. 4.16 and 4.17 show the results for helium

Electron Impact Energy 80 eV
Faraday Cup Current 0.5μA
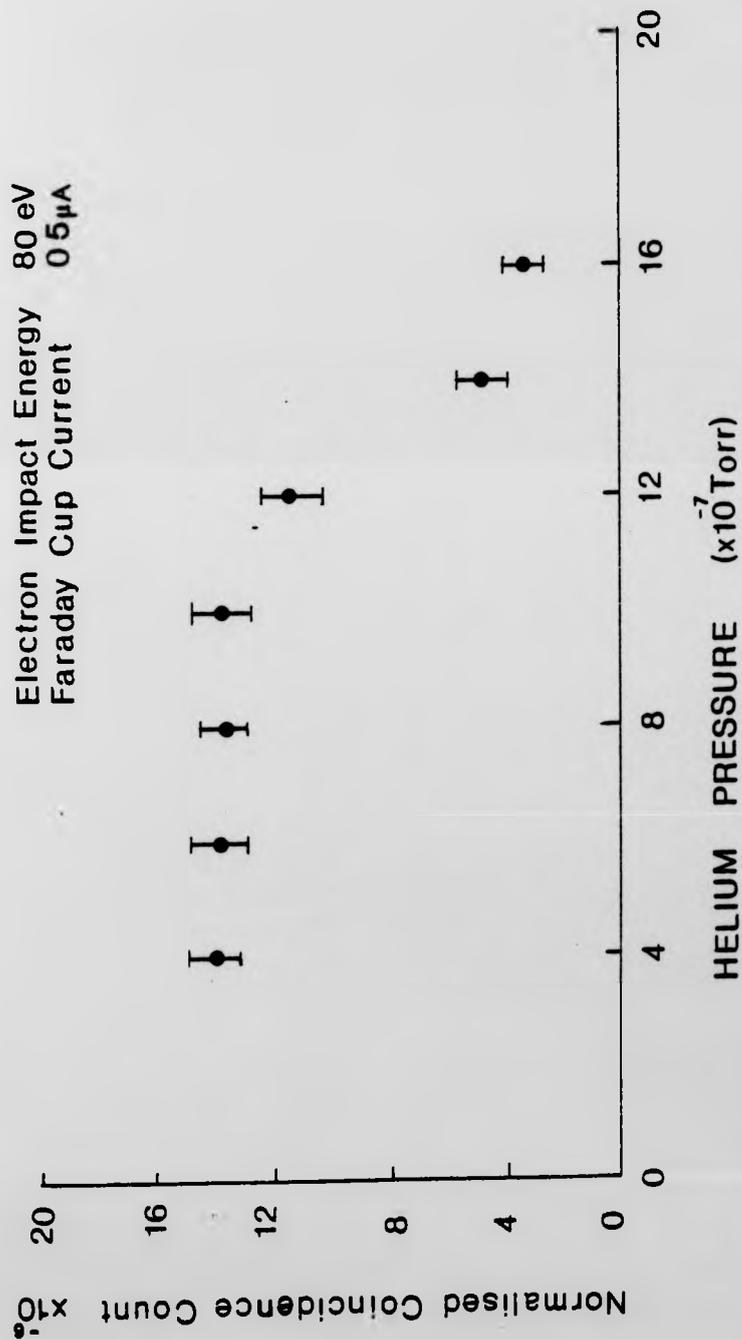
Fig. 4.16:

Dependence of coincidence signal on pressure at an incident electron energy
of 80 eV, electron scattering angle of 30° and photon multiplier at 122°.
Error bars indicate ±1 standard deviation.
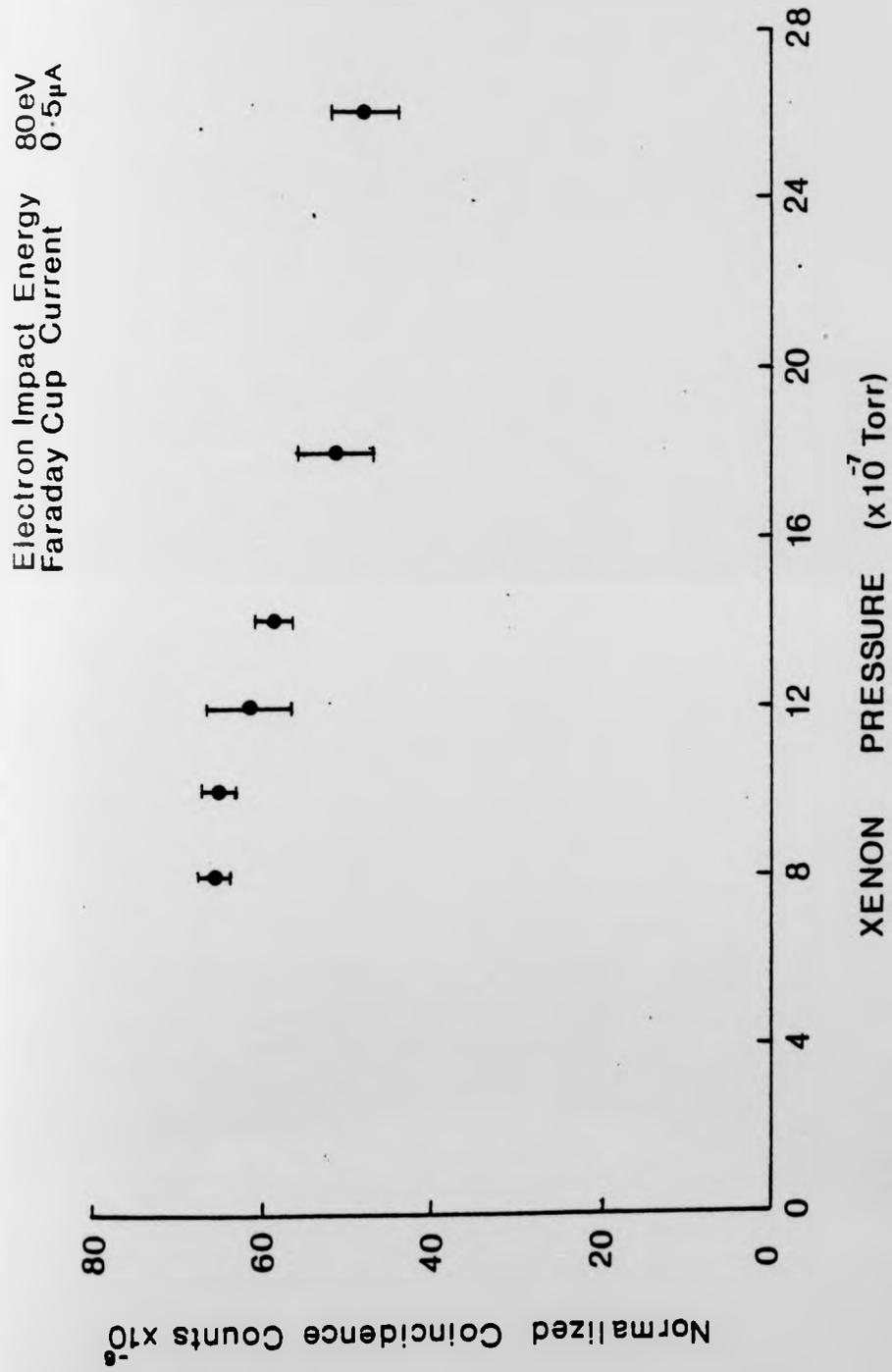
Fig. 4.17:

Dependence of coincidence signal on pressure at an incident electron energy of 80 eV, electron scattering angle of 20° and photon multiplier at 122°. Error bars indicate ±1 standard deviation.

and xenon respectively. It is evident that the normalised coincidence counts start reducing significantly at pressures in excess of 7×10^{-7} Torr for helium and 1.4×10^{-6} Torr for xenon (correction factor was not applied to the pressure measurements). In this experiment therefore the operating pressures have been always kept lower than 7×10^{-7} Torr in the case of measurements on helium, while in the case of xenon, the operating pressure was maintained below 1.4×10^{-6} Torr to avoid any effect on the data collected, due to resonance trapping.

4.13 Test for the Effect of Polarization of Photons

A check has been carried out to study if there were any errors being introduced in the measured angular correlation due to the polarization of the photons. This could cause birefringence effects in the magnesium fluoride window used in the photon multiplier (UV Bendix 762). For this at the existing position of the photon multiplier at 122° where the maximum number of counts were expected, and the electron scattering angle of 20° the normalised coincidence counts were measured. The photon multiplier was then axially rotated through 90° and the measurement was repeated keeping all other parameters the same. The measured coincidence counts were equal in both cases within the experimental error which was lower than 10%.

A third measurement with the photon multiplier axially rotated through 45° from the initial position was finally made to confirm the results of the previous two measurements.

The three measured values of the normalised coincidence

counts were found equal within the limits of experimental error. These values would have been different from each other if the magnesium fluoride window in the photon multiplier had exhibited any birefringence effects due to the polarization of the photons. The intensity of the dipole radiation in a direction making an angle θ with the dipole axis is given by (Percival and Seaton 1958)

$$I(\theta) \; \alpha \;\; (1 - P \cos^2 \theta) \tag{4.4}$$

where

$I(\theta)$ = number of photons per unit solid angle emitted in a direction θ with respect to the incoming electron beam

and P is the degree of polarization.

Eq.(4.4) shows that the value of $I(\theta)$ at three different points 45° apart on the cosine curve will be different which will give rise to different values of normalised coincidence counts. The present test therefore indicates that the data is not affected significantly due to the birefringence effects in the magnesium fluoride window.

4.14 Sources of Systematic Errors

The following possible sources of systematic errors were considered in addition to the imprisonment of radiation as discussed in section 4.12, the differential non linearity check mentioned in section 4.4 and the supression of spurious electrical noise described in section 3.16:

(i)   A pile up distortion of the time spectrum caused by proper stop pulses being unrecorded due to prior arrival of another stop pulse originating from an uncorrelated event, could result in a loss of coincidence signal at longer delay times. The possibility of such a pile up distortion was minimized by keeping the start and stop counting rates low ($\approx 10^4$ Hz), by keeping the ratio of the electrons to photons small and if the stop rate was much higher than the start rate, by interchanging the start and stop channels.

(ii)   The variations in the sensitivity of the electron and photon detectors can also affect the measurements. These variations for a fixed constant fraction timing discriminator setting can be due to ageing of the channeltron electron multiplier or phototube and also arise from the variation of the amplitude of the output pulses at high count rates. These effects were minimised by using pulse amplifiers in cascade to ensure measurement of low amplitude pulses originated from the detectors. This allowed measurement of pulses down to about 200 μV in cases where the saturated pulse height was about 200 mV.

(iii)   Electrons and photons reflected from the metal surfaces inside the vacuum chamber can cause false contributions to the coincidence signal. In order to reduce the reflection coefficient of the surfaces visible to the particle detectors and the interaction region, such surfaces were blackened with soot.

(iv)   Any uncertainty in the setting of the electron
scattering angles θ_e and photon angles θ_γ can give
rise to a significant effect in the derived values
of λ and $|\chi|$ particularly at small electron scattering
angles and those photon angles at which the normalised
coincidence counts are expected to be large.

In the present experiment, the mechanical
angular resolution of the detectors was 0.1 degree.
The 0° axis for the actual electron beam was marked
by taking an angular scan of the primary beam current
through the analyser and plotting a current versus
angle graph as described in section 4.2.2. The
position of the analyser with the maximum electron
current in the channeltron when measured in the d.c.
mode, was taken as the 0° axis of the electron
scattering angle. The angular calibration of the
photon detector angle θ_γ was checked by verifying
that the photon counts from 2^1P state of He were
maximum at the 90° position of the detector.

(v)   The reproducibility of the values of λ and $|\chi|$
for helium at small scattering angle ($\theta_e = 30^O$) and
their comparability with the presently confirmed
experimental and theoretical values, assured that
no significant systematic error was affecting the
data.

5 - RESULTS AND DISCUSSION

5.1 Helium

The present experimental results are summarized in Table 1. The investigation covered the electron scattering angular range from 8° to 108° at an incident electron energy of 80 eV. In addition to the derived values of λ and $|\chi|$, the values of the components of the alignment tensor A^{col}, the orientation vector $|O_{1-}^{col}|$ and θ min are also presented.

Figs. 5.1 (a) to (i) show the angular correlations obtained at electron scattering angle θ_e of 8°, 18°, 30°, 35°, 50°, 60°, 80°, 100° and 108°. The dashed curves represent the predictions of the first Born approximation (FBA). It is apparent that there are marked differences between the FBA and the experimental data, both in the angular position of the minima and in the amplitude of the angular correlations. The minimum of the angular correlation curve becomes less pronounced at larger scattering angles. These discrepancies highlight the limitations of the FBA which predicts no angular momentum transfer to the atom along the direction of linear momentum transfer $\bar{K}$ for which $\Delta M = 0$, implying that $\chi = 0$. For a theory for which $\chi = 0$, e.g. FBA, the radiation pattern is that of a single dipole lying along the momentum transfer direction. In this case the angular correlation curve should fall to zero in the direction of the dipole axis, which lies along the momentum transfer direction and therefore

TABLE 1. Values of the parameters derived from the measured electron-photon angular correlation as a function of the electron scattering angle θ_e for an incident energy of 80 eV (helium)

Electron Scattering Angle θ_e	λ	$|\chi|$ rad	θ min(deg)	$|O_{1-}^{col}|$	A_o^{col}	A_{1+}^{col}	A_{2+}^{col}
8°	0.531±0.008	0.699±0.015	42.76±0.33	0.309±0.006	-0.296±0.004	0.392±0.008	-0.469±0.012
18°	0.317±0.012	0.328±0.068	56.26±0.61	0.150±0.031	0.024±0.010	0.441±0.012	-0.683±0.018
30°	0.431±0.046	1.398±0.053	64.54±6.77	0.488±0.009	-0.146±0.026	0.085±0.046	-0.569±0.069
35°	0.577±0.059	0.983±0.056	37.13±2.35	0.411±0.018	-0.366±0.023	0.274±0.059	-0.423±0.089
50°	0.714±0.007	1.842±0.016	-14.73±0.77	0.435±0.005	-0.571±0.007	-0.121±0.007	-0.206±0.010
60°	0.948±0.064	2.177±0.605	- 7.87±6.13	0.182±0.181	-0.922±0.100	-0.126±0.064	-0.052±0.097
80°	0.736±0.037	1.984±0.091	-18.45±3.37	0.404±0.032	-0.604±0.035	-0.177±0.037	-0.264±0.056
90°	0.615±0.037	1.099±0.032	-31.27±1.64	0.433±0.010	-0.422±0.014	0.221±0.034	-0.385±0.051
100°	0.437±0.037	1.941±0.056	-35.33±2.50	0.463±0.012	-0.156±0.026	0.179±0.037	-0.563±0.056
108°	0.677±0.045	1.283±0.064	-18.42±3.85	0.448±0.017	-0.516±0.030	0.133±0.045	-0.323±0.068

Fig. 5.1 (a) to (i)

Electron-photon angular correlations in helium showing the normalised coincidence count rate as a function of photon scattering angle for electron scattering angles of 8°, 18°, 30°, 35°, 50°, 80°, 100° and 108°, at an incident electron energy at 80 eV. The solid line curves are chi-squared optimization of eqn. 2.8 to the experimental data. The dashed curves are the predictions of the first Born approximation.

Error bars indicate ±1 standard deviation.

HELIUM
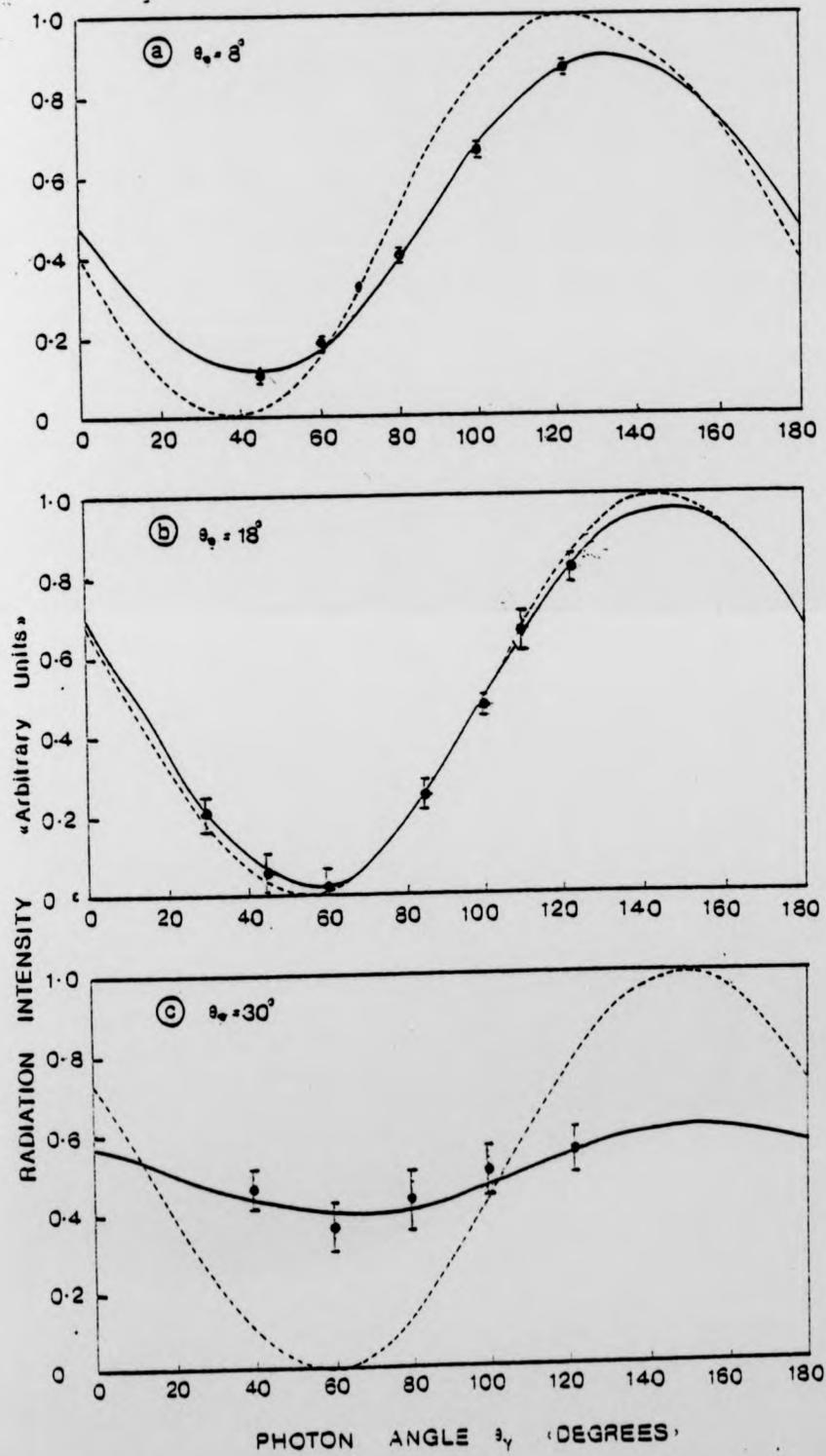
Fig. 5.1 (a) to (c)

HELIUM

Fig. 5.1 (d) to (f)

HELIUM

PHOTON ANGLE θ_γ (DEGREES)
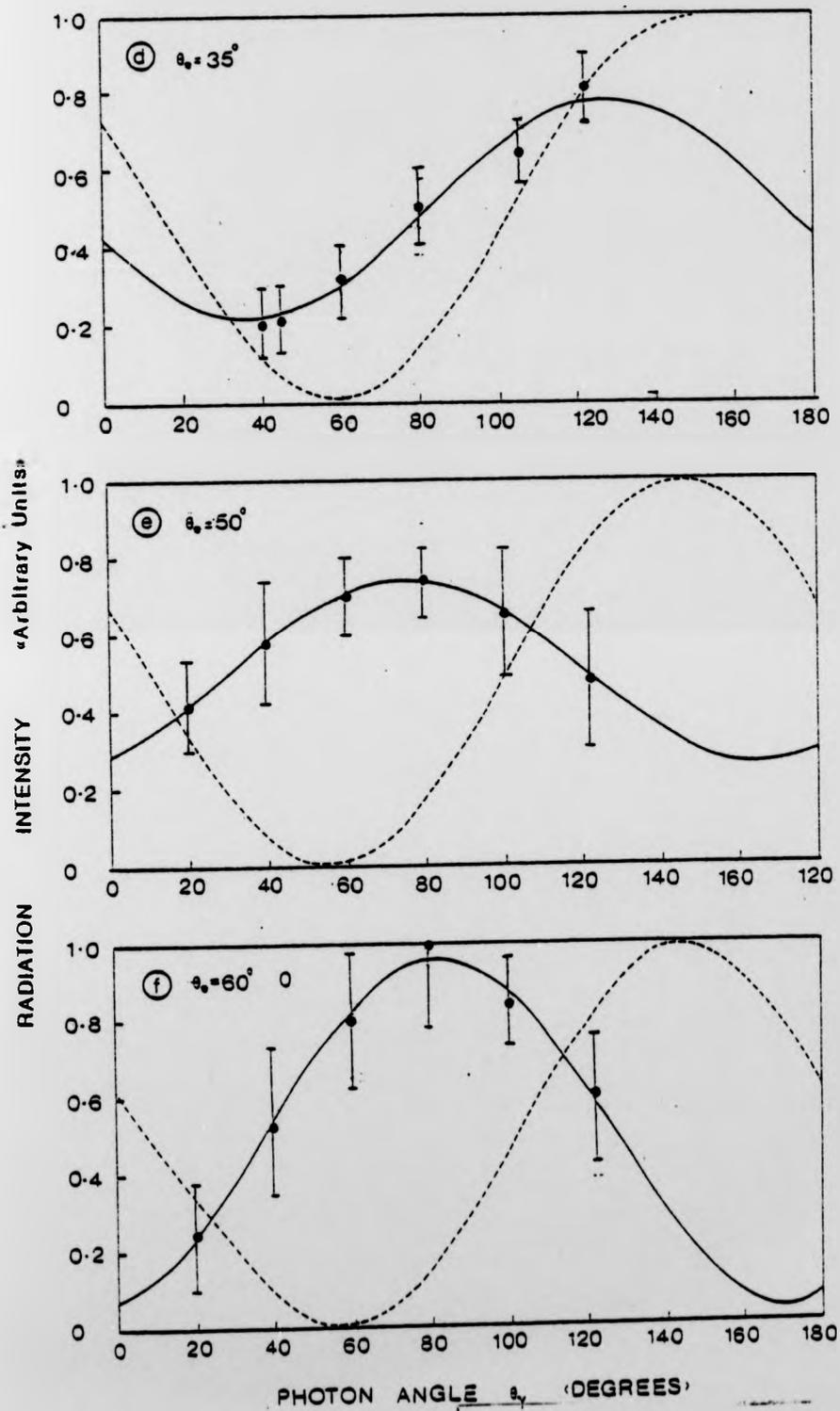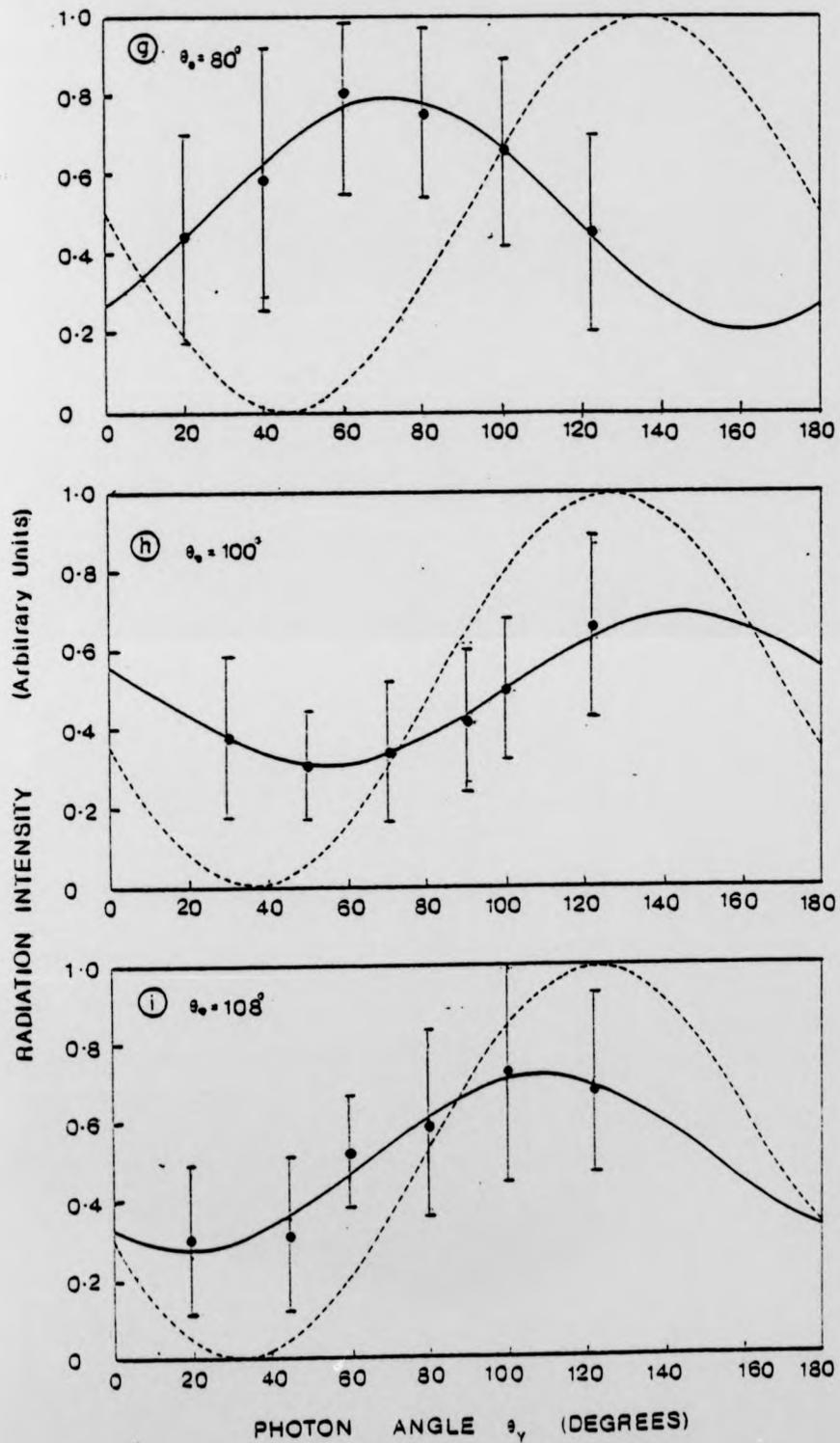
Fig. 5.1 (g) to (i)

zero should occur at the photon angle where no momentum transfer is taking place. The angular correlation curve predicted by the FBA will therefore have a $\sin^2\theta$ dependence about the momentum transfer axis. This agrees with the experimental data only at small scattering angles. Even at $\theta_e = 30^\circ$ the FBA curve lies much outside the 70% confidence limits of the measured angular correlation.

At large scattering angles, the radiation pattern can be described in terms of a dipole picture by assuming the presence of two dipoles with a relative phase difference of χ and amplitudes a_1 and $\sqrt{2}\ a_1$ aligned along the Z and X axis respectively. Variation in the relative phase and amplitudes of the two dipole oscillators will then account for both the shift in the angular position of the minimum and the decrease in the amplitude of the angular correlation function. Macek and Jaecks (1971) assume the presence of two dipoles differing in phase by $\frac{\pi}{2}$ and with amplitudes $|a_0\cos\theta_{min} + a_1\sqrt{2}\sin\theta_{min}|$ and $|a_0\sin\theta_{min} - a_1\sqrt{2}\cos\theta_{min}|$ aligned along the major and minor axes of the observed radiation pattern. As the dipoles oscillate their resultant traces out an ellipse in the scattering plane. The radiation patterns i.e. the angular correlation curves in Fig. 5.1 can then be interpreted in terms of a progressive broadening of the ellipse and a re-alignment of its major axis away from $\theta_{\bar{K}}$ as the scattering angle increases.

Fig. 5.2 shows the variation of θ_{min} with electron scattering angle in the present measurements. The results are compared with those of Hollywood et al. (1979),

Fig. 5.2.

Variation of θ_{min} with electron scattering angle for an incident energy of 80 eV in helium.

⬓ , Present work; ⍦ , Hollywood et al.(1978);

⬡ , Eminyan et al. (1974)   ⬓ ,Ugbabe et al. (1977)

⬥ , Steph & Golden (1980)
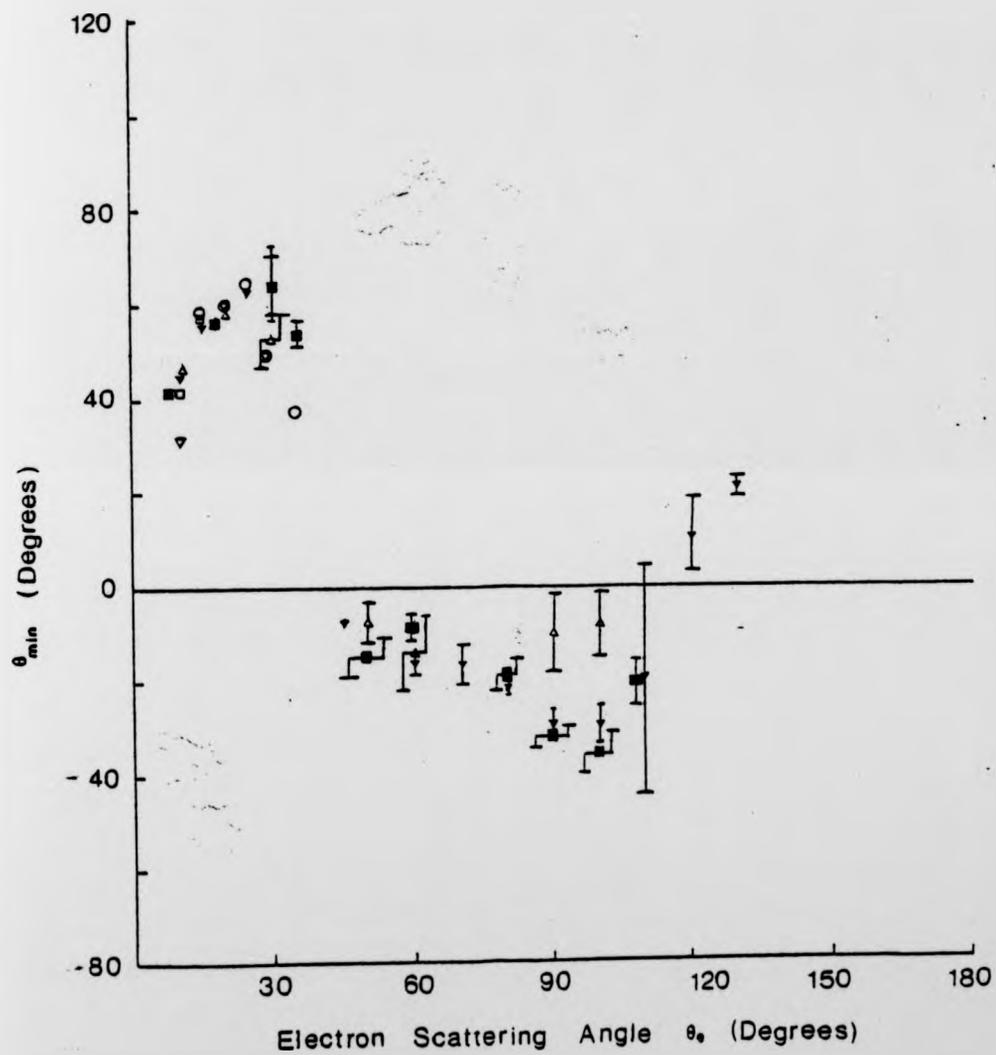
Eminyan et al. (1974), Ugbabe et al. (1977), Slevin et al. (1980) and Steph and Golden (1980).

The measured variation of λ with electron scattering angle θ_e is presented in Fig. 5.3. The present results are compared with the results of previous experiments and also with theoretical calculations.

An examination of the present data shows an overlap with all the previous data at small scattering angles. The error bars represent one standard deviation or 70% confidence limits which show the present results to be in good agreement with those obtained by Hollywood et al. (1979) and Sutcliffe et al. (1978). The present value of λ at $\theta_e = 50^O$ is somewhat below and at $\theta_e = 60^O$ is somewhat above the values obtained by Hollywood et al. (1979) and Sutcliffe et al. (1978) but follow the general pattern of the variation of λ at these scattering angles.

At large scattering angles (above $\theta_e = 60^O$) the present results tend to agree with the data of Hollywood et al. (1978), Slevin et al. (1980) and are widely different from the observations of Sutcliffe et al. (1978). Steph and Golden (1980) have extended the range of their previous measurements (Sutcliffe et al, 1978) by making another measurement at $\theta_e = 100^O$ but unfortunately did not proceed systematically between 100° and 155° scattering angle range. These measurements therefore do not give a clear picture of the variation of λ at scattering angles between 100° and 155°.

Because of the wide differences between the results of Hollywood et al. (1979) and Sutcliffe et al. (1978)

Fig. 5.3

Variation of λ with electron scattering angle for an incident electron energy of 80 eV in helium.

⬍ , Present data; ⬍ , Eminyan et al. (1974);

⬍ , Ugbabe et al. (1977); ⬍ , Tan et al. (1977);

⬍ , Sutcliffe et al. (1978) and Steph and Golden (1980);

⬍ , Hollywood et al. (1978); ⬍ , Slevin et al. (1980).

The theoretical predictions are the first Born approximation

------ ; Madison et al. (from Sutcliffe et al. 1978)
———— ; Thomas et al. (1974) — O —; Scott and
McDowell (1976) — · — ; and Fon et al. (1979) — -- — .

Error bars indicate ±1 standard deviation.

ELECTRON SCATTERING ANGLE (degrees)

later extended by Steph and Golden (1980) great care has
been taken in the design of the present apparatus and
collection of data so as to ensure that it was free from
any systematic errors. The angular resolution of 0.1
degree for the apparatus and the precise measurement of
the electron scattering angles (θ_e) and the photon angles
(θ_γ) with a large number of tests carried out to check the
validity of the measurements before the present set of
data was taken, gives confidence in the authenticity of
the present results. As seen in figure 5.3, the value of
λ constrained by conservation of angular momentum to be
unity at $\theta_e = 0^O$ and 180°, falls from 1 to a deep minimum
around 18° rises to a maximum at $\theta_e \simeq 60^O$ and falls to a
minimum again at $\theta_e \simeq 100^O$ adds to the claim of Hollywood
et al. (1979).

Fig. 5.4 shows the dependence of $|\chi|$ upon electron
scattering angle for an incident electron energy of 80 eV.
The measured values are generally in good agreement with
the previous experimental measurements of Eminyan et al.
(1974) and Ugbabe et al. (1977) for small scattering angles
and those of Hollywood et al. (1979), Steph and Golden (1980)
and Slevin et al. (1980) for small as well as large scatter-
ing angle measurements. The general shape of the variation
of $|\chi|$ with electron scattering angle (θ_e) is also in fair
agreement with the theoretical values predicted by Scott
and McDowell (1976) and by Fon et al (1979). FBA however,
predicts the value of $\chi \equiv 0$ throughout the angular range.

By studying the variation of the alignment tensor
and the orientation vector with electron scattering angle

Fig. 5.4:

The variation of $|\chi|$ with electron scattering angle for and incident electron energy of 80 eV in the excitation of the 2^1P state of helium.

⬥ , Present data; ⭗ , Eminyan et al. (1974);

⬓ , Ugbabe et al. (1977); ⬥ , Hollywood et al. (1979);

⬦ , Steph and Golden (1980); ⬦ , Slevin et al. (1980).

The theoretical predictions are by Scott and McDowell (1976)

— · — ;   and Fon et al (1979) — -- — .

Error bars indicate ±1 standard deviation.

Fig. 5.4:

The variation of $|\chi|$ with electron scattering angle for and incident electron energy of 80 eV in the excitation of the 2^1P state of helium.

⬥ , Present data; ⏁ , Eminyan et al. (1974);

⏁ , Ugbabe et al. (1977); ⬥ , Hollywood et al. (1979);

� , Steph and Golden (1980); ⬇ , Slevin et al. (1980).

The theoretical predictions are by Scott and McDowell (1976)

— · — ; and Fon et al (1979) — -- — .

Error bars indicate ±1 standard deviation.

θ_e, an alternative description of the excitation process can be obtained (Fano and Macek, 1973). The expectation value of atomic orbital angular momentum perpendicular to the plane of scattering that is transferred in collision is

$$\langle Ly \rangle = - 2 \left[\lambda (1-\lambda) \right]^{\frac{1}{2}} \sin \chi$$

The deviation of χ from zero therefore measures the extent to which 2^1P atoms are produced in an oriented state by scattering at a given energy and scattering angles. The quantity $\langle Ly \rangle$ can in principle be measured directly in a coincidence experiment since the circular polarization factor $P^{circ} = \dfrac{(I_+ - I_-)}{(I_+ + I_-)}$ of coincidence photons emitted perpendicular to the plane of scattering is equal to $\langle Ly \rangle$. This measurement is not feasible for the 58.4 nm radiation from the 2^1P state of helium because of the short wavelength involved. From the angular correlation measurements in the scattering plane, therefore only the magnitude of χ can be determined and hence only $|O_{1-}^{col}|$ can be deduced. From the definition (Fano and Macek 1973)

$$O_{1-}^{col} = \frac{\langle Ly \rangle}{L(L+1)} \quad \text{the deduced}$$

relationship

$$2 \, O_{1-}^{col} = - \langle Ly \rangle = P^{circ}$$

shows that the radiation emitted normal to the scattering plane ($\theta_\gamma = \phi_\gamma = \frac{\pi}{2}$ and $\phi_e = 0$) would be expected to be 100% circularly polarized at angles in the region of 30° and 100° (Fig. 5.5). If we assume the sign of χ from the theory of Scott and McDowell (1976), this radiation is

θ_e, an alternative description of the excitation process can be obtained (Fano and Macek, 1973). The expectation value of atomic orbital angular momentum perpendicular to the plane of scattering that is transferred in collision is

$$\langle L_y \rangle = - 2 \left[\lambda (1-\lambda) \right]^{\frac{1}{2}} \sin \chi$$

The deviation of χ from zero therefore measures the extent to which 2^1P atoms are produced in an oriented state by scattering at a given energy and scattering angles. The quantity $\langle L_y \rangle$ can in principle be measured directly in a coincidence experiment since the circular polarization factor $P^{circ} = (I_+ - I_-) / (I_+ + I_-)$ of coincidence photons emitted perpendicular to the plane of scattering is equal to $\langle L_y \rangle$. This measurement is not feasible for the 58.4 nm radiation from the 2^1P state of helium because of the short wavelength involved. From the angular correlation measurements in the scattering plane, therefore only the magnitude of χ can be determined and hence only $|O_{1-}^{col}|$ can be deduced. From the definition (Fano and Macek 1973)

$$O_{1-}^{col} = \frac{\langle L_y \rangle}{L(L+1)} \quad \text{the deduced}$$

relationship

$$2 \, O_{1-}^{col} = - \langle L_y \rangle = P^{circ}$$

shows that the radiation emitted normal to the scattering plane ($\theta_\gamma = \phi_\gamma = \frac{\pi}{2}$ and $\phi_e = 0$) would be expected to be 100% circularly polarized at angles in the region of 30° and 100° (Fig. 5.5). If we assume the sign of χ from the theory of Scott and McDowell (1976), this radiation is

right handed circularly polarized (σ^+) at $\theta_e \simeq 30^O$ and left handed circularly polarized (σ^-) at $\theta_e \simeq 100^O$. The radiation has zero circular polarization at $\theta_e \simeq 60^O$. It also follows from Fig. 5.4 that at $\theta_e \simeq 50^O$ and 108° $\bar{\chi}$ passes through π while A_{1+}^{col} passes through zero (Fig. 5.5) and there is minimum photon intensity in the forward direction.

A_O^{col} is a measure of the anisotropy of the population of the magnetic substates referred to the Z axis as quantization axis. For $\theta_e \simeq 0^O$ or 180° the conservation of angular momentum requires only $m_L = 0$ substates to be excited, and the relation

$$\text{(Fano and Macek, 1973)} \quad A_O = \frac{<3L_z^2 - L^2>}{L(L + 1)}$$

gives $A_O^{col} = -1$ $(\Delta M_L = 0)$

Fig. 5.5 shows that $A_O^{col} = 0$ when $\theta_e = 16^O$ and 27°. At these scattering angles then, the three substates are equally populated. This behaviour of A_O^{col} alone would imply an isotropic photon angular distribution for an incoherent excitation process, but the present experimental data show both A_{1+}^{col} and A_{2+}^{col} having non-zero values at these angles. The observed anisotropic distributions result from interference between the coherent excitation amplitudes.

5.2 Krypton and Xenon

The experimental results obtained for the electron-photon angular correlation measurements on the $4p^5$ ($2P_{3/2}$) $5s^3P_1$ and $4p^5$ ($^2P_{1/2}$) $5s^1P_1$ states of krypton at incident electron energies of 36 eV and 60 eV are presented in Table 2. Table 3 contains the results of these measurements on the

right handed circularly polarized (σ^+) at $\theta_e \simeq 30^O$ and left handed circularly polarized (σ^-) at $\theta_e \simeq 100^O$. The radiation has zero circular polarization at $\theta_e \simeq 60^O$. It also follows from Fig. 5.4 that at $\theta_e \simeq 50^O$ and 108° $\overline{\chi}$ passes through π while A_{1+}^{col} passes through zero (Fig. 5.5) and there is minimum photon intensity in the forward direction.

A_O^{col} is a measure of the anisotropy of the population of the magnetic substates referred to the Z axis as quantization axis. For $\theta_e \simeq 0^O$ or 180° the conservation of angular momentum requires only $m_L = 0$ substates to be excited, and the relation

$$(\text{Fano and Macek, 1973}) \quad A_O = \frac{<3L_z^2 - L^2>}{L(L + 1)}$$

gives $A_O^{col} = -1 \ (\Delta M_L = 0)$

Fig. 5.5 shows that $A_O^{col} = 0$ when $\theta_e = 16^O$ and 27°. At these scattering angles then, the three substates are equally populated. This behaviour of A_O^{col} alone would imply an isotropic photon angular distribution for an incoherent excitation process, but the present experimental data show both A_{1+}^{col} and A_{2+}^{col} having non-zero values at these angles. The observed anisotropic distributions result from interference between the coherent excitation amplitudes.

5.2 Krypton and Xenon

The experimental results obtained for the electron-photon angular correlation measurements on the $4p^5$ $(2P_{3/2})$ $5s^3P_1$ and $4p^5$ $(^2P_{1/2})$ $5s^1P_1$ states of krypton at incident electron energies of 36 eV and 60 eV are presented in Table 2. Table 3 contains the results of these measurements on the

Fig. 5.5:

The variation of the components of the alignment tensor and the orientation vector with the electron scattering angle in the electron excitation of 1^1S state of helium to 2^1P state at 80 eV.

⦿ , Present data; ⦿ , Hollywood et al. (1978);

------ represents the theoretical calculations of Fon et al. (1979).

Error bars indicate ±1 standard deviation.
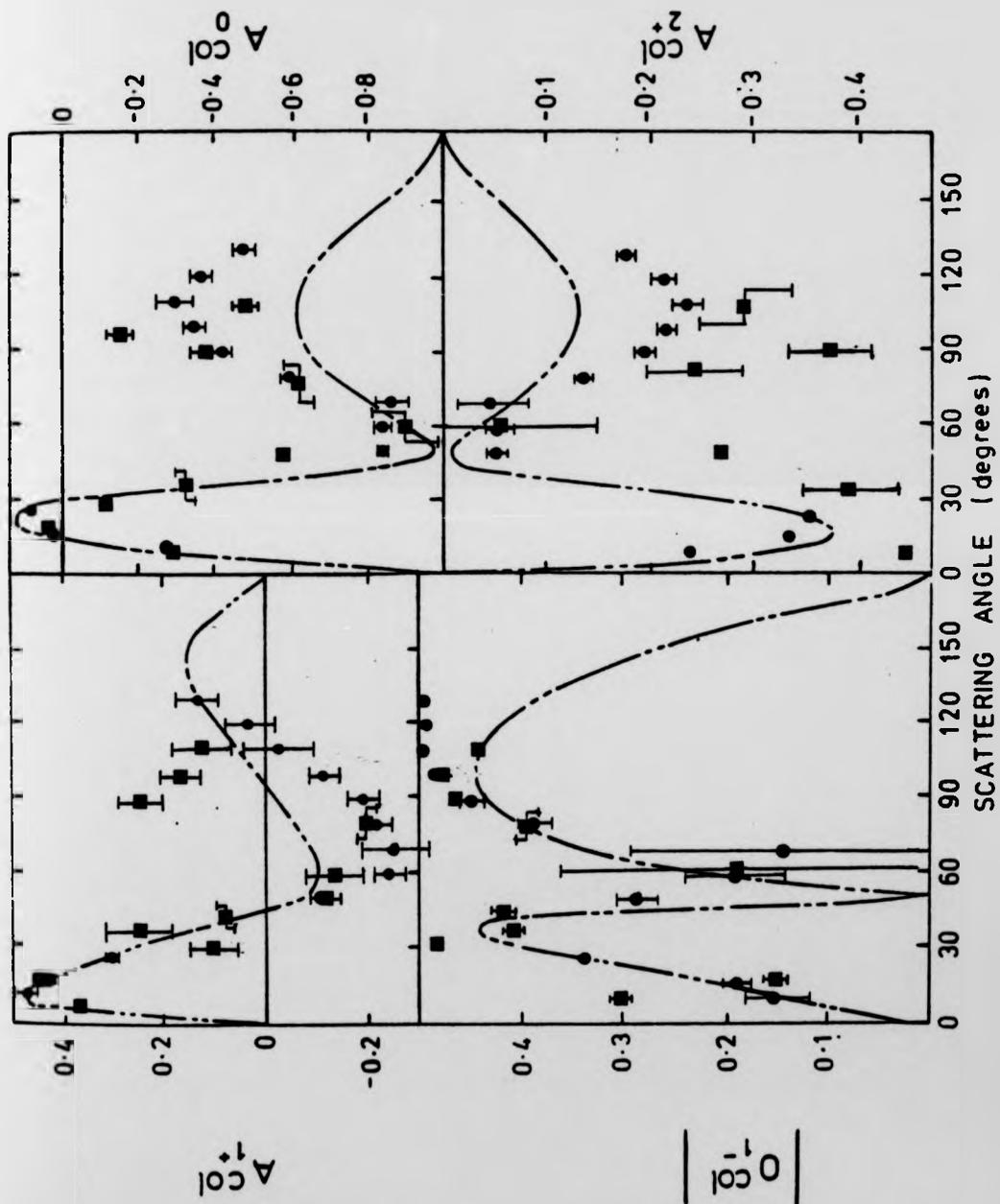
Table 2: Values of the parameters derived from the measured electron-photon angular correlations as function of the incident electron energy E_i and the electron scattering angle θ_e for $^3P_1$ and $^1P_1$ states of krypton

Incident electron energy E_i	State	Electron scattering angle θ_e (deg)	λ	$\bar{\chi}$ (rad.)
36 eV	$^3P_1$	20	.584 ± 0.124	1.633 ± 0.084
	$^3P_1$	30	.517 ± 0.081	1.716 ± 0.079
	$^1P_1$	20	.510 ± 0.073	1.960 ± 0.050
	$^1P_1$	30	.449 ± 0.073	-1.360 ± 0.080
60 eV	$^3P_1$	20	.829 ± 0.289	1.988 ± 0.249
	$^3P_1$	30	.782 ± 0.157	1.451 ± 0.178
	$^1P_1$	20	.717 ± 0.217	-1.806 ± 0.130
	$^1P_1$	30	.583 ± 0.098	-1.352 ± 0.107

Table 3: Values of the parameters derived from the measured electron-photon angular correlations as function of the electron scattering angle θ_e for $^3P_1$ state of xenon.

Incident Electron Energy E_i	Electron Scattering Angle θe	λ	$\bar{\chi}$	$\cos \varepsilon$
80 eV	20°	.499 ± .033	1.239 ± .019	1.426 ± 1.696
	30°	.403 ± .034	1.504 ± .035	.349 ± .071

$5p^5(2P_{3/2})$ $6s^3P_1$ state of xenon at an incident electron energy of 80 eV. Both these investigations were carried out for the electron scattering angles of 20° and 30°.

Unlike helium, LS coupling is not valid for krypton and xenon. In these target atoms the spin-orbit interaction affects the phase information and more than two parameters are needed to describe the electron-photon angular correlation process. Following a suggestion by Blum et al. (1980) the angular correlation measurements for this study have been made in two planes, one in the scattering plane X-Z (Fig. 2.1b) with azimuthal angles $\phi_\gamma = 180^O$ and $\phi_e = 0^O$ and the other out of the scattering plane at azimuthal angle $\phi_\gamma = 135^O$ and $\phi_e = 0^O$.

Figs. 5.6 (a) to (h) show the angular correlations obtained by measuring the emitted radiation from krypton (123.6 nm and 116.5 nm) in and out of the scattering planes. Similarly Figs. 5.7 (a) and (b) show the angular correlations obtained with 146.9 nm radiation emitted from xenon.

In the case of xenon the parameters λ, $\cos \bar{\chi}$ and $\cos \varepsilon$ are derived from the measured electron-photon normalised coincidence count rates by fitting the data to the angular correlation expressions given by eqns. 2.13 and 2.14 in Chap. II. A value of $\cos \varepsilon$ equal to 1 indicates the absence of spin-orbit interaction. The deviation of value of $\cos \varepsilon$ from 1 is a measure of the strength of the spin orbit interaction experienced by the target atom. The derived value of $\cos \varepsilon$ at an electron scattering angle of 30° which differs significantly from 1 indicates the presence of spin orbit interaction in xenon atom. At

Fig. 5.6 (a) to (h):

Electron-photon angular correlations in krypton showing the
the normalised coincidence count rate as a function of
photon scattering angle (i) out of the scattering plane
with azimuthal angle $\phi_\gamma = 135^\circ$ and (ii) in the scattering
plane with azimuthal angle $\phi_\gamma = 180^\circ$. Solid curves are
the least square fits to the experimental data.

Error bars indicate ± 1 standard deviation.

123
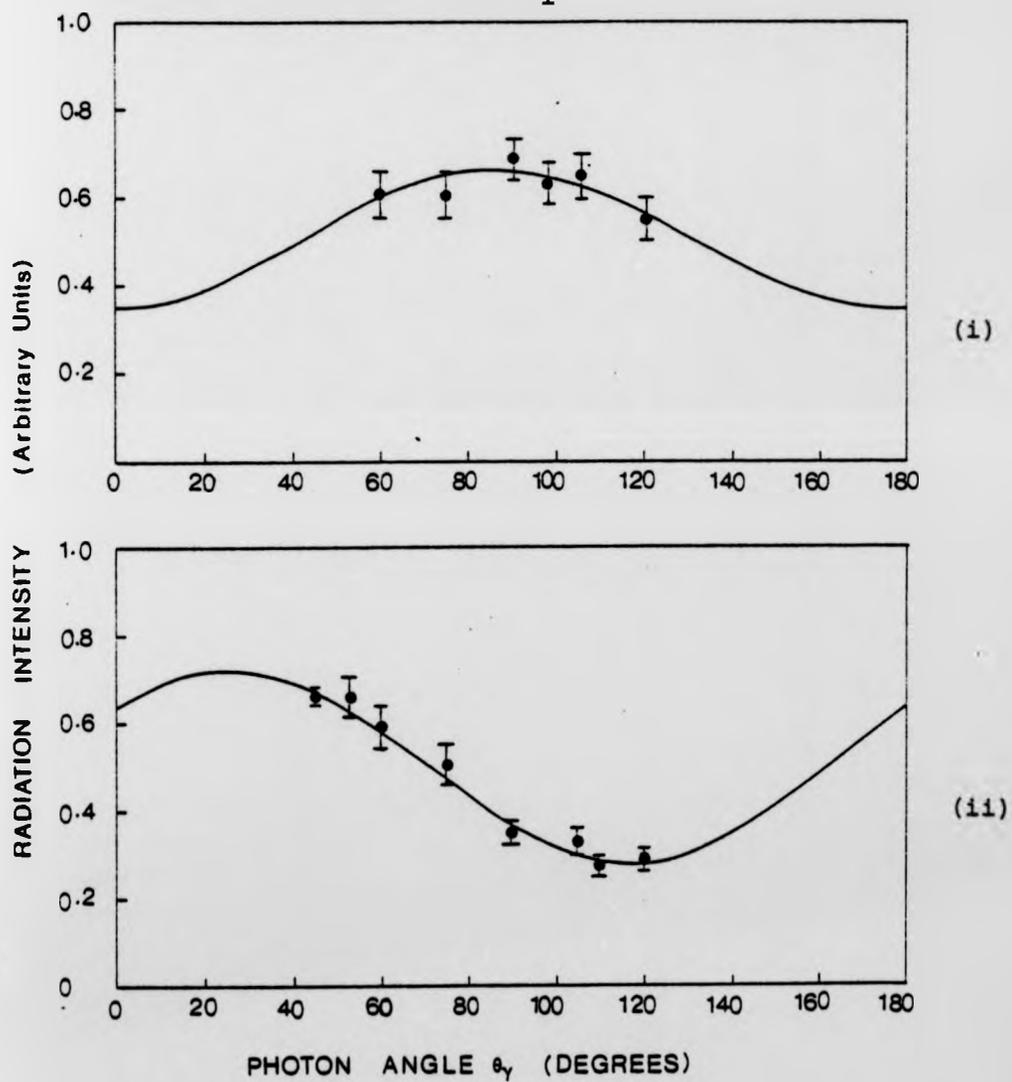
Fig. 5.6 (a) (i) and (ii)

KRYPTON $^3P_1$

Electron Scattering Angle $\theta_e = 30^O$
Incident Electron Energy $E_i = 36$ eV

(i)

(ii)

PHOTON ANGLE θ_Y (DEGREES)
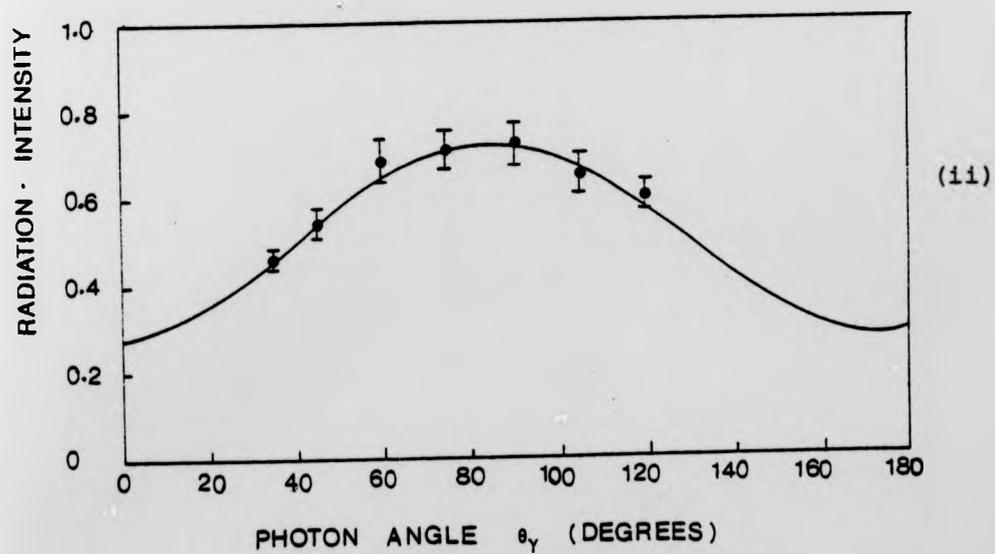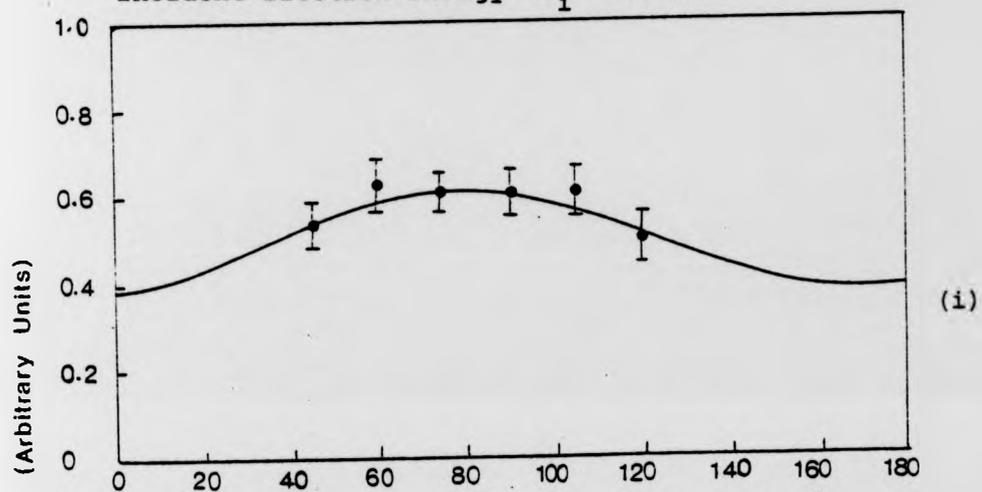
Fig. 5.6 (b) (i) and (ii)

KRYPTON $^1P_1$

Electron Scattering Angle $\theta_e = 20^o$
Incident Electron Energy $E_i = 36$ eV
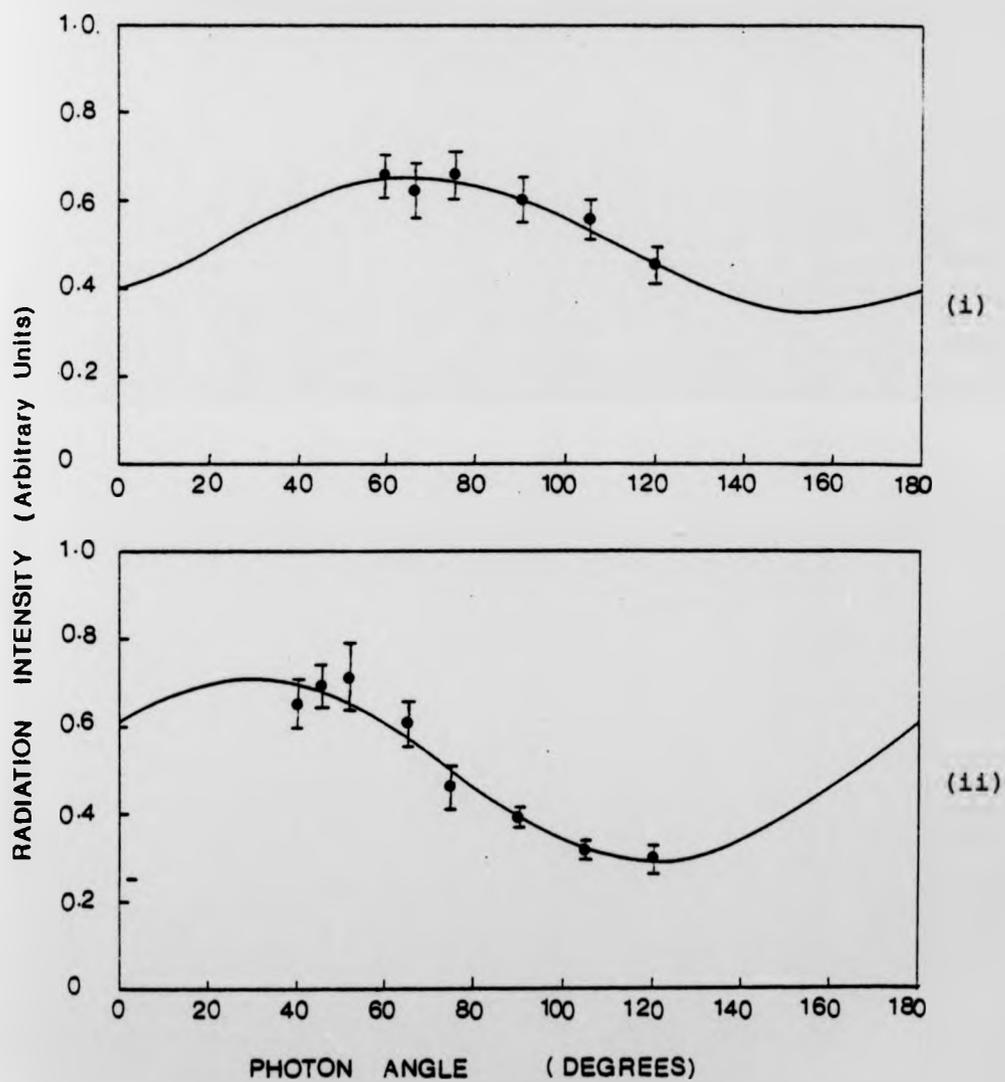
Fig. 5.6 (c) (i) and (ii)

KRYPTON $^1P_1$

Electron Scattering Angle $\theta_e = 30^o$
Incident Electron Energy $E_i = 36$ eV
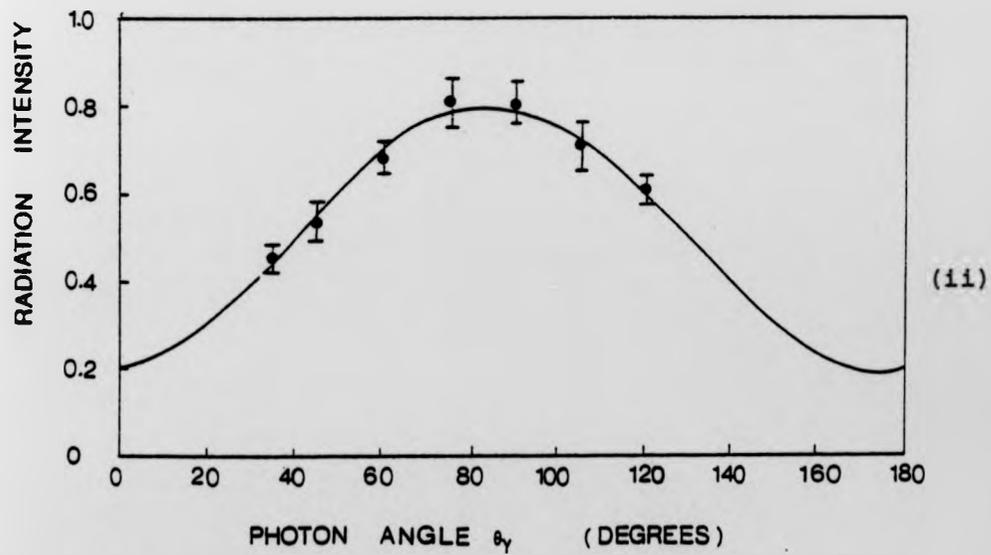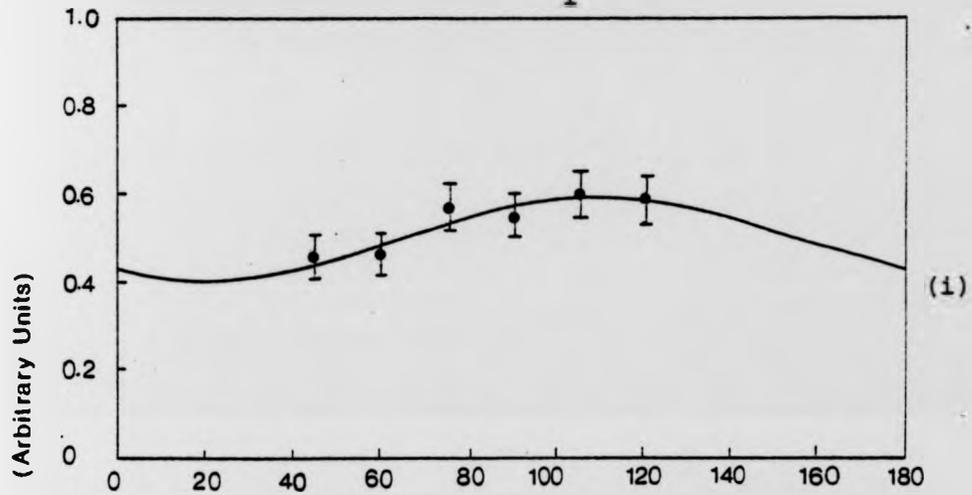
Fig. 5.6 (d) (i) and (ii)

KRYPTON $^3P_1$

Electron Scattering Angle $\theta_e = 20^\circ$
Incident Electron Energy $E_i = 60$ eV

(i)

(ii)

RADIATION INTENSITY   (Arbitrary Units)

PHOTON ANGLE θ_γ (DEGREES)
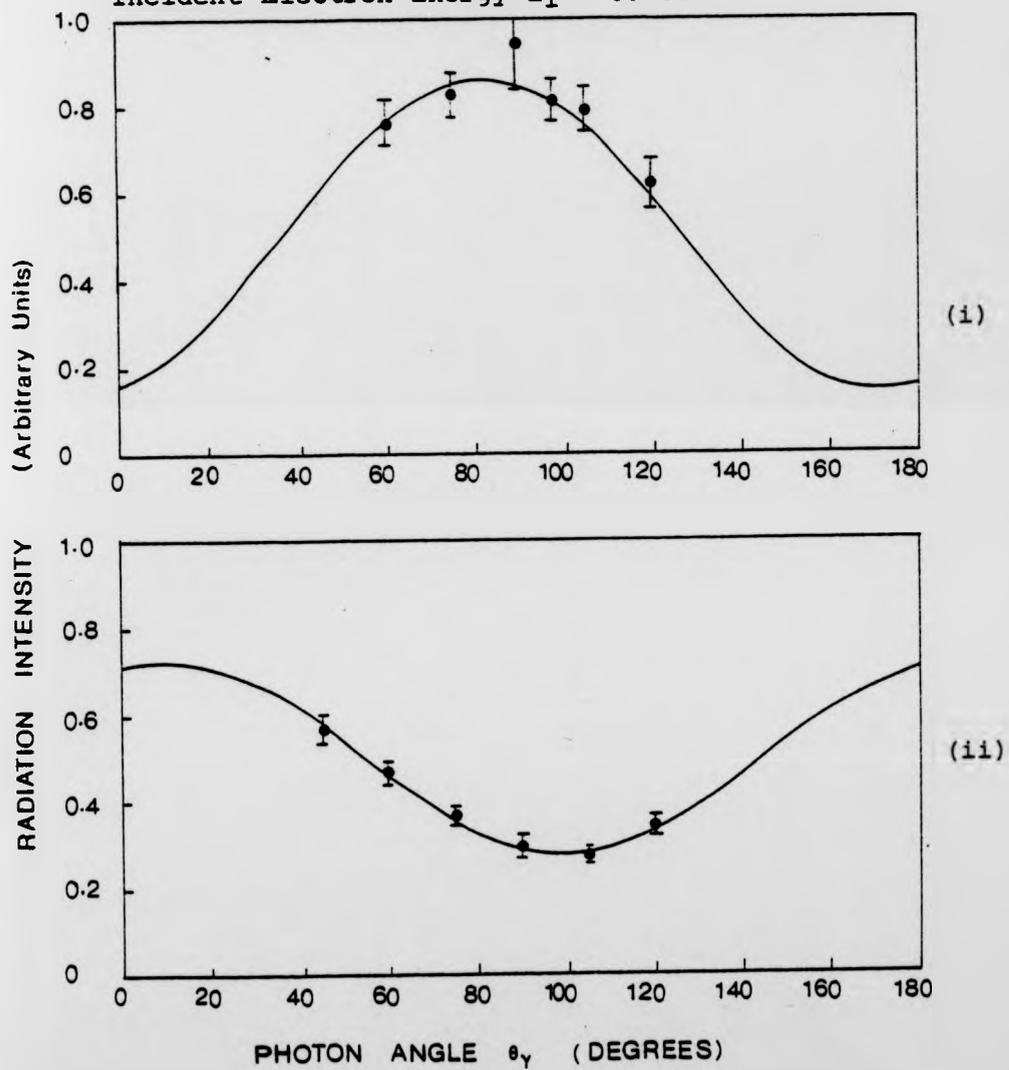
Fig. 5.6 (e) (i) and (ii)

KRYPTON $^3P_1$

Electron Scattering Angle $\theta_e = 30^O$
Incident Electron Energy $E_i = 60$ eV
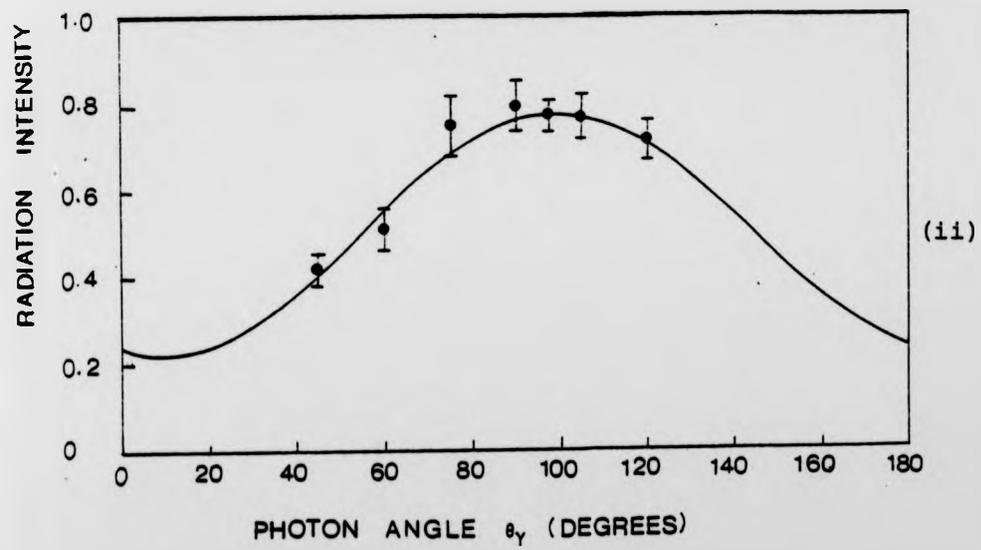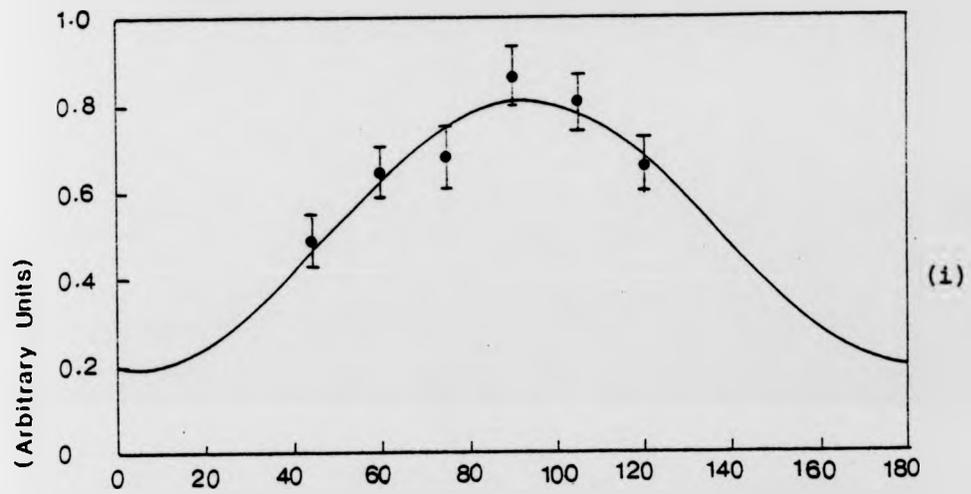
Fig. 5.6 (f) (i) and (ii)

KRYPTON $^1P_1$
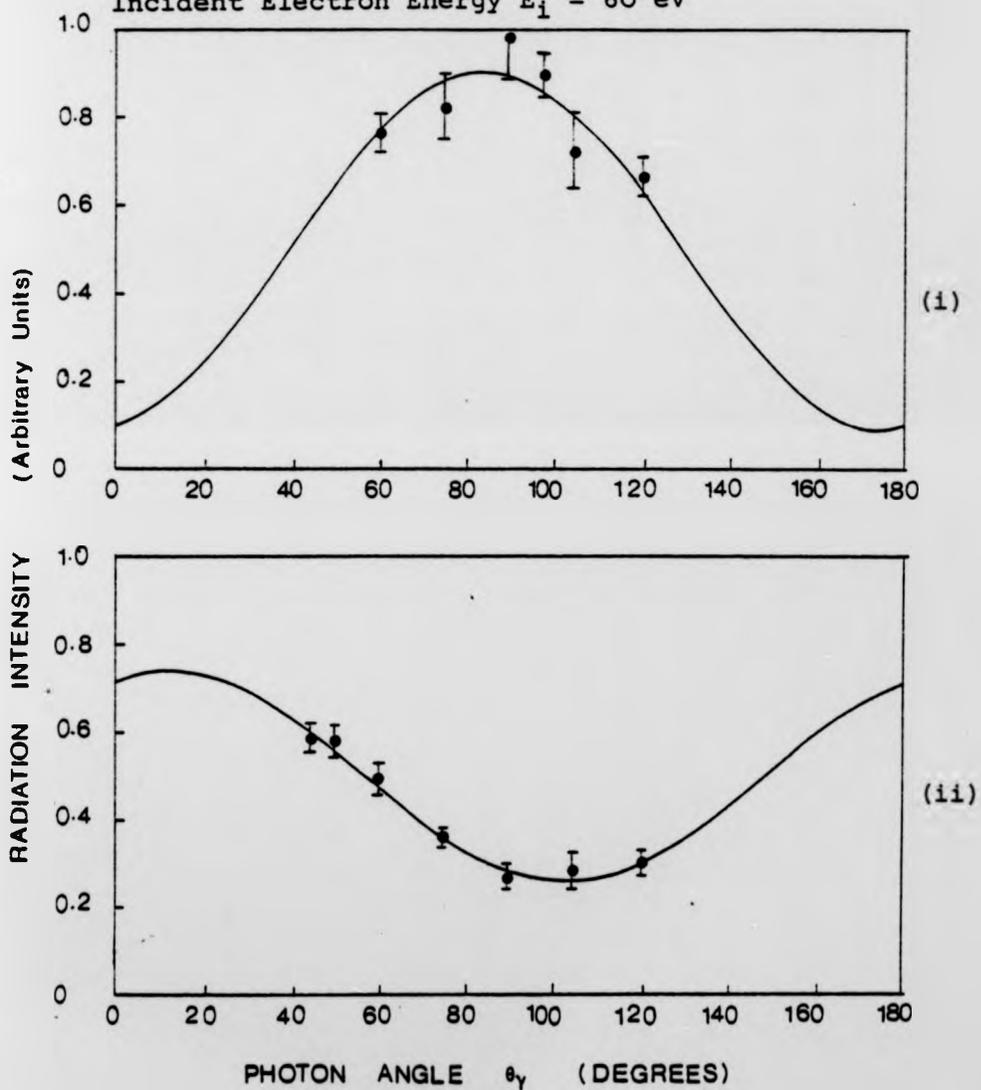
Electron Scattering Angle $\theta_e = 20^\circ$
Incident Electron Energy $E_i = 60$ eV

Fig. 5.6 (g) (i) and (ii)

130

KRYPTON $^1P_1$

Electron Scattering Angle $\theta_e = 30^o$
Incident Electron Energy $E_i = 60$ eV

RADIATION INTENSITY (Arbitrary Units)

PHOTON ANGLE θ_γ (DEGREES)

(i)

(ii)
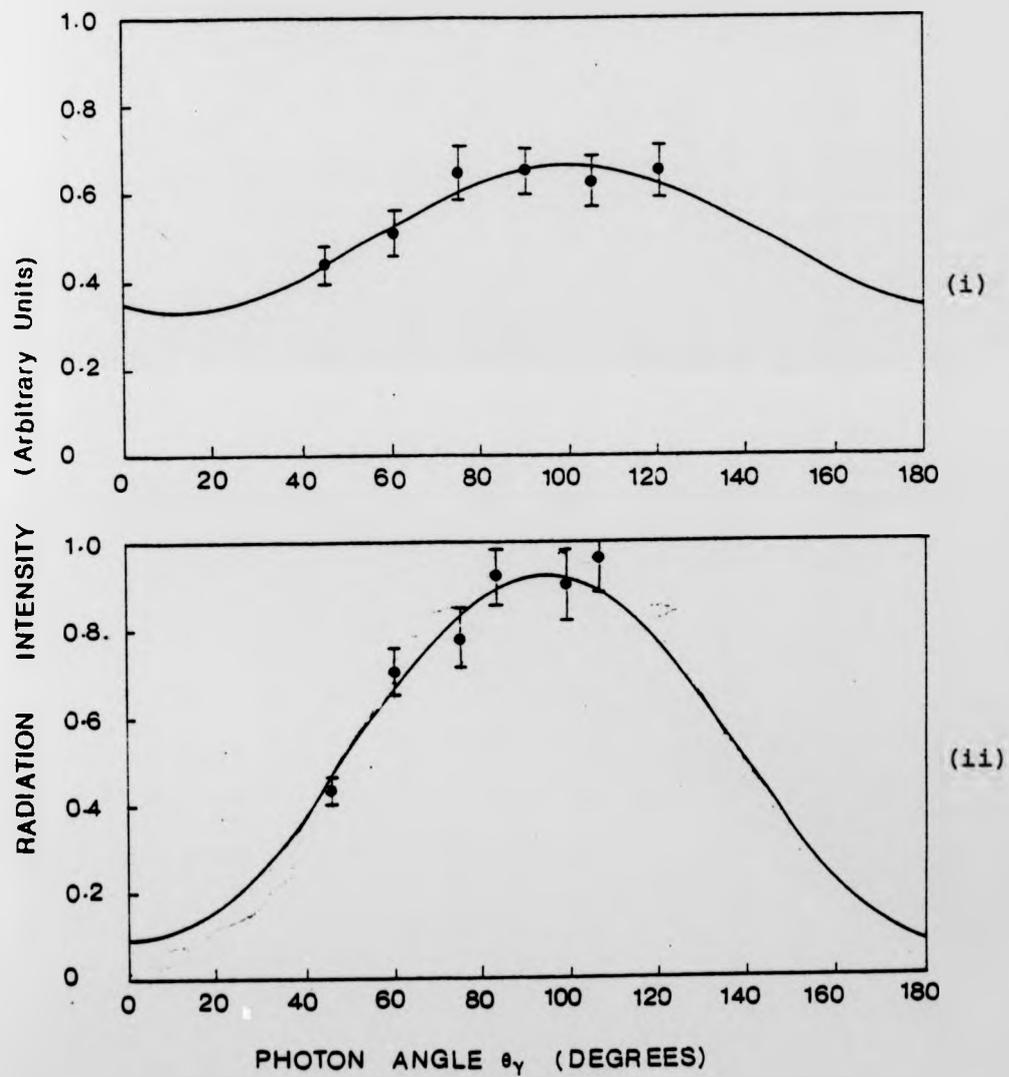
Fig. 5.6 (h) (i) and (ii)

Fig. 5.7 (a) and (b):

Electron-photon angular correlations in xenon showing the
normalised coincidence count rate as a function of photon
scattering angle (i) out of the scattering plane with
azimuthal angle $\phi_\gamma = 135^\circ$ and (ii) in the scattering
plane with azimuthal angle $\phi_\gamma = 180^\circ$. Solid curves
are the least square fits to the experimental data.

XENON $^3P_1$

Electron Scattering Angle $\theta_e = 30^O$
Incident Electron Energy $E_i = 80$ eV

(i)

(ii)

RADIATION INTENSITY (Arbitrary Units)

PHOTON ANGLE θ_γ (DEGREES)
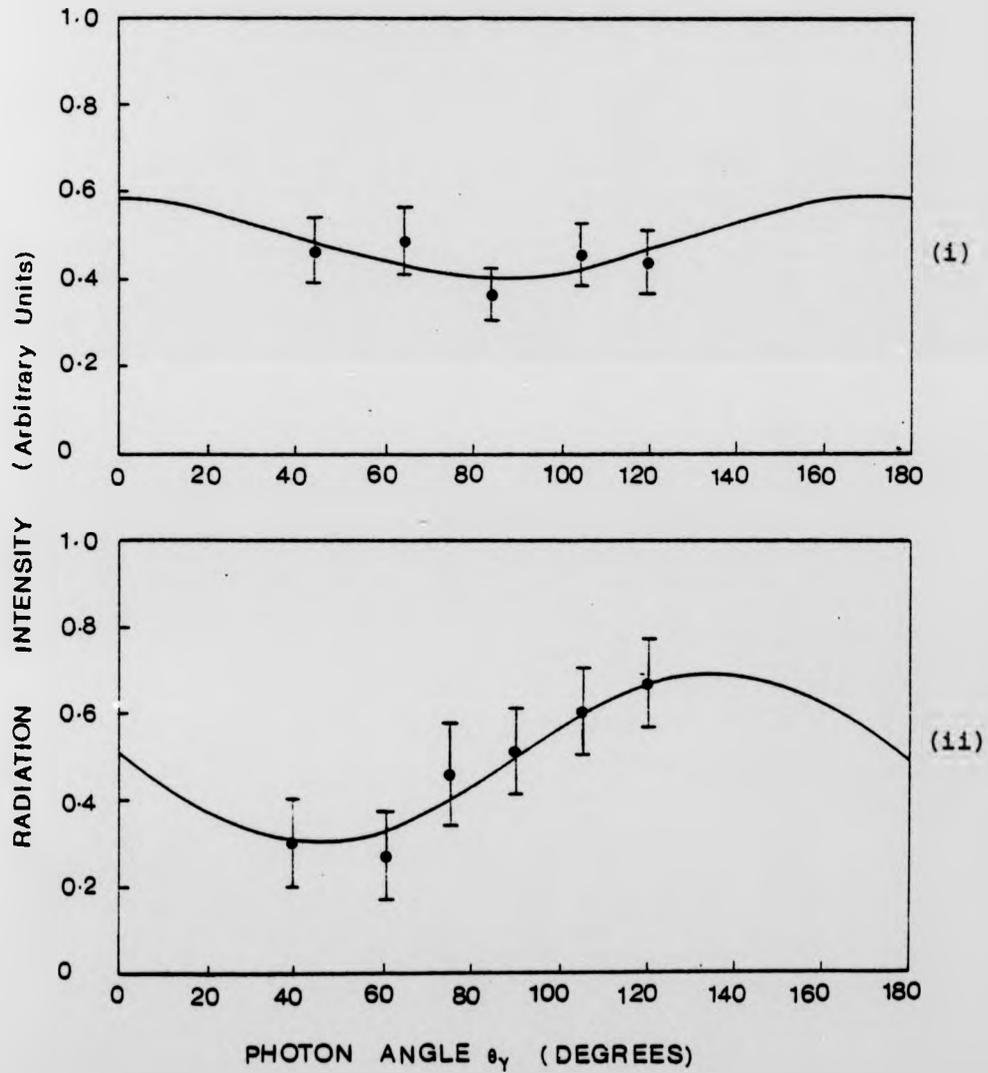
Fig. 5.7 (a) (i) and (ii)

XENON $^3P_1$

Electron Scattering Angle $\theta_e = 20^o$
Incident Electron energy $E_i = 80$ eV
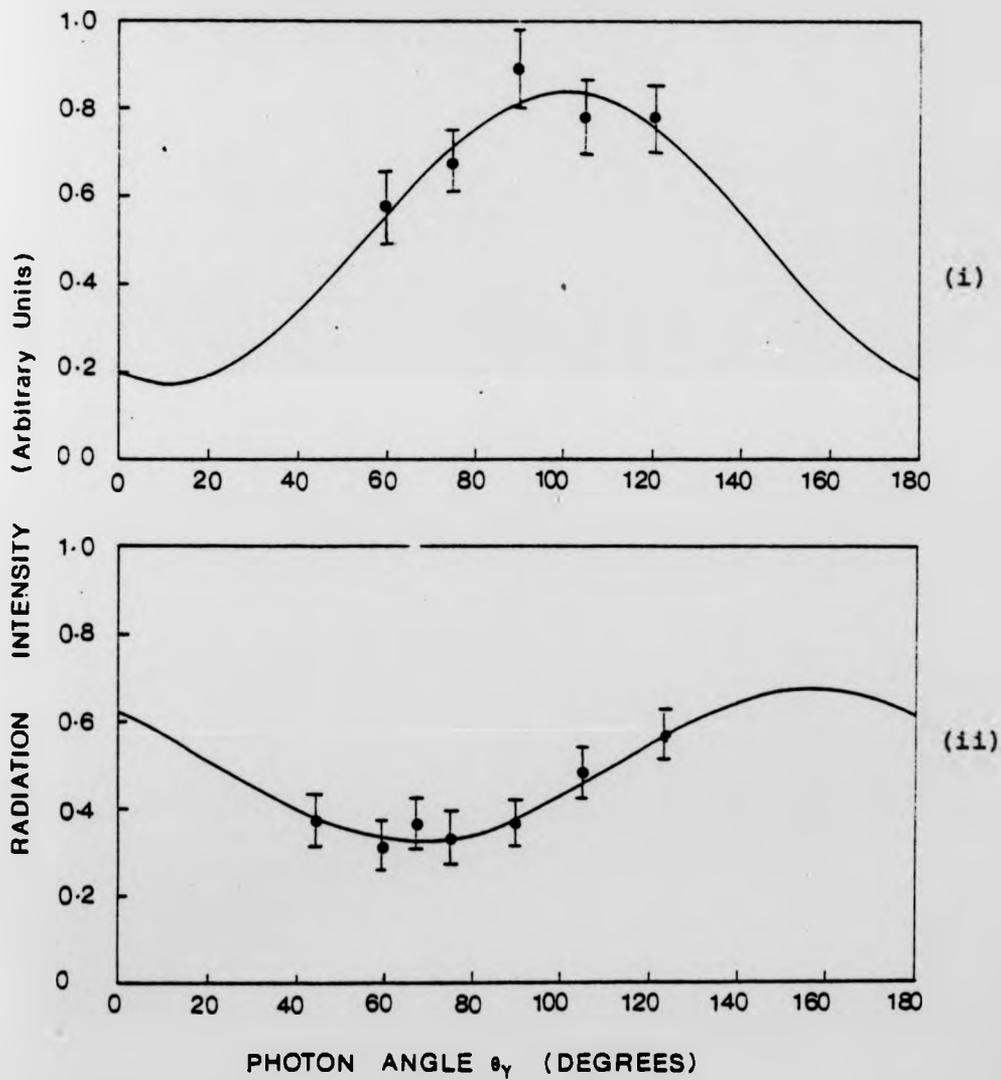
Fig. 5.7 (b) (i) and (ii)

$\theta_e = 20^\circ$, the derived value of cos ε is slightly greater than 1 due to a larger statistical error in the value of λ. In the case of krypton, the derived values for cos ε are also found greater than 1 which is due to the present statistical uncertainties in λ and are therefore not presented in the Table 2. For the future a longer period of collection of data should reduce the uncertainty in λ further in order to yield statistically significant values for cos ε.

The experimental measurements of λ, cos $\overline{\chi}$ and cos ε for heavy target atoms (Kr and Xe) have been carried out for the first time and as to date there are no known theoretical calculations for these parameters.

6 - <u>CONCLUSIONS</u>

The introduction of the electron-photon coincidence technique in the study of inelastic scattering of electrons by atoms has resulted in valuable information about the collision physics and coherence properties of the excitation process. The parameters λ and χ which are extracted from these coincidence experiments are a sensitive test of various theoretical models used to describe electron scattering processes. While total and differential cross-section measurements reveal a kind of "gross structure" of the excitation process, measurements of angular correlations between electrons and photons provide "fine structure" information on scattering and target parameters. The scattering parameters are the excitation amplitudes and their relative phase differences and the target parameters are represented by the orientacion, alignment and multipole moments of the collisionally excited atoms.

Helium atoms are well described by LS coupling scheme and the complete analysis of the excitation process has been achieved for the 2^1P state (Eminyan et al. 1973, 1974). The observed discrepancies in the experimental results of Hollywood et al. (1979), Sutcliffe et al. (1978), and Steph and Golden (1980) are of great interest for those involved in this field of atomic physics.

A lot of time and effort has been devoted to the design and construction of the apparatus for the electron-photon angular correlation measurements during the present study to ensure that the data collected were free from systematic errors. A number of validity tests carried out

on the individual parts of the apparatus and the system as a whole give us confidence that the present data are free from major systematic errors.

The scattering and target parameters have been derived for 10 different electron scattering angles ranging from 8 to 108°, covering reasonably well the whole angular range studied so far by other groups. It has been found from the results that up to an electron scattering angle $\theta_e = 60^{\circ}$, the values of λ agree fairly well with previous experimental data and theoretical calculations. For scattering angles $\theta_e > 60^{\circ}$ the present values for λ follow the general trend observed by Hollywood et al. (1978), and Slevin et al. (1980). They also confirm the existence of a minimum in λ at large scattering angles ($\sim 100^{\circ}$).

The present experimental data show that there is a need for further theoretical calculations to clarify the existing discrepancies between theory and experiment. This should cover the whole range of electron scattering angles specially at an incident electron energy of 80 eV which has been under experimental study in the recent past.

In the case of heavy atoms the presence of spin-orbit interaction in the target atom has a significant effect on the phase information obtainable from electron-photon coincidence experiments. Spin-orbit effects have been experimentally observed in krypton and xenon at small electron scattering angles at 36 eV, 60 eV and 80 eV incident electron energies. A value of cos ε equal to 1 indicates the absence of spin-orbit interaction effects

in the target atom. The deviation of the values of cos ε
from 1 determines the strength of the spin-orbit inter-
action experienced by the atom. The derived values of
cos ε from the present measurements on krypton and xenon
show the extent of the spin-orbit interaction in the
target atoms.

The present results of the experiment on heavy rare
gas atoms (Kr & Xe) are important because the effect of
spin-orbit interaction on the phase information obtainable
from electron-photon coincidence experiment has been
explicitly identified. The newly introduced parameters
cos $\bar{\chi}$ and cos ε (Blum et al. 1980) therefore lead to a
better characterization of the scattering process.

REFERENCES

Al-Shamma S H and Kleinpoppen H, 1978, J. Phys. B: Atom. Molec. Phys. $\underline{11}$ L367.

Al-Shamma S H, 1978, Ph.D Thesis, University of Stirling.

Anderson N, Anderson T, Coke C L and Horsdal Pedersen E, 1979, J. Phys. B: Atom. Molec. Phys. $\underline{12}$ 2541-51.

Arriola H, Teubner P J O, Ugbabe A and Weigold E, 1975, J. Phys. B: Atom. Molec. Phys. $\underline{8}$ 1275-9.

Baranger E and Gerjuoy E, 1958, Proc. Phys. Soc. $\underline{72}$ 326-36.

Bell R E, 1966, Alpha, Beta and Gamma Ray Spectroscopy, Vol.2 ed. K Siebahn (Amsterdam: North Holland) 905-29.

Branden B H and McDowell M R C, 1977, Phys. Rep. $\underline{30}$ 207-303.

————————— 1978, Phys. Rep. $\underline{46}$ 250-294.

Blum K, 1979, Proc. 11th Int. Conf. on Physics of Electronic and Atomic Collisions (Kyoto: Society for Atomic Collision Research).

Blum K and Kleinpoppen H, 1975, J. Phys. B: Atom. Molec. Phys. $\underline{8}$ 922.

————————— 1979, Phys. Rep. $\underline{52}$ 203-61.

————————— 1976, Electron and Photon Interactions with Atoms, eds. H Kleinpoppen and M R C McDowell (New York: Plenum) p.501.

————————— 1980, Invited paper presented at the International Workshop on Electron-Atom and Molecular Collisions, Zentrum für Interdisziplinare Forschung, Universitat Bielefeld, to be published.

Blum K, da Paixao F J and Csanak Gy, 1980, J. Phys. B: Atom. Molec. Phys. $\underline{13}$ L257-L261.

Camhy-Val C and Dumont A M, 1970, Astron. Astrophys. 6 27.

Candler C, 1964, Atomic Spectra (London: Hilger and Watts Ltd).

Delage A, Roy D and Carrett J D, 1975, Abstracts of Papers of IXth International Conference on the Physics of Electronic and Atomic Collisions, Seattle, Vol.2, p.1099.

Dixon A J, Hood S T and Weigold R, 1978, Phys.Rev.Lett. 40 1262-6

Elanbaas W, 1929, Z. Phys. 59 289.

Eldridge J A and Olsen H F, 1926, Phys. Rev. 28, 1151.

Ellet A, Foot P D and Mohler F L, 1926, Phys. Rev. 27 31.

Ehlers V J and Gallagher A, 1973, Phys.Rev.A 7, 1573-85.

Ehrhardt H, Schulz M, Tekaat T and Willmann K, 1969, Phys. Rev.Lett. 22 89-92.

Ehrhardt H, Hesselbacher K H, Jung K, Schubert E and Willmann K, 1974, J. Phys. B: Atom.Molec.Phys. 7 69178.

Eminyan M, MacAdam K B, Slevin J and Kleinpoppen H, 1973, Phys.Rev.Lett. 31 576-9.

———————————— 1974, J. Phys.B: Atom. Molec.Phys. 7 1519-42.

Eminyan M, MacAdam K B, Slevin J, Standage M C and Kleinpoppen H, 1975, J.Phys.B: Atom. Molec. Phys. 8 2058-66.

Eminyan M, Kleinpoppen H, Slevin J and Standage M C, 1976, Electron and Photon Interaction with Atoms, eds. H Kleinpoppen and M R C McDowell (New York: Plenum) p 455.

Fano U and Macek J H, 1973, Rev. Mod. Phys. 45 553-73.

Fedorov V L and Mezentsev A P, 1965, Opt. Spectrosc. 19 5-8.

Fon W C, Berrington K A and Kingston A E, 1979, J. Phys.B:
Atom.Molec.Phys. 12 L171-3.

Frank J and Hertz G, 1914, Verch. der Phys. Ges. 16 457.

Froitzheim H, Ibach H and Lehwald S, 1975, Rev.Sci.Instrum.
46 1325-8.

Giordmaine J A and Wang T C, 1960, J.Appl. Phys. 31, 463-71.

Grivet P, 1972, Electron Optics (Oxford: Pergamon).

Hanle W, 1929, Z. Phys. 54 848.

Hanne G F and Kessler J, 1974, Phys.Rev.Lett. 33, 341.

Hanle W and Schaffernicht W, 1930, Ann. Phys. Leipzig 6 905.

Hertel I V and Stoll W, 1974, J. Phys. B: Atom.Molec.Phys.
5 583.

Harting E and Read F H, 1976, Electrostatic Lenses
(Amsterdam: Elsevier).

Heddle D W O, 1968, in Methods of Experimental Physics
Vol.7 (New York: Academic).

Heddle D W O, 1976, Contemp. Phys. 17, 443-60. also 1976
in Electron and Photon Interactions with Atoms, eds.
H Kleinpoppen and M R C McDowell (New York: Plenum) p.671.

Heddle D W O, Keesing R G W and Parkin A, 1976, Proc. Roy.
Soc. Lond . A 337 443-50.

Heddle D W O, Keesing R G W and Kurepa J M, 1974, Proc.
Roy. Soc. Lond. A 337 435-41.

Heddle D W O and Keesing R G W, 1967, Proc. Roy. Soc. Lond.
A. 299, 212-20.

Heideman H G M, Smit C and Smit J A, 1969, Physica 45 305-20.

Hermann H W and Hertel I V, 1978, in Coherence and Correlation in Atomic Collisions, eds. H Kleinpoppen and J F Williams (New York: Plenum).

Hils D, McCusker M V, Kleinpoppen H and Smith S J 1972, Phys. Rev. Lett. 29 398.

Hollywood M T, Crowe A and Williams J F, 1979, J. Phys. B: Atom. Molec. Phys. 12, 819-34.

Holt R A and Pipkin F M, 1974, Phys. Rev. A 9, 581-4.

Hood S T, Weigold E and Dixon A J, 1979, J. Phys. B: Atom. Molec. Phys. 12 631-48.

Hughes A L and McMillan J H, 1929, Phys. Rev. 34 291-5.

Hughes A L and Rojansky V, 1929, Phys. Rev. 34, 284-90.

Imhof R E and Read F H, 1969, Chem. Phys. Lett. 3 652-4.

——————————— 1971a J. Phys. B: Atom Molec.Phys. 4 450-60.

——————————— 1971b J. Phys. B: Atom.Molec.Phys. 4 1063-9

——————————— 1971c Chem.Phys.Lett. 11 326-8.

——————————— 1977 Rep.Prog.Phys. 40 1-104.

Kaul R D, 1966, J.Opt.Soc.Am. 56 1262-3.

King G C and Adams A, 1974, J.Phys.B: Atom.Molec.Phys. 7 1712-8.

King G C, Adam A and Cvejanovic D, 1975a, J.Phys.B: Atom. Molec.Phys. 8 365-71.

King G C M, Adam A and Read F H, 1972, J.Phys.B: Atom.Molec. Phys. 5 L254-7.

King G C, Read F H and Imhof R E, 1975b, J.Phys.B: Atom. Molec.Phys. 8 665-73.

King G C, Mohamed K A, Read F H and Imhof R E, 1976,
    J.Phys.B: Atom.Molec.Phys. 9 1274-50.

Kleinpoppen H, 1967, Columbia University, unpublished report.

Kleinpoppen H, 1975, Atomic Physics 4, eds. G Zu Putlitz,
    E W Weber and   Winnacker (New York: Pleum)
    p.449-85.

Kleinpoppen H, 1969, Physics of the One- and Two-Electron
    Atoms, eds. F Bopp and H Kleinpoppen (Amsterdam:North-
    Holland) p.612-31.

——————————— 1977, Advances in Quantum Chemistry Vol.10, p77.

Kleinpoppen H and McGregor I, 1979, in Coherence and Corre-
    lation in Atomic Collisions, eds. H Kleinpoppen and
    J F Williams (New York: Plenum).

Klemperer O and Barnett M E, 1971, Electron Optics (Cambridge:
    Cambridge UP).

Koschmieder H,1974, Ph.D Thesis, University of Stirling.

Kuppermann A, Rice J K and Trajmar S, 1968, J.Phys.Chem.
    72 3894.

Kuyatt C E and Simpson J A, 1967, Rev.Sci.Instr. 38 103.

Kuyatt C E, 1968, Methods of Experimental Physics, ed.
    L Marton Vol.7a 11.

Lew H, 1967, Methods of Experimental Physics, Vol.4, Part A,
    eds. V W Hughes and H L Schultz (New York: Academic)
    p.160.

Macek J and Jaecks D H, 1.971, Phys.Rev.A 4 2288-300.

Macek J and Hertel I V, 1974, J.Phys.B: Atom.Molec.Phys.
    7 2173.

Malcolm I C and McConkey J W, 1979, J.Phys.B: Atom.Molec.
    Phys. 12 511-9.

Marmet P and Kerwin L, 1960, Can.J.Phys. 38 787-96.

McFarland R H, 1964, Phys. Rev. A133, 986-90.

————————— 1967, Phys.Rev. 156 55.

McGregor I, Hippler R and Kleinpoppen H, 1980, Proc. 7th
    Int. Conf. on Atom.Phys. August 4-8, 1980, Cambridge,
    Massachusetts (USA).

Moiseiwitsch B L and Smith S J, 1968, Rev.Mod.Phys. 40
    238-353.

Moore C E, 1949, Atomic energy levels as derived from the
    analysis of Optical Spectra Circular 467, Vol.1.

————————— 1952, Vol.2.

————————— 1958, Vol.3.

Mott N F, 1932, Proc.Roy.Soc.Lond. A 135 429.

Oppenheimber J R, 1927, Proc.Nat.Acad. Sci. 13 800-5.

————————————1928, Phys.Rev. 32 361-76.

Ottley T W and Kleinpoppen H, 1975, J.Phys. B: Atom.Molec.
    Phys. 8 621-7.

Pavlovic Z, Boness M J W, Herzenberg A and Schulz G J, 1972,
    Phys.Rev.A 6 676-85.

Penney W G, 1932, Proc.Nat.Acad.Sci 18 231-7.

Percival I C and Seaton M J, 1958, Phil.Trans. R.Soc. A
    251 113-38.

Pichanic F M J and Simpson J A, 1968, Phys.Rev. 168 64.

Pochat A, Rozvel D and Peresse J, 1973, J. de Physique 34 701.

Purcell E M, 1938, Phys.Rev. 54 818-26.

Quarder von B, 1927, Z.Phys. $\underline{41}$ 675.

Raible V, 1974, Ph.D Thesis, University of Stirling.

Ramsauer C, 1921, Annalen de.Physik $\underline{64}$ 513, $\underline{66}$ 546.

Ramsey N F, 1963, Molecular Beams (Oxford: Clarendon)
        pp. 12-21.

Roy D, Delage A and Carette J D, 1975, J.Phys.E: Atom.
        Molec. Phys. $\underline{8}$, 109-14.

Rubin K, Bederson B, Goldstein M and Collins R E, 1969,
        Phys.Rev. $\underline{182}$ 201-14.

Rudu M F, 1972, Low Energy Electron Spectroscopy, ed.
        K D Sevier (New York: Wiley-Interscience) pp. 3-34.

Schulz G J, 1963, Phys. Rev.Lett. $\underline{10}$ 104.

——————— 1973, Rev.Mod.Phys. $\underline{45}$ 378-486.

Scot T, McDowell M R C, 1976, J.Phys.B: Atom.Molec.Phys.
        $\underline{9}$ 2235.

Shaw D A, Adam A and King G C, 1975a, J.Phys.B: Atom.Molec.
        Phys. $\underline{8}$ 2456-60.

Shull C G, Chase C T and Myers F E, 1943, Phys.Rev. $\underline{63}$ 29.

Simpson J A and Kuyatt C E, 1963, Rev.Sci.Instrum. $\underline{34}$ 265-8.

————————————————, 1966, J.App.Phys. $\underline{37}$ 3805.

Skinner H W B, 1926, Proc.Roy. Soc.Lond. A $\underline{112}$ 642.

Skinner H W B and Appleyard E T S, 1927, Proc.Roy.Soc.Lond.
        A $\underline{117}$, 224-44.

Slevin J, Porter H Q, Eminyan M, Defrance A and Vassilev G,
        1980, J.Phys.B: Atom.Molec.Phys. $\underline{13}$ L 23-L 25.

Smith A J, Read F H and Imhof R E, 1975, J.Phys.B: Atom.
    Molec.Phys. 8 2869-79.

Smith A J, Imhof R E and Read F H, 1973, J.Phys.B: Atom.
    Molec.Phys. 6 1333-8.

Standage M C and Kleinpoppen H, 1976, Phys.Rev.Lett. 36
    577-80.

Steph N C and Golden D E, 1980, Phys.Rev.A 21, 759-70.

Sutcliffe V C, Haddad G N, Steph N C and Golden D E, 1978.
    Phys.Rev.A 17 100-7.

Swanson N, Celotta R J and Kuyatt C E, 1976, Electron-Photon
    Interactions with Atoms, eds. H Kleinpoppen and
    M R C McDowell (New York: Plenum) p.661.

Tan K H, Fryar J, Farago P S and McConkey J W, 1977,
    J.Phys.B: Atom. Molec.Phys. 10 1073-82.

Thomas L D, Csanak G, Taylor H S and Yarlagadde B S, 1974,
    J.Phys.B: Atom.Molec.Phys. 7 1719.

Townsend J S and Bailey V A, 1922, Phil.Mag. 43 593.

Ugbabe A, Teubner P J O, Weigold E and Arriola H, 1977,
    J.Phys.B: Atom.Molec.Phys. 10 71-9.

Weigold E, Hood S T and Teubner P J O, 1973, Phys.Rev.Lett.
    30 475-8.

Whitteker J H and Dalby F W, 1968, Can.J.Phys. 46 193.

William J F, 1975, The Physics of Electronic and Atomic
    Collisions, eds. J S Riseley and R Geballe (University
    of Washington, Seattle, Washington) pp.139-50.

Williams J F and Crowe A, 1975, J.Phys.B: Atom.Molec.Phys.
    8 2233.

Williams J F and Willis B A, 1975, J.Phys.B: Atom.Molec.Phys.
    8 1670.

Williams J F, 1978, J.Phys.B: Atom.Molec.Phys. 11 2015.

Williams W L and Fry E S, 1968, Phys.Rev. Lett. 20 1335-38.

Williams W, Trajmar S and Kuppermann A, 1973, Abstracts of
    Papers VIIIth Int. Conf. on the Physics of Electronic
    and Atomic Collisions, Beograd, Vol.I, p.328.

Wykes J, 1972, J.Phys.B: Atom.Molec.Phys. 5 1126-37.

Zaidi A A, McGregor I and Kleinpoppen H, 1978, J.Phys.B:
    Atom.Molec.Phys. 11 L 151-5.

Zehnle L, Clemens E, Martin P J, Schauble W, ed. V Kempter,
    1978, J.Phys. B. 11 2865-74.